ON THE RHEOLOGY AND MORPHOLOGY DEVELOPMENTS OF TERNARY LIQUID/LIQUID/PARTICLES SYSTEM WITH CAPILLARY FORCE

by

Junyi Yang

Bachelor of Science, University of Missouri-Columbia, 2012

Bachelor of Science, East China University of Science & Technology, 2012

Submitted to the Graduate Faculty of

Swanson School of Engineering in partial fulfillment

of the requirements for the degree of

Doctor of Philosophy

University of Pittsburgh

2018

UNIVERSITY OF PITTSBURGH

SWANSON SCHOOL OF ENGINEERING

This dissertation was presented

by

Junyi Yang

It was defended on

March 20th, 2018

and approved by

Robert M.Enick, Ph.D., Professor, Department of Chemical and Petroleum Engineering

Joseph John Mccarthy, Ph.D., Professor, Department of Chemical and Petroleum Engineering

Jung-Kun Lee, Ph.D., Professor, Department of Mechanical Engineering & Materials Science

Dissertation Director: Sachin Velankar, Ph.D., Professor, Department of Chemical and Petroleum Engineering

ON THE RHEOLOGY AND MORPHOLOGY DEVELOPMENTS OF TERNARY LIQUID/LIQUID/PARTICLES SYSTEM WITH CAPILLARY FORCE

Junyi Yang, PhD

University of Pittsburgh, 2018

This dissertation is focused on understanding the relationship between rheology and morphology of capillary suspension under various shearing conditions. A model ternary liquid/liquid/particle system is constructed for experimental propose. Particularly in this system, one of the liquid has some preferentiality in wetting towards particles so that liquid meniscus can be formed between particles. Formation of such meniscus can create a network which endows the suspension with a yield stress. Four specific topics are presented: 1) to investigate rheology of pendular network (i.e. only pair-wise connection form between fully wet particles), by examining the dependence of the yielding behavior on flow history, quantify their viscoelasticity, and relate these to the microstructural picture of meniscus rupture; 2) to verify the effect of various wetting conditions on rheology of the capillary suspension. Results show a diminishing solid-like property of such suspension as the particles become less wetting by the minority fluid, which induced particle aggregation; 3) to map the rich variety of morphologies for a model ternary system containing particles which were equally wetted by both polymers, analogous to: Picking emulsions, particle-stabilized foams and bijels [1, 2]; 4) to correlate the dynamic morphology of ternary model blend with rheological measurement during creep-recovery via in-situ visualization.

TABLE OF CONTENTS

LIST OF TABLES

LIST OF FIGURES

PREFACE

Foremost, I would like to express my sincere gratitude to my research advisor, Professor Sachin Velankar, for his support over the past five years. I would like to thank him for his contributions of time, ideas and funding to make my Ph.D. experience productive and stimulating. As a tremendous mentor for me, Professor Velankar. always showed me his patience, diligence and painstaking attention to research, which encourages me a lot in my research.

I want to acknowledge Dr. Trystan Domenech for providing me the guidance of doing preliminary research. He recommended many good papers and books, which helps me greatly during my Ph.D. research.

I am also grateful to Professor McCarthy, Professor Lee, and Professor Robert Enick, for serving as my committee members. I would like to thank them for their insightful comments and suggestions.

I would like to thank to all of my colleague members and collaborators, including Junyu Yang, Derrick Amoabeng, Ya Gao, Dave Roell, Martin Echavarria and Nicole Heinichen. It is my great pleasure to work with all of you and I wish you all the best. I would like to thank Dr. Susheng Tan and Mike McDonald for training me on Scanning Electron Microscope (SEM).

I would like to thank my parents for their support and courage over my eight years study aboard. Now I’m ready to go home.

1.0 INTRODUCTION

1.1 BACKGROUND

By adding a small amount of water to dry sand, sand castles can be built because the water wets the sand, forming capillary bridges binding the particle together. Such capillary-driven attractive particulate systems find their significance in not only scientific literature but providing an approach to fabrication of new materials[3]. Previous studies have focused on how the added liquid affects the original suspension system in terms of rheology and morphology. For instance, addition of a small amount of wetting fluid to a suspension of particles in a non-wetting fluid, the suspension would form a *pendular* network shown in Figure 2, where particles are connected by pair-wise menisci, giving the suspension a yield stress[4-7]. In general, this dissertation is to examine multiple effects such as the dependence on composition, on deformation history and particle wettability on particulate suspensions using an idealized "model system": The model system consists of two immiscible polymers polyethylene oxide (PEO) and polyisobutylene (PIB), and silica particles whose wettability for the liquids can be tuned. One of the advantages of such system is that it flows at a modest temperature, but its structure can be preserved by simply cooling to room temperature, and characterized by examining one of the polymer phases in scanning electron microscope after selective removal of the other. Thus the rheological properties of ternary systems and their morphology can be related. Later in this research, a slightly different model system consisting LIR-

30/PEO/glass particle was used to examine the *in-situ* morphology deformation during shear. Detailed description on this system as well as correlation between rheology and morphology during creep-recovery process is available in Chapter 5.0 . For rest of the dissertation, Chapter 1.1 gives the background and literature review on four specific topics accomplished; Chapter 1.2 summarized the materials and experimental technique used through this work. Chapter 2.0 examines the dependence of the yielding behavior on flow history for pendular network; Chapter 3.0 verifies the effect of various wetting conditions on rheology of the capillary suspension by conducting surface medication on silica particles to alter their hydrophobicity; Chapter 4.0 constructs a map of rich variety morphologies for the model ternary PIB/PEO/silica system containing particles which were equally wetted by both polymers.

1.1.1 Establishment of model ternary liquid/liquid/particle system

In particulate systems, capillary forces can bind discrete particles together into a space-spanning network with a yield stress. The most familiar example is of sand, which when wetted with small amounts of water, develops sufficient yield stress to allow construction of elaborate sand castles[8-11]. The same is true for particles-in-liquid suspensions: addition of a small amount of a second immiscible liquid can create a network which endows the suspension with a yield stress[4-7, 12-17].

Such suspensions in which capillarity forces are important are practically useful in materials science. Specifically, the very simple method – "add liquid and mix" – of realizing a yield stress offers a convenient way of stabilizing a structure temporarily before it can be made permanent e.g. by sintering or crosslinking[3]. Furthermore, open pore morphologies can be realized readily in such systems[16, 18-20] with immediate relevance to applications in which chemical transport or fluid retention must be combined with mechanical strength. Indeed applications to

materials science are not restricted to suspensions with capillary forces – a diverse set of particle/fluid/liquid mixtures can, depending on the materials and composition, yield a variety morphologies of potential interest to materials science[3], including, particle-stabilized foams[21-23], bijels[19, 24], wet granular materials[8, 25, 26] and liquid marbles[27, 28].

Previously in our group, a model system composed of immiscible polyethylene oxide (PEO), polyisobutylene (PIB) and silica particles that were fully-wetted by PEO was constructed to examine the morphology of capillary suspensions. These mixture constituents were selected not for any specific application, but for experimental convenience: the wetting fluid PEO melts at a modest temperature (~65), which facilitates the rheological measurements of the ternary system, and it can be solidified by cooling to room temperature which helps morphology characterization by electron microscopy. Previous experiments showed that ternary system morphology as well as rheology are sensitive to the volumetric ratio of PEO to particles[5]: $\varrho = \phi_{PEO}/\phi_p$. As ϱ ϱ increases from ~0.01 to ~0.2, particles became bound together by small menisci of the wetting liquid, forming a percolating network which was dubbed a *pendular network*. A further increase in ϱ at fixed particle loading led to encapsulation of particles due to excess PEO, and the system reached the compact *capillary aggregation* regime. Detailed morphology evolution upon composition for systems with fully wetting particles is discussed later and shown in Figure 2. Rheologically, *pendular networks* were found to behave analogous to other attractive suspensions: they showed yield stress in steady shear, solid-like behavior and *G'-G"* crossover in large amplitude oscillatory shear (LAOS), and delayed yielding in creep[5].

A PIB/PEO/silica model system was used to examine the rheology of pendular networks. Since such mixtures are far from equilibrium, and their deformation history is expected to affect the microstructure and rheological properties[4]. Even at same composition, either pendular network

or capillary aggregate structures may appear depending on the mixing conditions. Nevertheless, capillary aggregates can be reduced or eliminated by pre-dispersing the PEO with a drop size comparable to or smaller than that of the particles. In addition, pendular menisci may be ruptured under applied flow deformation and re-formed simultaneously as particles that already have wetting fluid on their surface come into contact with each other. This raises several questions: does high shear rate induce structural breakdown, and if so, do the rheological properties depend on shear history? In addition, can changes in rheological properties be restored by sufficiently long flow? Or is flow-induced structural breakdown long-lived, and thus induce nearly-permanent changes in properties? Are pendular networks viscoelastic, e.g. do they show significant recovery upon cessation of shear? Incidentally, very similar questions have been addressed in another system with capillary forces, viz. droplet-matrix blends of immiscible fluids [29-31]. In that case, flow induces both drop breakup and drop coalescence (analogous to breaking and reforming menisci). In those systems, shearing at high rate can reduce drop size and affect the rheology, but subsequent shearing at lower rate can usually (but not always) restore the original drop size and rheological properties. The questions stated above are answered and this portion of the thesis is described fully in Chapter 2.0 .

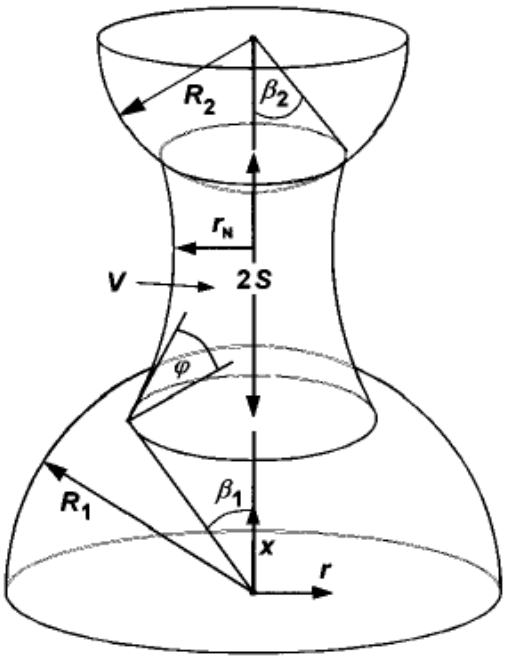

Figure 1. A schematic representation of a liquid bridge of volume V and surface tension γ between two spheres.

1.1.2 Effect of wettability on capillary clusters

While the above-mentioned case involving unmodified silica particles with PEO and PIB is dubbed the *fully-wetting* situation, i.e. the contact angle at fluid-particle interface is zero, forming hour-glass shaped meniscus. However, the case when the surface of the particles is less-favorably wetted by the minority fluid, which is dubbed the *partially-wetting* situation (Figure 1 where the angle φ is not close to zero), has not been fully discussed. Here we focus on only a narrow composition range with ϱ ranging from 0 to 0.25, i.e. the volume fraction of PEO is much less than the particle

volume fraction to ensure pair-wise menisci, at least approximately. In such particulate systems with capillary forces, the wettability of the particles towards the minority liquid plays a crucial role in determining the blend rheology and microstructure[1, 3, 32]. Because the inter-particle attractive force has a joint contribution of surface tension and Laplace pressure difference[33]:

$$F = 2\pi r_N \alpha + \pi r_N 2\,\Delta P \tag{1}$$

where r_N is the neck radius of the meniscus, α is the surface tension, and $\Delta P = \frac{\alpha}{\bar{r}}$ is the Laplace pressure difference inversely proportional to the curvature $\bar{r}$ of the meniscus. As the contact angle increases, the pressure term becomes less dominant with the decreasing curvature and eventually changes the sign, making the overall capillary interaction repulsive[34]. Although, the full dependence of contact force between individual pair of particles on yielding behavior for overall particulate system is predicted to be more complex[35], we speculate that capillarity-induced aggregation, and hence yield stresses developed in the fully wetting situation will diminish or even disappear in the partially wetting situation. Therefore, silica particles carrying three different degrees of hydrophobicity from surface modifications (including the unmodified fully wet ones) will be examined. The modification process involves two different silane agents: dichlorodimethylsilane (DCDMS) and octadecyltricholorosilane (OTS), both replace the silanol groups on silica surface with the hydrophobic groups[36, 37]. Using these three different particle types, we examined the dependence of linear viscoelastic storage modulus on particle loading under oscillatory shearing condition, and yielding behavior by conducting steady state shear experiments. Details of experimental process on surface treatments is available in Chapter 1.2.3. Detailed results on both particles are described in Chapter 4.0 .

1.1.3 Morphology evolution for ternary system with various wettabilities

Ternary liquid/liquid/particle mixtures show a wide diversity of microstructures resulting from how the particles interact with two fluids, such as: pairwise attraction through capillary bridging[4, 5, 13], many-body cohesion through capillary clustering [5], interfacial assembly of particles [24, 38, 39] or particle bridging of drops[15, 40]. Even a single ternary system can display several of the above morphologies depending on its composition and particle wettability. In a previous paper[5], a previous group member examined the morphology of ternary blends composed of PEO, PIB, and silica particles that are almost completely wetted by one of the polymer phases. Five types of morphology were identified in a single system, and the corresponding morphological map is shown in Figure 2: (1) *pendular/funicular* network, (2) capillary aggregates network, (3) filled drops, (4) co-continuous and (5) drops-in-suspension. These results highlight the central role of capillary interactions in the formation of percolated structures in the case of pendular, funicular and capillary aggregates bicontinuous networks, where the cohesion between the particles forming the network is dominated by capillary forces. For a fixed particle volume fraction, the increase in wetting phase volume fraction induces a change in the building blocks of the capillary-driven network from single particles to capillary aggregates. In addition, the particle volume fraction was found to have a strong influence on phase inversion of the ternary system. However, the effects from changing wettability of particle surface in blend morphology remain unknown. Indeed in small molecule systems, one well-studied example of three-phase liquid/liquid/particle systems is Ramsden–Pickering emulsions [15, 36]. The particles act as surfactants by adsorbing at the liquid–fluid interface, hence inhibiting drop coalescence and stabilize the emulsion. Additionally, a coherent monolayer of particles will stay at the interface that may bridge the droplets and assemble the droplets into volume-spanning networks due to capillary adhesion[15, 40]. Mostly important, the presence of

interfacially active particles can stabilize bicontinuous structure through arrested spinodal decomposition of the fluids[41, 42]. Analogous to Figure 2, a morphological map for particles that are partially-wetted by both of the immiscible liquid phases during melt-mixing is constructed in Chapter 4.0 .

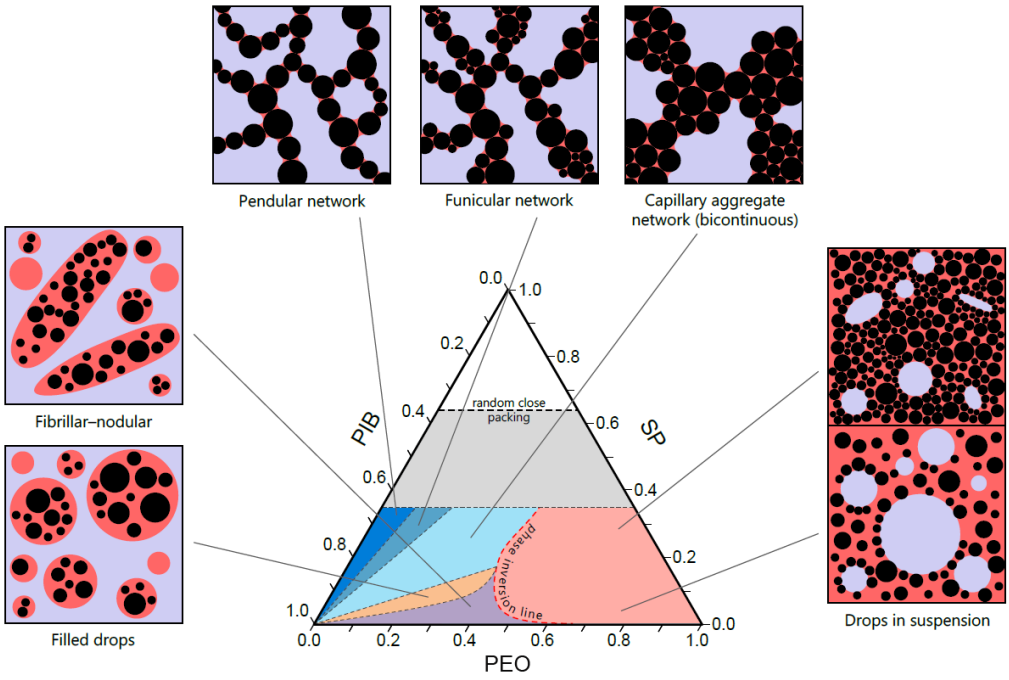

Figure 2. Morphological map and schematic structures of the investigated PIB/PEO/fully wettable silica ternary system. The ternary composition diagram is based on volume fractions. The red dashed path in the ternary diagram represents the phase inversion boundary, with the liquid continuous phase being PIB (non-wetting phase) on the left-handside and PEO (wetting phase) on the right-handside. The grey region of the ternary diagram corresponds to high particle concentrations, which was not explored. Figure reproduced from T. Domenech and S. S. Velankar, J. Rheol., 2017, 61, 363-377. with permission.

1.1.4 Advantages of in-situ visualization on creep-recovery for model blend

As mentioned above, with a small amount of wetting fluid, a pendular network will form which endows the suspension with a yield stress[5, 13]. Such a ternary mixture is unquestionably "solid-like", nevertheless, at a small strain on the order of 1%, it yields and shows very little elastic recoil (Chapter 2.4.3). Thus after yielding, a pendular network is almost purely viscous and not viscoelastic. However further increasing the amount of wetting fluid will engulf the particles and, if there is sufficient wetting fluid, one expects to obtain a particle containing droplet-matrix microstructure. Such droplet-matrix morphologies are known to be viscoelastic, for instance, immiscible polymer blends with a droplet-matrix morphology show elastic recovery that is substantially larger than that of their pure components due to the interfacial tension[43, 44]. Other viscoelastic properties can be measured and related to the morphology including normal stresses in shear flow and stress relaxation behavior, e.g. the stress relation behavior has been categorized with different morphological changes mechanism after cessation of flow: shape-recovery of slightly deformed droplets, breakup of a deformed droplet due to end-pinching, and breakup of a highly elongated droplet[45]. While little research has been done on the stress-strain response during creep-recovery test for such particle-filled droplets blend, for pure binary droplet-matrix blends, the polymer blend literature suggests that both the level and time scale of the immiscible blend recovery after steady state shear are very sensitive to the morphology[43, 46].

In order to clarify relationship between rheology parameters and the morphology during creep-recovery process, both need to be observed simultaneously. Rapidly quenching the structure at step shear strain enables ex-situ observation on the shape of dispersed droplets during recovery[47]. Yet such method failed to capture the deformation evolution of single droplet. Because the blend quenching is an irreversible process, several blends at different strain deformation are

needed to make a comprehensive comparison. In order to overcome such limitation, I therefore conducted an in-situ visualization of structural evolution under shearing conditions using a microscope-equipped rheometer, and correlated them with rheological phenomena. Preliminary tests show that the reflective index mismatch between silica particles and continuous PIB phase makes the image crowded and difficult to interpret at even modestly higher particle loadings. However, a nearly-perfect index match was found for glass particles in liquid isoprene rubber (LIR-30) suspension. Liquid bridges formed by addition of low molecule weight PEO give excellent optical visibility of capillary aggregates even at up to 20 ^{vol}% of particles. Thus, the study in Chapter 5.0 utilize this LIR-30/PEO/glass particle system to investigate the relationship between in-situ dynamic microstructure and rheological response for pendular network and capillary aggregates.

1.2 EXPERIMENT AND EXPERIMENTAL SET UP

1.2.1 Materials and chemicals

Polyisobutylene (PIB, $\rho \approx 0.908$ g/ml, $Mw \approx 2{,}200$ g/mol) and polyethylene oxide (PEO, $\rho \approx 1.1$ g/ml, $Mw \approx 20{,}000$ g/mol, melting point $\approx$ 65°C) was purchased from Soltex and Fluka respectively. Spherical silica particles (diameter roughly 2μm) were purchased from Industrial Powders. As shown previously[4, 5], unmodified particle surfaces are fully wetted by PEO, which is the minority phase in the mixtures examined here.

Ternary blend materials tested in Chapter 5.0 are composed differently from above: Polyisoprene (LIR30 from Kuraray, viscosity 130Pa.s) is the continuous phase and low molecule

weight polyethylene oxide (PEO, ρ≈1.1 g/ml, Mw≈600 g/mol) is the wetting fluid. The particles used are hydrophilic glass particles with average diameter of $\sim 10\mu m$ ~ 10μm obtained from Karlsruhe Institute of Technology.

1.2.2 Sample preparation- Cold Mixing

All the samples studied in Chapter 2.0 and 3.0 were made through a mixing process dubbed as "cold mixing". The first step of cold mixing is to make a concentrated *masterbatch*. A small quantity of PIB and PEO were mixed together using a custom ball mixer[40]. 80 ^{wt}% of PIB and 20 ^{wt}% of PEO were held inside the mixer at 80 ℃ for 15 minutes to ensure complete melting, and then mixed at 600 RPM for 2 minutes. The mixed product was then transferred into a sealed plastic dish, and quenched in the refrigerator at about 10 ℃ for at least 30 minutes to complete crystallization of the PEO. The *masterbatch* blend produced has a PEO-in-PIB morphology, and after removal of PIB, the residual PEO drops are seen to be roughly 5 μm in diameter. PIB/PEO/silica ternary samples of the desired compositions were then prepared by blending appropriate quantities of *masterbatch*, pure PIB, and particles by hand with a spatula in a 40 mm petri dish at room temperature. Samples were placed in vacuum overnight to degas and then stored in the fridge to suppress particle sedimentation.

The intention of making masterbatch is to circumvent problems we had in previous experiments in which all three components were mixed all at once in a batch mixer. For instance, for a ~4 grams batch with wetting fluids volume fractions as low as ϕ_{PEO} =0.16%, this volume fraction corresponds to only 8 mg of wetting fluid. Apart from possible errors in weighing such small quantities, it is also possible that some of the wetting fluid may be "lost" if it wets the internal

parts of the mixer, making the actual mixture composition different from the target value. In addition, when the PEO/PIB ratio is itself varied for specific blend, the drop size will change, and this is expected to affect the morphology according to previous experimental results. Cold-mixing circumvents the previous direct mixing method so that: 1) very dilute PEO compositions (10-times lower than those used previously) can be examined without possible weighing errors; 2) the consistency of size of PEO drops can be kept from one sample to another.

Overall seven compositions were studied including the particle-free blend. For each blend, PEO to particle volumetric ratio (ϱ) varied from 0 to 0.32 and the particle loading was fixed at 20^{vol}%.

1.2.3 Sample preparation- Silica Surface Modification

For partially wetted particles studied in Chapter 3.0 and 4.0 , silane agents dichlorodimethylsilane (DCDMS) and octadecyltricholorosilane (OTS) are used to increase hydrophobicity of particle surface. The process of modification is similar to that used previously[40], although the final drying step is circumvented to avoid particle aggregation. For DCDMS modification, a gas stream with DCDMS vapor was fed into a tumbling vessel half-filled with particles for 60 minutes. This DCDMS modification was performed by Mr. Martin Echavarria, an undergraduate Chemical Engineering major at Pitt. For OTS modification, the silica particles are first heated up to 380℃ in the vacuum oven for 5 hours to remove the residual organic compound. Particles are then suspended in toluene, the silane is added, and allowed to stir at 99℃ for 7.5 to 13 hours to complete the silanization reaction. The particles are washed with reagent grade toluene 5 times before dried out in the hood. This OTS modification procedure was conducted by Ms. Yuening Wang, an undergraduate Chemistry major at Pitt.

SEM was performed on particle/PEO/PIB mixtures to verify that silanization makes the DCDMS-coated particles equally-wetted by the PEO and PIB, whereas the OTS makes them preferentially-wetted by the PIB (Figure 15).

The same "cold-mixing" method is used for sample preparation and is done by Ms. Nicole Heinichen. Overall eight compositions for each kind of the particle are selected ranging from 1^{vol}% to 30 ^{vol}% with a fixed PEO to particle volumetric ratio (ϱ) of 0.16 as is shown in the table below.

1.2.4 Sample preparation- Two step mixing

Two-step mixing method instead of cold-mixing was used in Chapter 4.0 . Different amount of PIB and PEO were first held inside the mixer at 80 ℃℃ for 15 minutes to ensure complete melting, then corresponding amount of particles were added and mixed at 600 RPM for 2 minutes. The mixed product was then immediately transferred into a sealed plastic dish, quenched in the refrigerator at about 10℃ for at least 30 minutes to solidify the PEO phase. This mixing process was performed by Mr. David Roell, an undergraduate Chemical Engineering major at Penn state university.

Sample stubs were prepared for SEM characterization. For samples with PIB as the continuous phase, a small quantity of sample is first transferred into a vial filled with n-octane, and held overnight to dissolve the PIB matrix. The residual sediment (network structure composed of particles and wetting fluid) is then collected and transferred onto a carbon-taped SEM stub with a piece of filter paper (Millipore, 0.1 μm pore size) attached, rinsed by octane several times. For samples with PEO as the continuous phase, a small bulk of sample was first cooled and fractured

in liquid nitrogen. the fractured surface was then washed several times with n-octane before placing on the sub. All SEM stubs with extraction were then left to dry, and coated with an Au/Pd sputtering target (Cressington) for 90 seconds at 40mA before sent into the SEM chamber.

1.2.5 Characterization

Rheological experiments were conducted on a TA Instruments AR-2000 stress-controlled rheometer (for composition study) and an Anton Paar rheometer MCR 302 (for deformation study). All the tests on PIB/PEO/silica system were carried out on a 25 mm parallel plate geometry profiled to prevent wall slip, at 80 degree to ensure melting. The geometry was pre-heated to 80 degree, then the sample was loaded within a gap of 1 mm. For steady state shear, measurements were carried out at shear rates ranging from $0.01s^{-1}$ to 100 s^{-1} with a maximum shearing time of 1 minute for each point. By fitting the results into modified Herschel-Bulkley equation, we are able to derive the yield stress for each blend as is discussed in Chapter 2.4. For dynamic oscillatory experiments, amplitude sweep tests (strain ranging from 0.005% up to 300% at 1 rad/s) were conducted to evaluate the viscoelastic behavior for each blend. Detailed results are also discussed in Chapter 2.4.

Effect of deformation history on rheology tests were mainly conducted on an Anton Paar rheometer MCR 302. Two deformation procedures were conducted and LAOS behavior for each sample were examined afterwards. For the first one, each sample was subjected to 1/s for 600 strain units, followed by an amplitude sweep at 1 rad/s up to a strain of 300%. Immediately following this, a second amplitude sweep was conducted, but with decreasing strain. For the second one, samples were sheared at three different rates, 0.1, 1, and 10/s. These rates span across the highest

rate in the oscillatory experiment (3/s s^{-1}corresponding to 300% strain). Each shear step was conducted for 10 minutes, followed by an amplitude sweep at 1 rad/s. The corresponding results are discussed in Chapter 2.4.3. In the same Chapter, creep-recovery tests on PIB/PEO/silica system were conducted at stresses lower than the yield stress estimated from previous steady shear measurements. Creep times were varied, whereas a fixed recovery time of 250 seconds was set.

Creep-recovery tests on LIR50/PEO/glass particle system were also conducted on the Anton Paar rheometer with a 40 mm parallel glass plate geometry and built *in in-situ* microscope at 20 ℃. The sample will be loaded within a gap of 200 μm. *In-situ* visualization will be carried out while the rheology tests are in progress. The video capture function is activated to simultaneously record the rheological parameters and corresponding optical image of localized microstructure. It is for the optimization of the image quality that we will use LIR-50/PEO/Glass system for the *in-situ* experiments at higher particle loading (>5 ^{vol} %). The light scattering from the particles can be reduced due to the near-perfect index match between glass particles and continuous polyisoprene phase as is shown in the example below. Preliminary tests on PIB/PEO/silica system showed in-situ visualization is only accessible under dilute conditions (particle loading less than 2 ^{vol} %, not shown here).

Oscillatory shear, steady state flow and creep-recovery tests will be conducted in order to test the viscoelasticity of ternary system. Detailed testing protocol is shown in Chapter1.0 5.3.2: the sample was first sheared at 480 Pa for 2 minutes in order to attain enough strain units to reach steady state flow condition. A 0.7-second step shear was applied at same stress level (480Pa) and ceased for 5 minutes to record the strain recovery. The creep-recovery process was repeated three times and the video recording starts from the end steady state flow toward the end of third recovery

to 1) capture the instantaneous elongated particle filled droplet morphology; 2) measure the time required for such structure to recover; 3) investigate the relaxation and aspect ratio dependence on stress and composition. Such testing protocol was conducted three time at different stress level (480Pa/240Pa/120Pa). The initial steady state shearing time varied for different stresses to ensure same strain units were applied before the following creep-recovery process (ie. 480Pa for 2 minutes and 240Pa for 4 minutes, etc). An oscillatory shear experiment was conducted right after the creeping, both storage and loss moduli were retrieved from a frequency sweep range of 0.05% to 300% at fixed strain amplitude of 1%. The modulus results along with the in-situ visualization can be used to determine whether the system is in pendular network state or capillary aggregate state. Limited steady state flow experiment were also conducted to measure the yield stress and infinite shear viscosity by increasing shear rate from 0.1/s to 100/s for selected compositions.

Aggregate structures were examined by SEM using ZEISS Sigma500 VP microscope and JEOL JSM6510 over a wide range of length scales. The sample stubs for SEM were made after solidifying the PEO by cooling and removal of PIB with octane. A small amount of sample was transferred into a vial filled with n-octane, and held overnight to dissolve the PIB matrix. The residual sediment (a composite structure comprising particles and PEO) was then collected, transferred onto a filter (Millipore, 0.1 μm pore size) stuck onto a carbon-taped SEM stub, and rinsed with octane several times, followed by metal coating using an Au/Pd sputtering target (Cressington) for 90 s at 40 mA.

2.0 COMPOSITION AND FLOW HISTORY DEPENDENCE OF YIELDING

2.1 CHAPTER FREFACE

Materials contained in this chapter were published as a research article in RSC Advancestitled "*Preparation and yielding behavior of pendular network suspensions*" in Journal of Rheology; figures used in this chapter have been reprinted with permission from: J. Rheol., 61 (2017) 217-228. (listed as reference 76 in the bibliography section).

List of Authors: Junyi Yang and Sachin S. Velankar

2.2 INTRODUCTION

In particulate systems, capillary forces can bind discrete particles together into a space-spanning network with a yield stress. The most familiar example is of sand, which when wetted with small amounts of water, develops sufficient yield stress to allow construction of elaborate sand castles[8-11]. The same is true for particles-in-liquid suspensions: addition of a small amount of a second immiscible liquid can create a network which endows the suspension with a yield stress[4-7, 12-17].

Such suspensions in which capillarity forces are important are practically useful in materials science. Specifically, the very simple method – "add liquid and mix" – of realizing a

yield stress offers a convenient way of stabilizing a structure temporarily before it can be made permanent e.g. by sintering or crosslinking[3]. Furthermore, open pore morphologies can be realized readily in such systems[16, 18-20] with immediate relevance to applications in which chemical transport or fluid retention must be combined with mechanical strength. Indeed applications to materials science are not restricted to suspensions with capillary forces – a diverse set of particle/fluid/liquid mixtures can, depending on the materials and composition, yield a variety morphologies of potential interest to materials science[3], including Pickering emulsions[15, 36], particle-stabilized foams[21-23], bijels[19, 24], wet granular materials[8, 25, 26] and liquid marbles[27, 28].

In such particulate systems with capillarity, the wettability of the particles towards the minority liquid plays a crucial role in determining the suspension microstructure[1, 3, 32]. The above-mentioned case of wet sand is, in this article, dubbed the *fully-wetting* situation, i.e. the particles are fully-wetted by the minority liquid, water. The case when the particles are less-favorably wetted by the minority fluid is dubbed the *partially-wetting* situation. This article is concerned with the former situation.

In a previous paper[5], we examined the morphology of suspensions in the fully-wetting situation. The suspensions were composed of two immiscible polymeric liquids and silica particles that were fully-wetted by one of the two liquids. Experiments showed that when the wetting liquid was present in a small minority (in that paper, 16^{vol} % of the particle loading), the morphology consisted of particles bound together by small menisci of the wetting liquid. At very low particle loadings, such meniscus binding led to the formation of open (i.e. not compact) aggregates denoted *pendular aggregates*. When the particle loading exceeded a few percent, aggregates were found to join together into a percolating network which was dubbed a *pendular network*. This terminology derives from the term *pendular meniscus* used to describe an hourglass-shaped meniscus joining

two particles[26, 33, 48], which is our idealized picture of the basic building block of a network at low wetting fluid loadings. Rheologically, pendular networks were found to behave analogous to other attractive suspensions: they show yield stress in steady shear, solid-like behavior and G'-G" crossover in LAOS, and delayed yielding in creep[5].

The goal of this article is to examine the rheology of pendular networks in greater detail, for example quantifying how the yield strain changes with the wetting liquid loading, whether the networks have significant elasticity (in the sense of elastic recoil), and whether rheological properties can be related to microstructural details of the pendular bridges. A significant part of this paper is devoted to the effect of shear history on the rheological properties. Specifically as will be discussed in Chapter 2.5, pendular menisci are associated with a certain attractive force, and furthermore the meniscus breaks when the inter-particle distance is sufficiently large. This raises an obvious question: can a high preshear rate or a high preshear strain disrupt the pendular network and induce softening? On the other hand, a meniscus may also be re-formed under applied flow as particles that already have wetting fluid on their surface come into contact with each other. This raises a second question: can changes in rheological properties be restored by sufficiently long flow? Or is flow-induced structural breakdown long-lived, and thus induce nearly-permanent changes in properties? Furthermore, since a pendular meniscus can be stretched to some extent without rupture, can this induce viscoelastic phenomena in the suspension such as elastic recovery after cessation of shear?

Incidentally, very similar questions have been addressed in another system with capillary forces, viz. droplet-matrix blends of immiscible fluids. In that case, flow induces both drop breakup and drop coalescence (analogous to breaking and reforming menisci). In those systems, shearing at high rate can reduce drop size and affect the rheology, but subsequent shearing at lower

rate can usually (but not always) restore the original drop size and rheological properties[29-31]. Furthermore, the increase in interfacial area due to applied flow provides a means of storing mechanical energy, and hence induces viscoelastic effects[43, 44, 47]. This article seeks to address similar questions for particulate systems with capillary forces.

This paper is structured as follows. Chapter 2.3 provides experimental details and Section III discusses the experiments. In the first part of Chapter 2.4, we develop and validate a new method for preparing our three-component mixtures along with a rationale for why this new method is preferred over the mixing procedures followed previously. In the latter section Chapter 2.4.2, we address the questions of the previous paragraph through rheological experiments. Chapter 2.5 comments on the results in the context of the micromechanics of meniscus rupture, followed by Conclusions.

2.3 EXPERIMENTAL SECTION

2.3.1 Materials and sample preparation

Polyisobutylene (PIB, $\rho \approx 0.908$ g/ml, $Mw \approx 2{,}200$ g/mol) and polyethylene oxide (PEO, $\rho \approx 1.1$ g/ml, $Mw \approx 20{,}000$ g/mol, melting point $\approx$ 65℃) was purchased from Soltex and Fluka respectively. Spherical silica particles (diameter roughly 2μm) were purchased from Industrial Powders. All experimental materials are identical to those used previously[4-6]. As shown previously[4, 5], the particle surfaces are fully wetted by PEO, which is the minority phase in the mixtures examined here.

A small quantity of PIB and PEO were mixed together to make a concentrated "masterbatch" using a custom ball mixer[40]. 80 ^{wt}% of PIB and 20 ^{wt}% of PEO were held inside the mixer at 80℃ for 15 minutes to ensure complete melting, and then mixed at 500 RPM for 5 minutes. The mixed product was then transferred into a sealed plastic dish, kept in the refrigerator at about 10℃ for at least 30 minutes to complete crystallization of the PEO. The masterbatch blend has a PEO-in-PIB morphology, and after dissolving the PIB, the residual PEO drops are seen to be roughly 5μm in diameter (Figure 3).

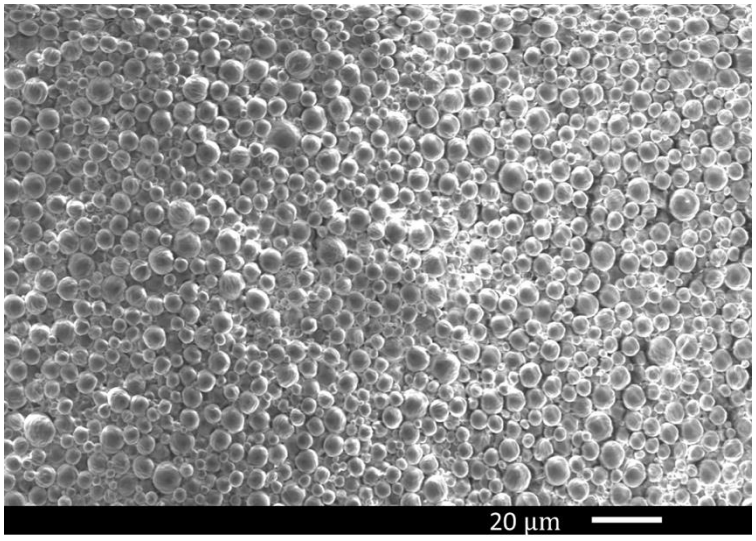

Figure 3. SEM image of solidified PEO dispersed phase extracted from the "masterbatch".

Ternary samples of the desired composition were prepared by blending appropriate quantities of this "masterbatch", pure PIB, and particles. This blending was performed by hand with a spatula in a 40 mm petri dish at room temperature. Samples were placed in vacuum overnight to degas. This mixing procedure is different than that used previously[5] and the reasons for this will be discussed in Chapter 2.4.

2.3.2 Rheolometer

Rheological experiments were conducted on a TA Instruments AR-2000 stress-controlled rheometer as well as Anton Paar rheometer MCR 302. All the experiments were carried out on a 25 mm parallel plate geometry profiled to prevent wall slip, at 80 ℃ to ensure that PEO was well above its melting temperature. The geometry was pre-heated to 80℃, the sample loaded, and set to a gap of no more than 1 mm.

Both continuous and oscillatory shear flow properties were measured. For continuous shear, steady shear measurements were conducted at shear rates ranging from $0.01s^{-1}$ to 100 s^{-1}. Each shear rate was maintained until deviation in torque was less than 3% for 1 minute. Creep-recovery tests were done at stresses lower than the yield stress estimated from steady shear measurements. Creep times were varied (discussed later) whereas a fixed recovery time of 250 seconds was set. For oscillatory experiments, amplitude sweep tests (strain ranging from 0.005% up to 300% at 1 rad/s) were conducted.

The compositions selected here are firmly in the regime in which pendular aggregates are expected, and hence morphological characterization is not the focus here. A limited amount of optical and electron microscopy was conducted using methods established previously.

These show that the samples have the expected structure of pendular aggregates, viz. particles that are connected by small menisci of the PEO. A typical example of the morphology is shown in Figure 34 in the Appendix A.

2.4 RESULTS

2.4.1 Validation of the "cold mixing"

Our previous research[4] considered ternary mixtures using the same constituents as the present paper with a composition of 10 [vol] % particles and 2.8 [vol] % PEO. Various mixing methods were considered including premixing the particles into the PIB before adding the PEO or vice versa (predisperse the PEO before adding particles). Different combinations of mixing speed were also used. In all cases, the temperature during the mixing was 80 ℃, and hence the PEO was molten when it was mixed. In general, two types of structures were evident: a network of particles bound by menisci of PEO, and large PEO-bound particle aggregates, called *capillary aggregates*. For convenience, examples of both structures, taken from that article[4], are shown in Figure 34. That article suggested that capillary aggregates were a "trapped state" which could not be broken up easily under mixing conditions. Achieving predominantly pendular networks required avoiding the formation of capillary aggregates in the first place, e.g. by pre-dispersing the wetting fluid PEO (preferably at a size smaller than of the particles) prior to adding particles.

Despite success in avoiding capillary aggregates, the previous methods still have some limitations. The first is that research on wet granular materials suggests that even extremely small quantities of wetting fluid (as low as 0.01 [vol] %) can affect the flow behavior[9]. Previously [5] we conducted experiments with wetting fluids volume fractions as low as $\phi_{PEO} =$ and found that pendular aggregation already had a major effect on rheological properties. For a ~4-gram batch, this volume fraction corresponds to only 8 mg of wetting fluid. Apart from possible errors in weighing such small quantities, it is also possible that some of the wetting fluid may be "lost" if it

wets the internal parts of the mixer, making the actual mixture composition different from the target value. Accordingly, volume fractions of wetting fluid lower than 0.16% were not examined. Second, the previous experiments showed that the size of the drops immediately prior to adding particles is an important parameter affecting the morphology development, with a small drop size reducing the formation of capillary aggregates. But when the PEO/PIB ratio is itself varied, the drop size may change, and this may be expected to affect the morphology. Finally, reproducing the same morphology using a different mixer, e.g. one with a larger capacity, is difficult, once again because different mixing characteristics are likely to create different drop sizes prior to adding particles.

The mixing process considered here, dubbed "cold mixing" is intended to circumvent these problems. Analogous to one of our previous mixing processes, the PEO is pre-dispersed as drops in the PIB, but then the blend masterbatch is cooled to solidify the PEO drops (shown in Figure 3). Particles are then mixed with this masterbatch at room temperature (along with additional PIB as needed). The sample is then heated in a rheometer to remelt the PEO drops, and then sheared to induce meniscus-bridging of particles. This cold mixing method offers several advantages. First, since samples in the pendular regime require very little PEO, a single PEO/PIB masterbatch is adequate to prepare a large number of ternary samples. Since the size of the frozen drops does not change during the room-temperature mixing step, all the ternary samples have identical drop size distributions across all samples. Second, the masterbatch can be diluted repeatedly to realize very low wetting fluid loadings without significant weighing errors, and moreover, since the PEO is solid until the sample is loaded in the rheometer, it cannot be lost by wetting parts of the mixer (the mixing dish and spatula in our case).

Finally, the first task of this paper therefore is to validate this cold mixing method as a means of preparing pendular morphologies.

Figure 4 validates this cold mixing approach. It compares the oscillatory behavior in amplitude sweep experiments for one specific blend with 20 ^{vol}% particles and 3.2 ^{vol}% PEO before melting vs after melting and shearing. The oscillatory behavior of the cold-mixed sample at 30°C ('-' symbols with thick curves) suggests liquid-like behavior with $G" \gg G'$ over the entire strain range. Such behavior is consistent with that expected for a suspension with a dispersed phase loading of 23.2 ^{vol} %. Note that the silica particles as well as the solidified PEO drops are both more polar than the PIB matrix, and this suspension is expected to behave not like a hard-sphere suspension but like a suspension of attractive particles. Indeed Figure 35 shows that under steady shear conditions at 30°C, this blend is somewhat shear-thinning, likely reflecting the influence of attractive interactions.

The sample was then melted, and sheared at 1 s^{-1} for 10 minutes. Upon repeating the amplitude sweep, a sharp change in rheology is apparent in Figure 7: $G'' < G'$ at low strain, followed by a crossover at intermediate strain. Such behavior is qualitatively similar to that observed in our previous research at the same composition, and was attributed to the formation of a pendular network (i.e. with pendular menisci bridging the particles), and the strain crossover was interpreted in terms of the microstructural breakdown of these menisci. This will be discussed further later. Subsequent to the amplitude sweep, the steady shear viscosity was measured at several different rates, and once again, the behavior (Figure 35) is qualitatively different from the unmelted sample: the sample shows yield-stress rheology (viscosity roughly follows $\dot{\gamma}^{-1}$) similar to that obtained from pendular networks previously[5].

Figure 4 and Figure 35 also show the behavior of a particles-in-PIB mixture without any PEO added at 80℃, and this suspension is liquid-like, not surprising for a suspension at 20 ^{vol} % particles. Thus, as previously, we firmly conclude that the strongly non-Newtonian behavior is attributable to capillary forces between particles.

In a later section of this paper, we will show that deformation history affects LAOS behavior significantly. Anticipating that, it is immediately relevant to ask whether the measured rheology changed if the sample was sheared for a longer duration. Accordingly Figure 4 shows two additional LAOS experiments, each conducted with an additional 600 strain units of shear at the same shear rate of 1 s^{-1}. These show negligible differences in moduli as compared to the first shearing step suggesting that sufficiently long shearing can establish a steady state rheology, at least under the conditions of Figure 4.

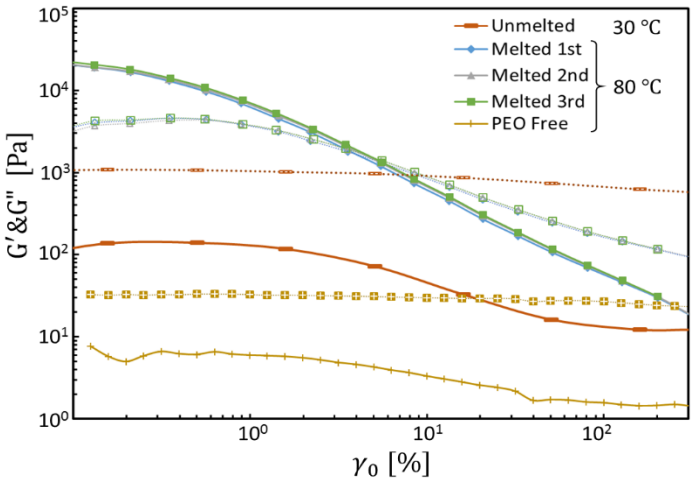

Figure 4. LAOS results for ternary mixture (PIB/PEO/silica =76.8/3.2/20) before and after melting and shearing, and binary suspension (PIB/silica = 76.8/23.2). Filled symbols with solid lines represent the storage modulus and open symbols with dashed lines represent the loss modulus.

2.4.2 Rheological changes with wetting fluid content

The cold-mixing approach can now be applied to examine the effect of wetting fluid content on the rheology. Previously we had shown that the rheological properties are non-monotonic in wetting fluid loading: at very low wetting fluid loadings, the formation of a pendular network leads to the rheological changes detailed in Figure 4 and Figure 35. But once the wetting fluid volume fraction became comparable to the particle fraction, the wetting fluid encapsulated the particles leading to a destruction of the pendular morphology, and the solid-like rheology diminished.

The corresponding results are best-represented in terms of the wetting fluid to particle volume ratio: samples with ϱ of about 0.1 to 0.3 had a roughly pendular structure whereas in samples with ϱ exceeding 1, the particles were engulfed by the wetting fluid, and had a diminished yield stress.

We seek to repeat those experiments for two reasons. First, as mentioned in the Introduction, preparing samples by direct mixing of the three components sometimes involved very small quantities of wetting fluid, with consequent uncertainty in composition. Second, more important, even the lowest wetting fluid loading that could be examined previously already showed a measurable yield stress. Thus we were not able to capture the transition between liquid and solid as fluid loading is increased. For instance, we could not establish whether there is a minimum amount of wetting fluid needed for developing a yield stress, or equivalently, if the yield stress appears gradually or abruptly as wetting fluid content changes. As mentioned above, one advantage of the cold mixing approach is that since mixing is performed when the PEO droplets are frozen, low wetting fluid loadings can be realized by sequential dilution. Accordingly, we examined the rheology of 20 ^{vol} % silica suspensions with PEO loadings varying from $\phi_{PEO} =$

$0.08\%\ to\ 6.4\%$. These results are shown in Figure 5. The numbers in the legend correspond to the value of ϱ, but since the particle loading is fixed at 20 [vol] %, the ϕ_{PEO} values are simply 0.2* ϱ.

In the absence of PEO, the particles-in-PIB suspension show strain sweep behavior similar to that of the unmelted sample in Figure 4: liquid-like rheology with $G" \gg G'$ over the entire strain range. Addition of wetting fluid at a loading $\phi_{PEO} = 0.08\%$ (which corresponds to $\varrho = 0.004$) has only a slight effect on the moduli. The next higher wetting fluid loading, corresponding to $\varrho = 0.016$ already shows all the features of the pendular network that were evident in Figure 4: much higher moduli, $G' > G"$ at low frequencies, and then a moduli crossover at some strain. Further increase in wetting fluid loading does not change the behavior qualitatively but the quantitatively, the moduli increase considerably up to $\varrho = 0.25$, followed by a modest decrease.

In steady shear (Figure 5b), the effects of PEO are felt even at the lowest PEO loading where the low-rate viscosity rises significantly at $\varrho = 0.004$. Upon further addition of PEO, the low-rate data show a clear yield stress, whereas there is only a modest change in stress at the highest shear rates accessible, and the stress vs strain rate data approach a slope of 1. These results suggest that significant solid-like behavior appears between 0.08% and 0.32% corresponding to $\varrho = 0.004$ and 0.016. It is difficult to reliably measure the value of yield stress at very low wetting fluid loadings within the maximum steady state shear maintaining time of 1 minute. Hence it is difficult to establish a percolation threshold above which a space-spanning network exists. Indeed there does not appear to be any wetting fluid loading at which the yield stress increases abruptly.

To quantify the yield stress in a consistent fashion across all samples, the data of Figure 5b were fitted to the modified Herschel Bulkley equation $\sigma = \sigma_y + k * \dot{\gamma}^n + \eta_\infty * \dot{\gamma}$, where σ_y represent the yield stress and η_∞ is a constant value measured from pure suspension at highest rate accessible. [49] The first two terms describe the stress-rate behavior at low rate regime and the third term mainly describe the higher rate regime. The solid lines in Figure 5b show the fits, and the corresponding values of the three fitting parameters σ_y, k and n are given in Table 1. The fitted yield stress (Figure 8a) increases almost linearly at low ϕ_{PEO} values, followed by a decrease in yield stress when ϱ exceeds 0.16 (i.e. ϕ_{PEO} exceeds 3.2 %). It must be noted that the yield stress obtained at the lowest ϱ value may not be entirely accurate since those stress vs rate data do not show a clear plateau at low rates. Furthermore, the lowest 2-3 points in Figure 5b may not have reached steady shear conditions due to the low shear strain corresponding to the 1 minute shearing time. It is useful to compare the results against those obtained previously[5]. The first comparison is against the yield stress measured at same composition, but prepared by the previous mixing method in which the PEO drops were molten during mixing. That case gave a somewhat higher yield stress (green triangle). The second is a series of ternary mixtures at 10 ^{vol} % particles, but spanning roughly the same range of ϱ values. The corresponding yield stresses (shown by the red squares in Figure 8a) are qualitatively similar, and in particular, at both 10 ^{vol} % and 20 ^{vol} % particles, samples approximately show the $\sigma_y \propto \phi_{PEO} \propto \varrho$ at low wetting fluid loadings and then a maximum yield stress when ϱ is on the order of 0.1.

Table 1. Summary of fitting parameters used in Modified Herschel-Bulkley equation:

$\sigma = \sigma_y + k * \dot{\gamma}^n + \eta_\infty * \dot{\gamma}$ for various ϱ values.

ϱ	k [SI units]	n	σ_y σ_y [Pa]
0.004	11.1	0.552	6.70
0.016	20.2	0.448	27.3
0.04	64.2	0.443	55.1
0.16	78.5	0.485	220.7
0.25	85.7	0.478	169.0
0.32	72.6	0.552	134.3

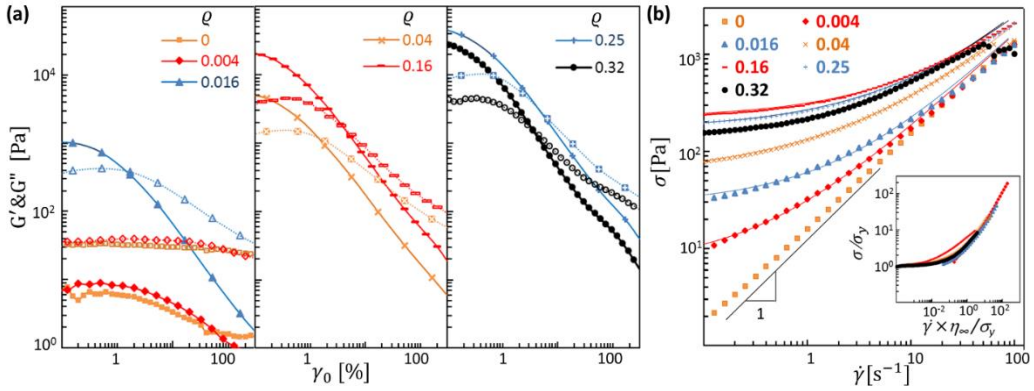

Figure 5. (a) LAOS results for ternary mixtures at fixed particle loading (20 [vol] %) and various PEO loadings. The ϱ values are listed in the legend. Filled symbols with solid lines represent the storage modulus and open symbols with dashed lines represent the loss modulus; (b) Stress versus shear rate curves. Continuous lines represent the best fit for each composition using the modified Herschel-Bulkley equation. The inset shows dimensionless plot for the same data.

Finally, we'd previously suggested a two-parameter scaling of the flow curve. Specifically we proposed scaling the steady shear data as follows: (1) normalize the shear stress by the yield stress σ_y, (2) the viscosity by the limiting high shear rate viscosity η_∞ ($12.63Pa*s$) for pure suspension at high shear rates, and (3) as a consequence, normalize the shear rate by the characteristic rate σ_y/η_∞. This scaling is suggested by drawing an analogy between suspensions in a pendular state and suspensions with attractive interactions between particles[5, 50]. At sufficiently low shear rates viscous forces are negligible, and hence the stress (which approaches the yield stress) embodies the attractive forces between particles. At sufficiently high rates viscous forces dominate, and hence the stress must simply represent the hard-sphere type contribution of the particles. In this physical picture, just two parameters – the yield stress that represents interparticle attractions, and the high-shear rate viscosity that represents viscous interactions between particles – suffice to scale all the steady shear behavior. Here we test whether the scaling applies as the PEO loading (rather than the particle loading) is varied. Since all the samples of Figure 7 have the same particle loading (20 ^{vol} %), they must necessarily have the same value of η_∞, and indeed we remarked above that the high-shear rate stress is only weakly sensitive to wetting fluid loading. Thus the only "shift" permissible is to normalize the stress using the yield stress. Figure 6b shows the results. With no further adjustable parameters (since σ_y was already determined in Figure 6a) a reasonable superposition of the various flow curves is obtained. The same scaling is shown in the form of a normalized stress vs normalized rate graph as an inset in Figure 7b. This confirms the validity of treating the flow curve of pendular suspensions as being an "interpolation" between a low rate regime dominated by capillary attractions, and a high rate

regime dominated by hard sphere suspension hydrodynamics. We must reiterate that at $\varrho = 0.004$, the flow curve is only weakly non-Newtonian (Figure 7b) and therefore the corresponding value of yield stress is susceptible to some error.

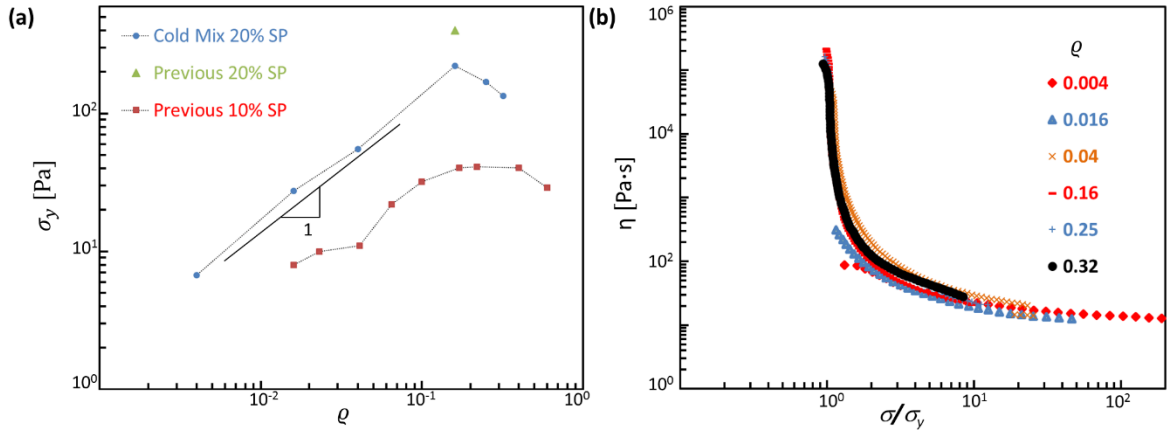

Figure 6. (a) Yield stresses corresponding to Fig. 3b compared with previous results. (b) Viscosity versus normalized shear rate curves for various ϱ values.

2.4.3 Dependence of flow conditions on microstructure

As explained in the Introduction, since such ternary blends are far from equilibrium, their microstructure can depend significantly on their deformation history. Above we already mentioned that adding the PEO after the particles led to formation of numerous capillary aggregates, whereas pre-dispersing the PEO before adding the particles gave a pendular structure with an almost complete absence of capillary aggregates. That same article[4] reported that different mixing approaches gave as much as a three-fold difference in yield stress. At least some of the difference

was attributable to formation of capillary aggregates which, being very compact, do not contribute much to the modulus. Some of the difference might also reflect more subtle differences in microstructure such as the number of pendular bridges per unit volume or average number of bridges per particle. Regardless, since the microstructure depends on mixing conditions, it is not surprising that the rheology does too. The cold mixing approach now provides a more consistent method of preparing samples across a range of compositions, and thus permits the effect of deformation history on rheology to be examined. We are chiefly concerned with three questions, all of which arise from the physical picture of particles held together by pendular menisci. The first concerns strain rate effects: we anticipate that capillary menisci are ruptured at high stress (indeed this is equivalent to regarding η_∞ as being independent of capillary attractions between particles as discussed in Chapter 2.4.2). Does this rupture also lead to softening, i.e. to a decrease in modulus? Indeed Koos and Willenbacher[51] measured the linear viscoelastic moduli after a high rate shearing and noted a gradual increase with time, suggesting some structural breakdown due to high rate shear, and subsequent recovery. The second concerns strain effects: we anticipate that capillary menisci rupture when deformed sufficiently. Does such large strain-induced meniscus rupture lead to softening as well? The third concerns elasticity (in the sense of recoverable deformation): since individual capillary menisci can be stretched (few ten percent as discussed in Section IV), can pendular networks show few ten percent recoverable strain after cessation of shear?

We will first illustrate the changes in rheology with deformation history with a simple shear protocol. A sample of the same composition of Figure 4 (PIB/PEO/silica=76.8/3.2/20) was subjected to 1/s shear for 600 strain units, followed by an amplitude sweep at 1 rad/s up to a strain of 300%. Immediately following this, a second amplitude sweep was conducted, but with

decreasing strain. A sharp decrease in low-amplitude modulus is evident (Figure 7a), presumably indicating some breakdown in the structure of the particulate network. This simple experiment shows clearly that shear history can – even within a single sample – induce moduli changes of as much as a factor of five. Yet this figure does not unambiguously identify whether the softening is a rate effect or a strain effect. In an oscillatory experiment at a strain amplitude γ_0 and frequency ω, the peak strain rate is $\gamma_0\omega$. Thus, an amplitude sweep at fixed frequency exposes samples to increasing strains as well as increasing rates.

To test the rate dependence more directly, we examined the LAOS behavior of the same composition of Figure 4 (PIB/PEO/silica =76.8/3.2/20) after shearing at three different rates, 0.1, 1, and 10/s. These rates span across the highest rate in the oscillatory experiment (3/s corresponding to 300% strain at 1 rad/s). Each shear step was conducted for 10 minutes, followed by an amplitude sweep at 1 rad/s. The results (Figure 7b) unambiguously show a significant softening: the low strain modulus decreases by almost three-fold after shearing the sample at 10/s. These changes in rheology were found to be completely reversible: upon shearing at 1/s for 10 minutes, the LAOS data overlaid almost exactly onto the 1/s results shown in Figure 9b. To our knowledge, these are the first data to show that the mechanical properties of suspensions with capillary interactions can be tuned reversibly by simply varying the shear rate imposed on the suspension. These experiments were performed for samples with various PEO fractions (all at 20^{vol} % particles), and in all cases, LAOS data were collected after three different preshear rates. The dependence of the corresponding linear viscoelastic modulus on ϱ after the three different rates is shown in Figure 36. All samples behave similarly (modulus reduces as preshear rate increases), but the decrease in modulus is more pronounced at low ϱ values. We speculate that this

is because the capillary network becomes increasing tenuous at low ϱ values, and can be destroyed readily by shearing. Incidentally it is interesting to note that the trend of Figure 36 – that the modulus becomes more dependent on rate at low ϱ - cannot continue to arbitrarily low wetting fluid loadings. This is because at $\varrho = 0$, capillary interactions must vanish and the rate dependence should disappear (as indeed it does experimentally, not shown).

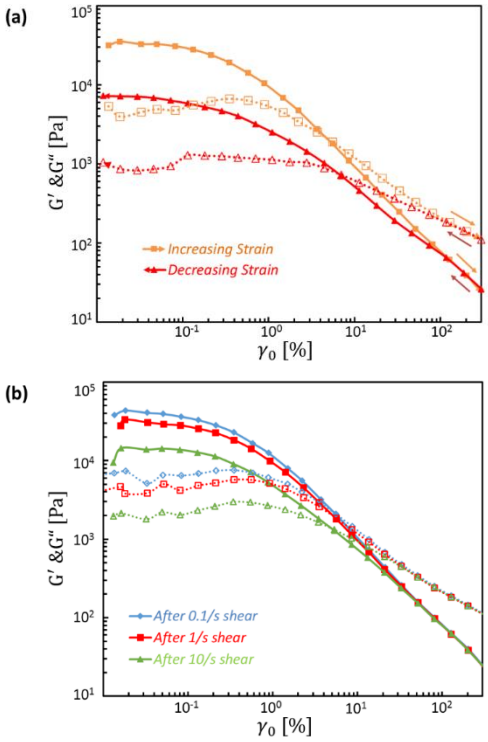

Figure 7. (a) LAOS results for ternary mixture (PIB/PEO/silica=76.8/3.2/20) where yellow squares indicate increasing strain and red triangles indicate decreasing strain. (b) LAOS results for ternary mixture after shearing at various rates indicated. Filled symbols with solid lines represent the storage modulus and open symbols with dashed lines represent the loss modulus.

It is also plausible that the capillary network may be broken by strain rather than by strain rate. Specifically, the process of breaking vs remaking a pendular meniscus is hysteretic (see Chapter 2.5) and hence we examined whether a modest strain imposed on a network that was created under steady shear conditions is itself disruptive. To test the strain dependence independent of rate effects, the following shear protocol (illustrated in the upper part of Figure 8) was used. A sample with $\phi_p = 20\%$ and $\varrho = 0.16$ was sheared at $1\ s^{-1}$ for 600 strain units. Shearing was paused, then resumed at the same shear rate for 1 strain unit, and then the oscillatory moduli measured. The entire process was repeated but with the latter strain being increased to 3, 60, and finally another 600 strain units. The corresponding data are shown in Figure 8, and it is clear that while strains of about 1 strain unit do indeed reduce the modulus as compared to much longer strains *at the same rate*, these modulus variations are modest, and much smaller than those in Figure 7. These observations suggest that while some menisci may be broken at large shear strain, new menisci are simultaneously formed, leading to little or no change in the overall network structure.

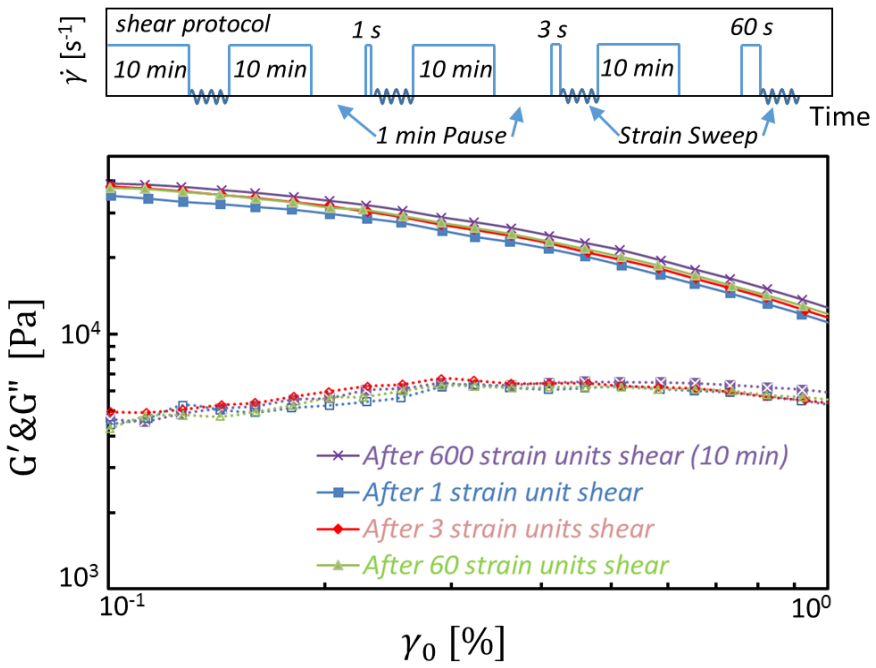

Figure 8. LAOS results for ternary mixture (PIB/PEO/silica=76.8/3.2/20) following the shear protocol sketched above. Filled symbols with solid lines represent the storage modulus and open symbols with dashed lines represent the loss modulus.

It is of immediate interest to ask whether such changes in modulus noted in Figure 7 can be related to underlying changes in microstructure. Previously we have used scanning electron microscopy (SEM) of samples in which the continuous phase was dissolved to qualitatively identify the microstructure (e.g. pendular vs capillary aggregates). However that approach is not suitable for testing for more subtle changes in network microstructure since the aggregates tend to undergo at least some damage when preparing samples for SEM. Here we attempted a different approach. Small samples of blends with 20 ^{vol}% particles were extracted from the rheometer (from near the edge of the parallel plate geometry) after shearing at $0.1\ s^{-1}$ and $10\ s^{-1}$ shearing, and placed in a polystyrene dish. These samples were too concentrated to permit any judgement on

whether structural breakdown occurred. A large drop of PIB was then placed on each sample in an attempt to gently to spread out the aggregates, and hence improve the images. This was unsuccessful: neither of the samples could be spread significantly, i.e. after both $0.1\ s^{-1}$ and $10\ s^{-1}$, the yield stress of the samples with 20 ^{vol} % particles was too high. This experiment was then repeated at a much lower particle loading of 3^{vol} %, while maintaining the same PEO/PIB ratio ($\varrho = 0.16$). Here the results proved clearer: the sample sheared at higher shear rate spread significantly, and discrete clusters can be readily identified by optical microscopy (Figure 9). In contrast, the sample sheared at the lower rate did not spread significantly suggesting a larger yield stress, presumably due to larger interconnected clusters. Thus we tentatively conclude that high rate shearing induces breakdown of capillary menisci, thus reducing the connectivity of the network. The shear thinning as noted in Figure 5 (at fixed particle loading) or previously (at fixed ϱ)[5] may be attributed to this decrease in network connectivity. Confirming this tentative conclusion requires *in situ* visualization[52]. The present experimental system is ill-suited for *in situ* visualization: the large refractive index mismatch between the particles and the continuous phase makes it impossible to image samples with 20 ^{vol} % particles. However we conducted experiments on an analogous system comprising glass particles, 1,4-polyisoprene as the continuous phase, and glycerol as the wetting fluid. Due to a near-perfect index match between the glass and polyisoprene, the particles are nearly invisible, and excellent images are obtained at 4.5 ^{vol} % particles. Those experiments (Figure 38 in the Appendix A) show beyond doubt that meniscus-bound aggregates do break down at high rates, and moreover, they readily form within a few strain units when sheared at low rate.

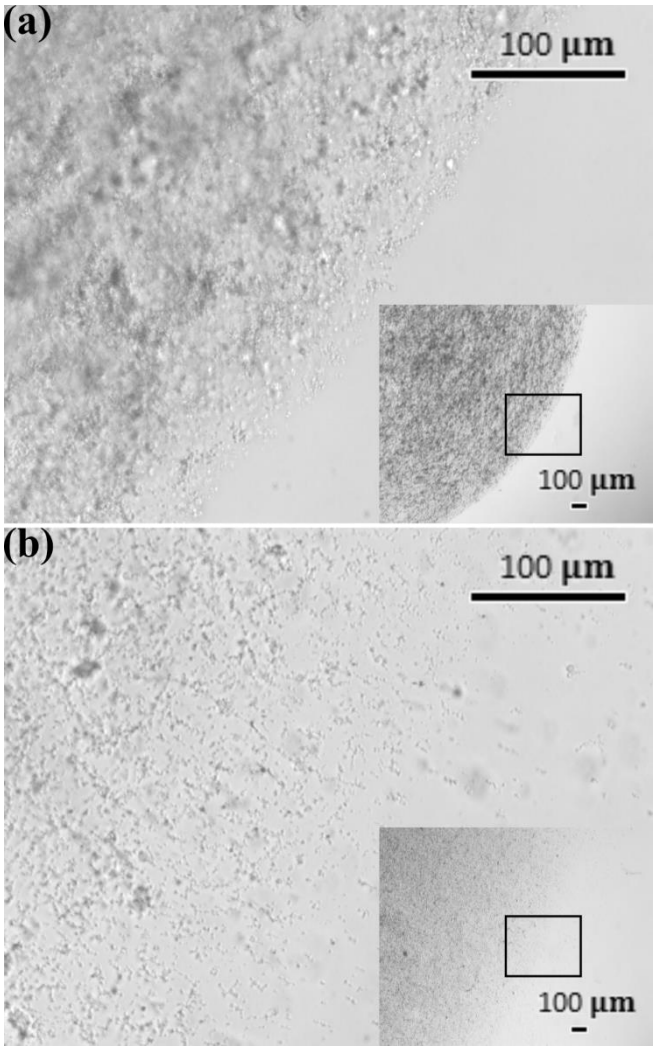

Figure 9. Optical microscope showing ternary mixture (PIB/PEO/silica=96.52/0.48/3) spread on a petri dish: (a) after 0.1/s shearing for 10 minutes; (b) after 10/s shearing for 10 minutes. The insets show the same sample with lower magnification.

The third question above – how much strain pendular networks can withstand without undergoing irreversible deformation – was addressed by creep-recovery experiments. A sample of the same composition as Figure 4 (PIB/PEO/silica=76.8/3.2/20) was subjected to creep at a stress of either 100 Pa or 150 Pa. Two stresses were needed to cover both "elastic" and "plastic" regimes of deformation (explained in the next paragraph), but note that both these stresses are lower than

the yield stress measured in steady shear experiments (Figure 6a and Table 1) for this same sample. The creep was interrupted at a small strain, following which recovery was monitored. This was repeated at several different creep times. In between each creep step, the sample was "reset" by shearing at 1/s for 600 strain units. These results are shown in Figure 10a.

The creep process (if not interrupted) comprises a rapid deformation to about 0.6% strain, followed by a slow increase in strain, as may be expected at a stress below the yield stress. Once interrupted, a portion of the strain recovered rapidly, followed by a slower recovery over several seconds. The ultimate recovery obtained from this experiment is shown in Figure 10b. If the applied strain is less than roughly 0.6%, almost all the strain can be recovered, i.e. the sample behaves elastically. Such elastic behavior is evident when the creep time is sufficiently small at 100 Pa strain. However for larger strains, the ultimate recovery remains fixed, i.e. deformation in excess of ~0.6% is almost purely plastic. These correspond to the longer duration creeps at 100 Pa, and all the cases at 150 Pa stress. Similar results were obtained at other compositions, and two such examples ($\varrho = 0.04$ and $\varrho = 0.25$) are shown in Figure 37 respectively.

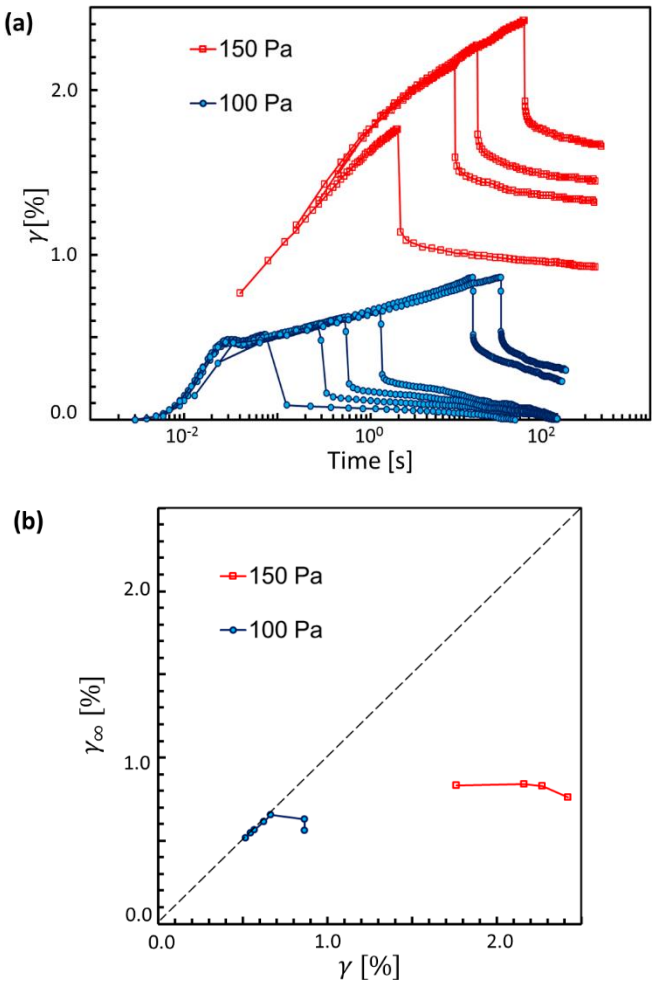

Figure 10. (a) Creep-recovery test results for ternary mixture (PIB/PEO/silica=76.8/3.2/20) at two stresses both below its yield stress. (b) Ultimate recovery strain (γ_∞) versus strain applied during creep (γ).

Plastic deformation is generally associated with irreversible microstructural changes. On the other hand, a glance at LAOS data such as Figure 4 or Figure 7a, shows that the modulus at 0.6% oscillatory strain is already less than half of its value at small-strain. This suggests that reversible strain softening occurs prior to plastic deformation. In order to verify this, one last experiment was conducted.

Samples were presheared at 1/s for 10 minutes, and then subjected to oscillatory amplitude sweep tests where the upper limit of the amplitude was increased in each successive step. For instance, in Figure 11, the first amplitude sweep ranged from 0.01% to 0.1% strain, the second from 0.01% to 1% strain, etc. It is clear that the modulus vs strain data remain reproducible at least up to 1% strain, a strain at which the modulus has reduced to less than half its low strain value. This confirms that significant modulus softening can occur reversibly, i.e. prior to irreversible decrease in modulus (see also [53] for further comments on this).

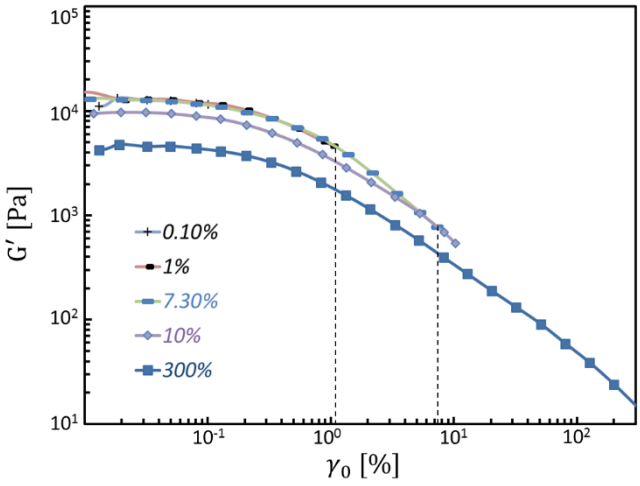

Figure 11. LAOS results of ternary mixture (PIB/PEO/silica=76.8/3.2/20) with sequentially increasing upper strain limit. Only storage modulus is shown.

Figure 12 now summarizes various strains that characterize the LAOS rheology: the limit of linearity ($\gamma_{critical}$) at which the G' reduces 10% from the value at the lowest strain accessible, the strain γ_{peak} at which the G" shows a maximum, and the strain γ_{fluid} at which the G' and G"

cross. Two of these strain measures increase gradually with PEO content, whereas γ_{peak} decreases slightly. We note that γ_{fluid} disappears at low PEO content since there is no crossover (G'<G" throughout the amplitude range). Furthermore, the sample with $\varrho = 0.004$ shows a weak peak in G" and hence the corresponding value of γ_{peak} is less reliable. At least one other article also mentions that the limit of linear viscoelasticity in LAOS experiments is only about 0.1%, although their crossover strains were larger[54]. Finally, above we also quantified two other measures of yielding: the strain at which irreversible changes in the linear viscoelastic modulus appear, and γ_∞, the recoverable strain. Both these are on the order of 1%, and both increase slightly with wetting fluid content.

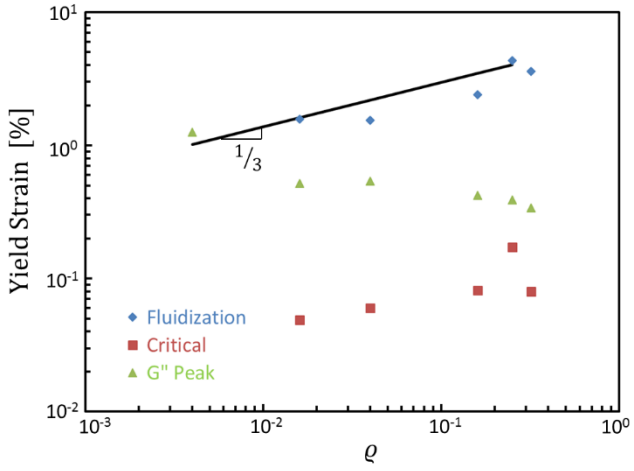

Figure 12. Summary of various measures of yield strains: γ_{fluid} (blue diamond), $\gamma_{critical}$ (red square) and γ_{peak} (green triangle). Solid line with a slope of 1/3 represents Eq. 4, but shifted down by a factor of 10.

2.5 DISCUSSION

Our microstructural picture of the suspensions in this study is of aggregates of particles held together by capillary forces, with the aggregates themselves percolating to form a network. In an ideal pendular network, all capillary interactions are strictly pairwise, i.e. each meniscus bridges exactly two particles, and there is no coalescence of menisci. The actual aggregates are not strictly pendular (indeed with polydisperse systems, multiple particles sharing a meniscus is highly likely). Nevertheless, as a first approximation, we will consider the mechanics of pendular networks for the idealized case of pendular menisci, monodisperse particles, and monodisperse menisci. With these assumptions, a "volume balance" readily yields[7]:

$$V_{meniscus} = \frac{8}{3z}\pi {R_p}^3 \frac{\phi_{PEO}}{\phi_p} \tag{2}$$

where the value of z is the coordination number representing the average number of menisci per particle ($z = 4$ will be adopted below), R_p is radius of the particles. One can therefore use Eq. 2 to estimate the mean meniscus volume from the composition of the ternary mixture. This meniscus induces an attractive force between the particles given by[33]:

$$F^* = \frac{\cos\theta}{1 + 2.1\left(\frac{S^*}{\sqrt{V^*}}\right) + 10.0\left(\frac{S^*}{\sqrt{V^*}}\right)^2} \quad for \quad V^* < 10^{-5} \tag{3}$$

or

$$\ln F^* = f_1 - f_2 \exp\left(f_3 ln\frac{S^*}{\sqrt{V^*}} + f_4\left(ln\frac{S^*}{\sqrt{V^*}}\right)^2\right) \quad for \ 10^{-5} < V^* < 0.1 \tag{4}$$

where the $f_j's$ are dimensionless variables depend on V^* and liquid-solid contact angle θ [33]. For the sample compositions examined here, V^* larger than 10^{-5} and hence only Eq. 4 is needed. In both these above expressions, $S^* = \frac{S}{R_p}$ is a dimensionless half-separation (i.e. $2S$ is the separation between the particle surfaces), $V^* = \frac{V_{meniscus}}{{R_p}^3}$ is a non-dimensional meniscus volume (which can be estimated from Eq. 2), and $F^* = \frac{F}{2\pi R_p \alpha}$ is the non-dimensional force. Note that F^* approaches 1 at small separations in Eq. 3. Beyond a certain separation, the meniscus ruptures, and the force jumps to zero. Previous results [55] show that the dimensionless half-separation for rupture is:

$$S_c^* = \frac{1}{2}(V^*)^{1/3} = \frac{1}{2}\left(\frac{8}{3z}\pi\frac{\phi_{PEO}}{\phi_p}\right)^{1/3} \quad (5)$$

where the latter equality is obtained from substituting from Eq. 2. The forces calculated from Eq. 4 (with Eq. 5 serving as the cut-off distance for meniscus rupture) are plotted in Figure 13 for a variety of sample compositions. Several comments can be made based on this idealized model.

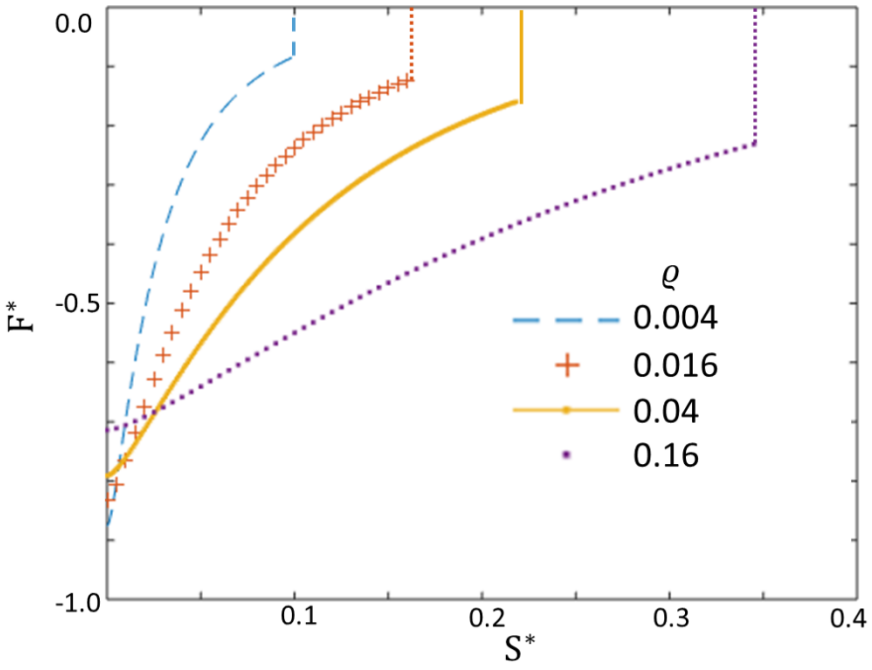

Figure 13. Normalized pair-wise capillary bridge attraction force as a function of dimensional separation distance for various ϱ values.

First, it is immediately tempting to ascribe rheological changes to breaking of the pendular menisci connecting the particles. For example, it is reasonable to expect that as the pendular network is sheared starting from quiescent conditions, irreversible changes appear when the particle separation exceeds that given by Eq. 5. This immediately suggests that if the deformation is affine, the breakdown strain should be roughly equal to S_c^*, and hence must scale as $\varrho^{1/3}$. Figure 12 shows that this scaling is approximately correct for all three measures of breakdown strain, although admittedly, the number of data points is small.

We emphasize that this prediction presumes that z is independent of wetting fluid loading – an assumption that is guaranteed to break down at high ϱ values as menisci coalescence begins.

Second, the actual value of S_c^* predicted from Eq. 5 is far higher than measured using any of the measures of breakdown. Specifically, the solid line in Figure 12 is shifted a factor of 10 lower than predicted by Eq. 5. This overprediction remains regardless of what value of z is adopted, or even whether z is independent of ϱ or not (note that z is a coordination number and hence only values between 2 and 12 are physically realistic, and hence z cannot be too far from 4). This may indicate that breakdown of the network involves processes other than (or in addition to) meniscus breakdown. One candidate for other processes is simply the rearrangement of particles within the cages defined by their nearest neighbors. Indeed past research on attractive suspensions suggests that such particle rearrangement can induce permanent structural and rheological changes that are in addition to those attributable to interparticle attractions[56, 57]. Another possibility is that breakdown may still involve meniscus rupture, but not homogeneously; instead localized deformation may cause rupture of relatively few menisci which experience far higher strain than the average.

Third, a key experimental observation is the rate dependence of the modulus which we have attributed to structural breakdown (i.e. rupture of menisci) at high rates. It is useful to define a particle-scale capillary number

$$Ca_p = \frac{viscous\ force}{interparticle\ adhesion} = \frac{\eta\dot{\gamma}R_p^2}{2\pi R_p\alpha} = \frac{\eta\dot{\gamma}R_p}{2\pi\alpha} \quad (6)$$

where α is the interfacial tension, η is the viscosity. The denominator is simply highest capillary force possible from Eq. 2. Thus we expect that when Ca_p is on the order of 1, almost all interparticle capillary bonds are broken and the morphology consists of discrete particles wetted by the PEO, possibly coexisting with PEO drops that are no bigger than the particles. For $Ca_p \ll 1$ on the other hand, large meniscus-bound structures can survive. Previously[58] we have reported the interfacial tension, $\alpha = 0.082\ N/m$, between PEO and PIB. The present polymers have somewhat different molecular weights, but in any case, α on the order of $0.01\ N/m$ can be expected. Then with $R_p = 1\ \mu m$ and $\eta = 10\ Pa.s$, we expect Ca_p to become on the order of 1 when $\dot{\gamma}$ is on the order of 6000 s^{-1}, a rate far exceeding the highest rate applied in our experiments. This simple dimensional analysis suggests that it is extremely unlikely that the shearing in our experiments is capable of breaking down the microstructure to the level of discrete particles. Thus all the structural breakdown reported here is likely the rupture of menisci connecting multiparticle clusters, and small pendular clusters likely survive to the highest accessible rates.

Fourth, although we have previously drawn an analogy between such non-colloidal pendular suspensions and attractive colloidal suspensions[5], Figure 13 illustrates some noteworthy features specific to the pendular suspensions. For instance, in Figure 13, the pairwise attraction extends to roughly 20% of the particle radius, whereas 5% of particle radius is more typical in attractive colloidal suspensions and gels (indeed some gels can be regarded as sticky hard spheres with negligible range of attraction[59-63]). Moreover, the pendular attraction is hysteretic: while an interparticle separation of ~20% of the particle diameter is needed to break the meniscus, the

particles must be brought nearly into contact to restore the attraction. This may be one reason why a strain on the order of 1 induces modest breakdown of the sample (as judged by the slight modulus decrease in Figure 8), which may be restored at higher strain. Indeed at low particle loading, such hysteresis may become increasingly important: reforming a meniscus requires the particles to collide with each other and thus we anticipate that once broken down after high-rate shearing, long shearing at lower rates may be needed to restore capillary menisci between particles. Lastly, the interparticle repulsion, which corresponds to contact between the particle surfaces, is extremely short range. Thus, for all practical purposes, the force-displacement curve for the particles has a positive slope at all separations (i.e. greatest attractive force is at zero separation). This suggests that a chain of pendular menisci cannot deform homogeneously; instead localized deformation and rupture of menisci is expected, analogous to pulling on a chain of magnets. Certainly a three-dimensional network can deform in more complex ways than a single chain, but nevertheless non-affine deformation may appear even at low strains. In fact we have conducted one preliminary experiment, albeit using the fluids and particles of Figure 38 (different from those used in the rest of this paper). This experiment is described Supplementary Figure 39 which shows that even at 300% strain, there is little or no deformation evident on the scale of single particles. Instead breakdown involves rotational motion of roughly-rigid segments of the pendular network. Unpublished results from Bossler, F., and Koos, E. (personal communication) support localized rupture as well.

Finally, a key result of this paper is that the rheology depends on the shearing conditions prior to the measurements. This immediately points to the difficulty of quantifying rheological properties as a function of composition. For instance, in a previous article, we examined pendular suspensions along a specific path in the ternary composition diagram where wetting fluid was 16%

of the particle loading. Along that path, we reported that the low-frequency plateau modulus as well as yield stress followed power laws, $G_p' \sim \phi_p^{4.9}$ and $\sigma_y \sim \phi_p^{3.3}$. In light of the results of this paper, if the shear history of the suspensions were changed, those power laws exponents may change or indeed the behavior may not be power law at all.

2.6 CONCLUSION

In summary, this article makes two chief contributions. The first, an operational issue, is to develop a new method of preparing pendular networks. The key merit of this method is to mix the particles and the drops together under conditions under which the drops are frozen. Thus the drop size distribution, contact angle, the stress under which drops collide with particles and wet them etc. can all be kept consistent across a wide range of sample compositions. Obviously this is only possible when the drop fluid can be frozen by crystallization or vitrification. The second is to elucidate fundamentals of pendular network rheology. In this context, the chief observations of this article are (1) pendular networks undergo a significant loss of modulus upon shearing at high rates, likely due to rupture of pendular menisci joining the particles, (2) at least for the compositions examined, the changes in rheology can be reversed, i.e. sufficiently long shearing can reset flow-induced rheological changes, (3) pendular networks can show elastic recoil strains on the order of 1%, and yield at larger strains, and (4) they also undergo significant reversible decrease of modulus prior to yield.

Overall the observations are consistent with the physical picture that a pendular network yields by rupture of the menisci joining particles. Nevertheless, the yield strains are far smaller

than may be expected by simple considerations of how much two particles need to separate before the meniscus between them breaks. We speculate that this is because yielding and flow involve rupture of a relatively few menisci connecting large particle aggregates.

3.0 THE EFFECT OF PARTICLE WETTABILITY ON YIELDING

3.1 Chapter Preface

Materials contained in this chapter were submitted as a research article titled “The effect of particle wettability on the of rheology particulate suspensions with capillary force” in Colloid and surface A;

List of Authors: Junyi Yang, Nicole Heinichen, and Sachin S. Velankar

3.2 INTRODUCTION

Capillary forces can sharply change the flow behavior of a particulate system[2, 7, 13, 14, 27, 64-67]. The most familiar example is of sand which can be poured easily when dry, but develops sufficient yield stress to support sand castles when wet. It has been long recognized that this change in rheology is attributable to the presence of small menisci between the particles which bind together the particles and induce a cohesive yield stress[9, 26]. A granular system such as sand typically has a high particle fraction typically around 60 vol%, but the same effect can be seen at much lower particle fractions in suspensions[5, 12, 13, 68, 69]. Specifically, if one starts with particles suspended in one fluid and adds a small quantity of a second fluid, the suspension can change from a free-

flowing liquid into a high viscosity paste[5, 12, 13, 70]. The central question motivating this paper is: how does the rheology of such a capillary-bound particulate system change as the particles become less wetting towards the minority fluid? Before proceeding, we clarify the simplified terminology in the rest of this paper: for the conciseness, the term the term "particle wetting" will be used rather than "particle wetting by the minority fluid". Thus a description such as "silanization makes particles less wettable" means "silanization makes particles less wettable by the minority fluid". Similarly "unmodified particles are fully-wetted" means "unmodified particles are fully-wetted by the minority fluid".

The simplest microscopic picture of such a capillary-bound particulate system (Figure 14a) involves a single pendular meniscus binding together two particles. Such pair-wise adhesion can bind particles together into large aggregates, which is generally denoted as the pendular state of the particulate system. At higher content of the minority fluid, multiple particles may become bound together by single menisci (Figure 14b), which has been called the funicular state[71]. Both these states presume that the minority fluid preferentially wets the particles, i.e. the contact angle (measured through the minority phase) is small, and indeed Figure 14a is drawn accordingly. This small contact angle is what guarantees that the pendular meniscus has a negative curvature (i.e. the meniscus has a negative Laplace pressure), and hence induces an adhesive force between particles. The situation when the minority fluid is less wetting towards the particles, i.e. the contact angle is near or above 90°, is more complex. In this case, a pairwise meniscus is unfavorable (its bulging shape, inset to Figure 14c, corresponds to a positive Laplace pressure) and induces a repulsive force between the particles at small interparticle separations[72]. Since the meniscus is unfavorable, when the minority fluid is mixed into the particulate system, it is unlikely to adopt the configuration of Figure 14c at all. Accordingly one would expect that if the contact angle of the

minority fluid is large, there should be little or no change in rheological properties of the particulate system. Remarkably however, Koos and Willenbacher reported that for several suspensions, a significant yield stress appeared due to addition of minority fluid even though the particles were poorly wetted[13]. Those experiments suggested that even a minority fluid that does not favor the particles can induce interparticle attraction and particle aggregation. Later calculations pointed to one possible reason: even though pair-wise menisci were not energetically favorable, multi-particle menisci may still be favorable[51]. Thus large-scale percolating networks could form using such multi-particle aggregates (dubbed capillary state clusters, Figure 14c) as their building blocks. The physical situation of Figure 14c bears a strong resemblance to the case of droplet-bridging by particles illustrated in Figure 14d. In both cases, one has neighboring "blobs" of the minority fluid that, because they share particles, can build large aggregates and endow the mixture with a yield stress. The quantitative difference is that the individual blobs of the minority fluid are much bigger than the particles in Figure 14d (hence may be called drops), whereas the blobs and particles have comparable size in the capillary clusters of Figure 14c.

In summary, addition of a minority liquid is able to create a particulate network due to capillary forces regardless of whether the minority fluid makes a small or a large contact angle on the particle surface. But the microstructure of this network is expected to change significantly with particle wettability, and one may therefore expect quantitative differences in the rheology as well. As yet however, there is no quantitative study of how particle wettability affects the rheology of such suspensions. The many examples given in original article by Koos and Willenbacher all used various particles made of different materials, sizes, and shapes which cannot be compared with one another[13]. More recently Bossler and Koos have reported an excellent confocal microscopy study of how contact angle affects the microstructure of the meniscus-bound particulate network[52].

The confocal microscopy in that paper supports the physical picture that a minority fluid with good wettability towards the particles forms pairwise pendular menisci between particles, whereas a minority fluid with poor wettability towards the particles forms multiparticle capillary clusters. However the rheological results reported in that paper used highly porous particles which tended to absorb the minority fluid. As a result, the rheology (as judged by the modulus of the capillary-bound suspension) changed non-monotonically as contact angle increased. The reason for this seems to be that the porous particles with good wettability absorbed the minority fluid altogether. Thus there was no minority fluid available to form pendular menisci, and the corresponding suspensions had an unexpectedly low modulus.

To our knowledge, there is no well-controlled study answering the question in the first paragraph of this paper: how does rheology change with particle wettability if other factors (particle sizes, system composition) are kept fixed? The present paper addresses this question for one specific composition "trajectory" along which the ratio of the minority fluid to the particles is held at a fixed value of 0.16. We have frequently represented compositions on a ternary composition diagram[5, 73-76], and the compositional trajectory for the set of samples studied in this paper are shown in Figure 40.

All the experiments in this paper are conducted using two molten polymers as the two fluid phases: polyisobutylene (PIB) as the continuous phase, and polyethylene oxide (PEO) as the minority phase. The particles are spherical, non-porous, and polydisperse silica. In past publications[4-7, 73-76], we have used this same ternary system for a host of experiments on microstructure and rheology, and it offers some specific advantages including: (1) the ability to quench the morphology by cooling, (2) the ability to selectively remove the PIB for scanning electron microscopic imaging, (3) the lack of any significant charge effects or trace surfactant

effects, which are often complications in water-based mixtures, and (4) lack of volatility, permitting long rheometric experiments without evaporation. For this specific research, the key advantage is that the particle wettability towards the minority fluid (PEO) can be modified while keeping all other factors constant. Specifically, the as-received particles are fully wetted by the PEO, whereas two different silane modifications are conducted to make them increasingly PEO-phobic.

This paper is organized as follows. Chapter 3.3 describes the experimental methods. Section 3.3.1 verifies the change in wettability of the particles due to silane modification. Chapter 3.4 describes the main results of changes in rheology with particle wettability. Chapter 3.5 discusses the results, and Chapter 3.6 is a summary and conclusion.

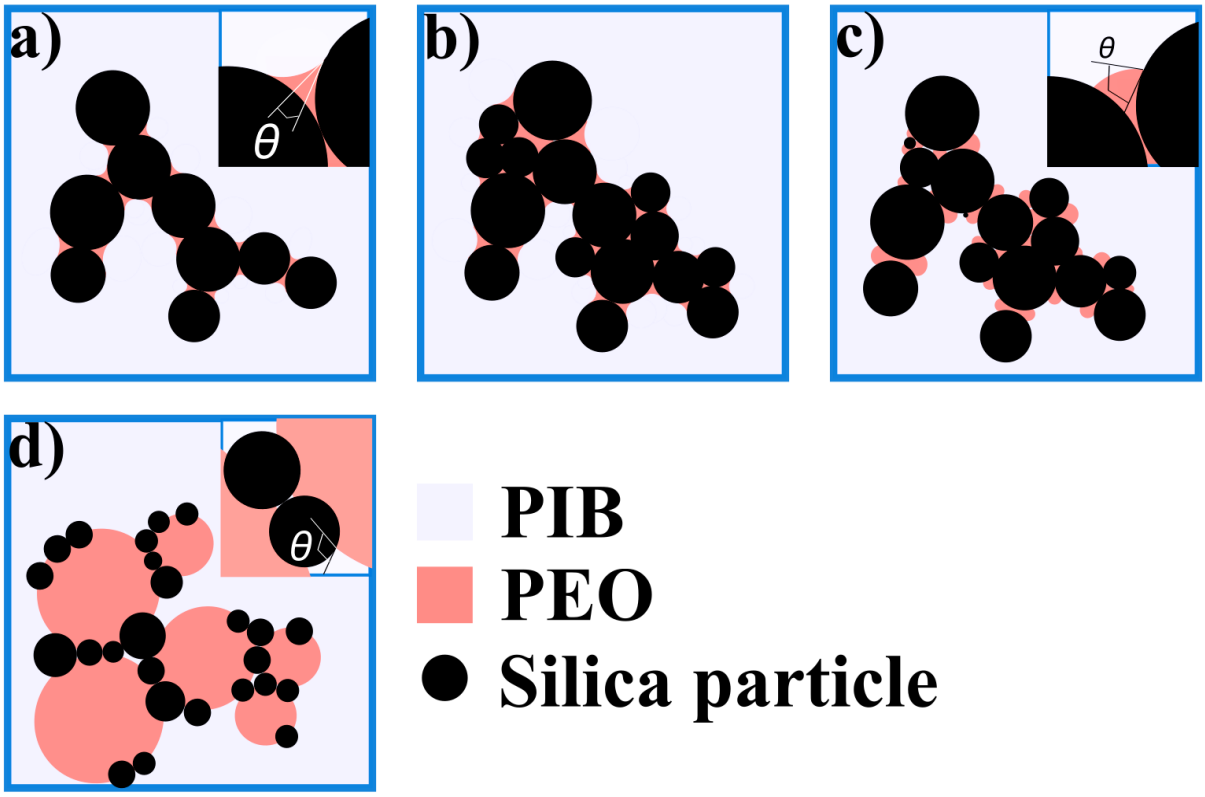

Figure 14.Structural sketch of different configurations of ternary blends containing silica particles with various wettability: a) pendular state; b) funicular state; c) capillary state cluster; d) particle-bridged droplets.

3.3 EXPERIMENTAL SECTION

3.3.1 Materials and hydrophobic modification

The two fluids used here are identical to those used in our previous research[1, 4-6, 73, 74, 76]: polyisobutylene (PIB, ρ=0.908 g/mL, MW = 2200 g/mol), and polyethylene oxide (PEO ρ=1.1 g/mL, MW = 20000 g/mol). The silica particles (mean diameter 2 μm μm and the size distribution is shown in Figure 41) were the same grade as used previously. Their surface was modified using dichlorodimethylsilane (DCDMS) and octadecyltricholorosilane (OTS). DCDMS modification was done through a gas phase silane deposition method[75], whereas OTS in a liquid phase deposition using toluene solvent. Both are described in detail in the electronic supplemental information as well as in our previous publication[75].

We acknowledge that the polydispersity may impact the behavior as compared to monodisperse particles at comparable fraction. One effect of polydispersity is that capillary forces increase with decreasing particle size. Hence when compared at the same composition, yield stress increases with decreasing particle size[77, 78]. Therefore – as long as the particles can be dispersed thoroughly – the small particles of a polydisperse sample may be expected to contribute more to the stiffness and strength of the suspension. Second, the polydisperse particles may be expected to form more compact clusters and perhaps allow clusters to become more stable, e.g. as contact angle changes.

3.3.2 Surface preparation

Samples for validating changes in wettability due to silane modification were prepared in a custom ball mixer as previously[73], by mixing the three components together at 80 °C when both polymers were molten. These samples were examined by SEM using ZEISS Sigma500 VP microscope after solidifying the PEO by cooling and removal of PIB with octane. This procedure only refers to Figure 15 (PIB:PEO:silica= 70:20:10).

The samples to be tested rheologically were all prepared by the "cold mixing" method described in Yang et al[76]. A PEO-in-PIB dispersion was first prepared under molten conditions and cooled to freeze the PEO drops. Particles were then mixed while still at room temperature at which the PEO drops are still solidified. The resulting physical mixture of solidified PEO drops and particles was then loaded into rheometer, heated to melt the drops, and sheared to allow capillary forces to bond together the particles. Details of mixing procedure are given in ESI. All the samples used for rheological experiments (i.e. except for Figure 15) used a PEO:particle ratio of 0.16 (Figure 40).

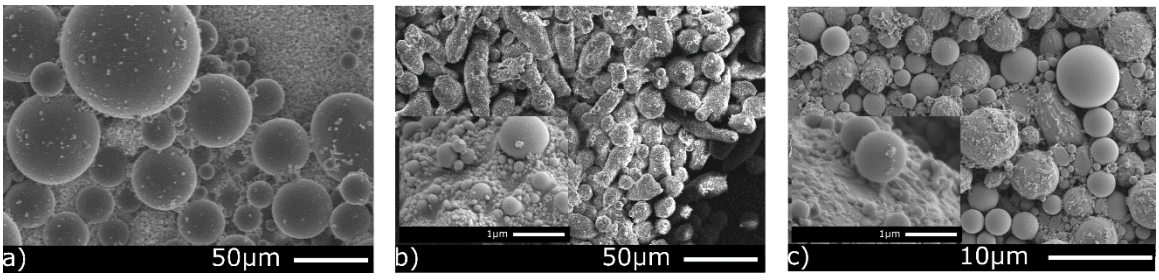

Figure 15.Effect of particle addition on morphology: (a) unmodified silica; (b) DCDMS-modified silica; (c) OTS-modified silica. All at composition PIB/PEO/silica= 70/20/10. Insets to (b) and (c) show magnified images of the appearance of particles on the surface of the PEO drops.

3.3.3 Rheological Measurements

An Anton Paar MCR 302 rheometer was used with 25 mm diameter profiled parallel plates to prevent wall slip. All samples were pre-heated and tested at 80°C to ensure that the PEO remained fully molten within a gap of 1 mm.

Both oscillatory and continuous shear tests were run. For each sample, the experiment began with a pre-shear test that ran for 10 minutes at a shear rate of 1 s^{-1}. This was followed by a large amplitude oscillatory shear test with strains ranging from 0.005% to 300%, at a constant frequency of 1 rad/s. Subsequent to the LAOS tests, continuous shear flow tests were conducted in the shear rate range of 0.01 s^{-1} to 100 s^{-1} with a maximum shearing time of 1 minute for each data point.

3.4 RESULTS

3.4.1 Validating the changes in wettability

We first verify that the DCDMS and OTS do actually change the wettability of the silica towards PEO and PIB. For this, blends were prepared with the PIB/PEO/particle volume fraction of 70/20/10 as is indicated by a red square in Figure 40. At this composition, the 70 vol% PIB becomes the continuous phase, whereas the relatively dilute PEO and silica become the dispersed phases. Thus, when the PIB phase is removed by dissolving into heptane, the PEO and particles can together be deposited on a filter paper and examined in SEM. Figure 15 shows the difference in microstructure of the three different particle types.

In the case of unmodified silica particles, SEM shows that the PEO is in the form of large spheres, with no particles visible. This exact structure has been noted repeatedly in our previous articles[74, 75] and suggests that the particles are present inside the PEO drops, testifying to their full wettability by PEO. Indeed previously we had verified by transmission electron microscopy that the PEO/PIB interface makes a near-zero contact angle on the surface of unmodified silica particle[5].

At the same composition, the blend with the DCDMS-modified particles (Figure 15b) has a sharply different morphology comprising an interfacially-jammed PEO dispersed phase that is highly irregular (i.e. non-spherical). A similar morphology was noted by Yang et al for the same system[75]. The interfacial adsorption (inset to Figure 15b) confirms that these particles are partially-wetted by PEO and PIB. The formation of such irregular shaped silica coated PEO droplets also indicates that particles are close to neutrally wetting, rather than having a contact angle far from 90°. Moreover, high magnification images suggest that the contact angle of the PEO/PIB interface at the DCDMS-silica surface is not too far from 90°.

A blend with the same composition, but with OTS-modified silica particles shows a further difference in structure. The particles can still adsorb on the surface of the PEO drops, but heavily protrude out (inset to Figure 15c). Indeed the largest silica particles seem to be completely unattached to the PEO. Previously we have also noted bridging of PEO drops by the OTS-modified silica particles[40, 75]. These images suggest that the OTS-modified silica is has a strong preferential wetting by PIB.

In summary, the particle silanization appears to be successful with the net result that the native silicas are almost completely PEO-philic, the DCDMS-silicas are roughly equally wetting towards PEO and PIB, and the OTS strongly prefer PIB.

Having verified the differences in particle wettability, we now turn to the effect of this wettability on the rheology of PIB/PEO/particle suspensions.

3.4.2 Effect of particle wettability on rheology

We will first examine the strain sweep behavior and the steady shear behavior at a single particle loading, and then summarize how particle loading affects the main rheological parameters. The primary goal of this article is to examine how particle wettability affects the capillary-induced changes in rheology of a suspension. Accordingly, the rheology of the suspensions in the *absence* of capillary forces (i.e. the silica-PIB suspension) is not the focus here. Nevertheless, below we will include a very brief discussion of the silica-in-PIB suspension only to illustrate the major changes induced by capillarity when PEO is added.

Figure 16 compares the LAOS behavior and Figure 17 the steady shear behavior of four blends, all at 20 vol% particles. In the absence of PEO, the silica-in-PIB suspension (made with unmodified silica particles) shows liquid-like rheology with $G'' >> G'$ in LAOS and stress nearly proportional to rate in steady shear. Upon addition of PEO there is a sharp qualitative change in the rheology. In LAOS, both moduli increase sharply, and $G' >> G''$ at low strain. With increasing oscillatory strain, there is a crossover which may be regarded as a yield point. In steady shear, Figure 17, an apparent yield stress appears at low rates. All of these features of the solid-like rheology were discussed extensively in previous articles[5, 76]. The focus of this paper is the effect of particle wettability. Figure 16 and Figure 17 show that decreasing PEO-philicity reduces the solid-like behavior, as evidenced by the decrease in both moduli, and the decrease in yield stress. These results suggest that addition of PEO leads to the formation of particulate networks regardless

of whether the particles are preferentially-wetted by PEO or by PIB; indeed we will confirm this microstructure in the next section). Figure 17 also shows that at the highest shear rates, the stress appears to be proportional to rate suggesting an apparent Newtonian behavior at high rate. Previously we had interpreted this in terms of a partial breakdown of the particulate network at high shear rate[5, 76].

Incidentally, Figure 17 shows the odd feature that at the highest rates, the sample with OTS-modified silica has an anomalously low viscosity. We have confirmed this results in multiple measurements. This is puzzling since at high shear rates, when viscous forces dominate over capillary forces, one should expect the viscosity to be similar for all samples with the same particle loading as seen previously[5]. We have no explanation for this odd observation.

Data such as Figure 16 and Figure 17 were gathered across a range of particle loadings, all while keeping the ratio of PEO to the particles fixed at 0.16. Examples of the raw data at two other compositions (10% particles and 30% particles) are shown in Figure 43 (LAOS) and Figure 44 (steady shear). Not surprisingly, the solid-like rheology becomes less pronounced with decreasing particle loading. Specifically, upon decreasing particle loading, both moduli reduce, but the storage modulus reduces much more than the loss modulus. Accordingly at low particle loadings, $G'' > G'$

. Moreover in steady shear, instead of a clear plateau in stress at low rates, the stress seems to drop monotonically (albeit still in a non-Newtonian fashion). These trends with particle loading were already explored for the fully-wetted unmodified silicas; the chief contribution of this paper to show that the same qualitative trends apply as the particles become less wetting. Further quantification of these data will be presented in the following section.

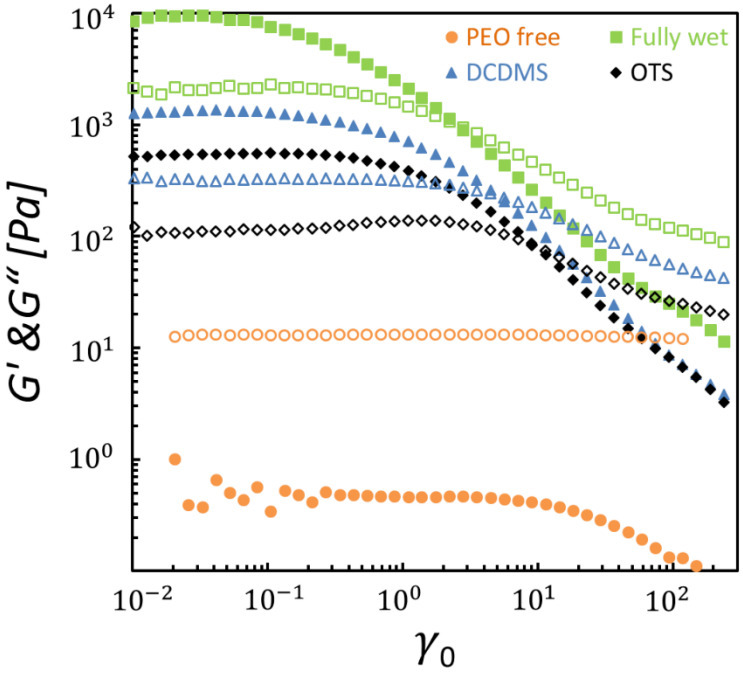

Figure 16. Oscillatory strain sweep results for ternary blends containing different silica particles at same composition (PIB/PEO/silica=76.8/3.2/20). Filled symbols show storage modulus, open symbols show loss modulus.

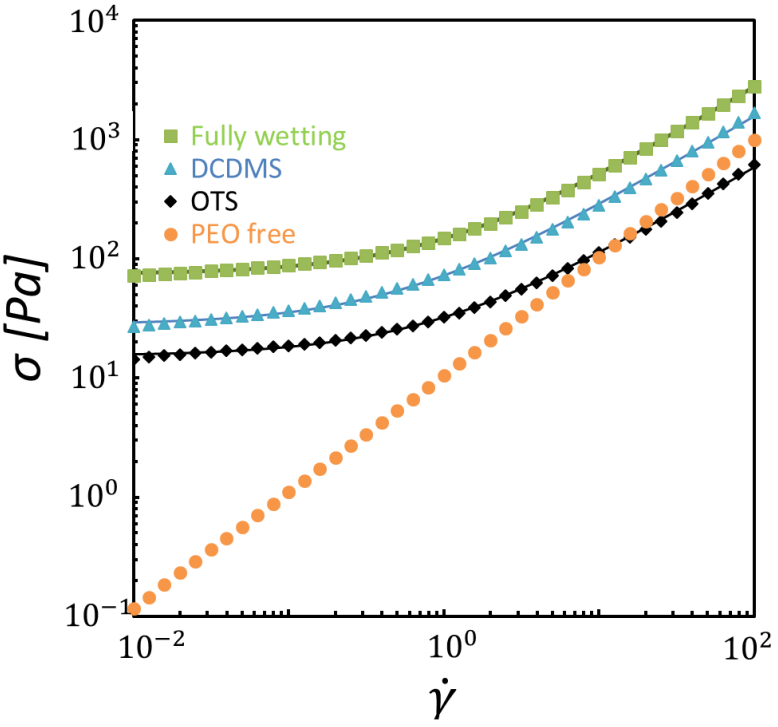

Figure 17. Steady state flow behavior for three ternary blends made consisting different silica particles but at same composition (PIB/PEO/silica=76.8/3.2/20), and binary PEO-free blend at (76.8/0/23.2). The solid lines show the fitting curves for each blend using modified Herschel-Bulkley equation.

3.5 DISCUSSION

As mentioned in the introduction, as the wettability of the particles reduces, we anticipate a weaker capillary attraction (or even a repulsion) between particles. Thus one should expect the solid-like properties to diminish as wettability of the particles reduces. Figure 16 and Figure 17 strongly support this expectation.

We extract two parameters from the experimental results: the plateau value of storage modulus at small strain amplitude (G_p') and the yield stress (σ_y). The plateau G_p' is obtained by averaging the storage modulus values in the linear regime at small amplitude. The corresponding values of G_p' are shown in Figure 18a. Yield stresses are estimated by using the following modified Herschel-Bulkley equation: $\sigma = \sigma_y + k * \dot{\gamma}^n + \eta_\infty * \dot{\gamma}$ as described previously[76]. This last term is well-able to capture the $(stress\ \sigma) \propto (rate\ \dot{\gamma})$ behavior at high rates. As in our previous paper[76], η_∞ is not a fitting parameter, but instead represents the viscosity expected for a hard-sphere suspension with the same particle loading, and is estimated from the Krieger-Dougherty equation[79]. Excellent fits are obtained (Figure 17) with σ_y, *k* and *n* as the three fitting parameters, and the corresponding values of σ_y are shown in Figure 18b. Values of n were all close to 0.76.

We acknowledge that at low particle loadings, the stress does not reach a convincing plateau at low rates, and hence the σ_y value is not entirely reliable. Visual inspection of the flow curves suggests that values above 10 Pa can be considered reliable.

Figure 18 shows that both G_p' and σ_y parameters increase with particle loading, and their absolute values decrease with decreasing wettability of the particles. In all cases, the dependence of these quantities on particle loading can be captured by power laws with the exponents noted in the figures. Given the noise in the data and the relatively few points, we cannot judge with confidence whether the exponents depend on particle wettability or not. As discussed previously[76] we re-emphasize that all such ternary mixtures of two immiscible fluids and particles are always

far from thermodynamic equilibrium and hence the values of plateau modulus and of the yield stress, as well as the exponents, are expected to change if the sample preparation method or flow conditions prior to measurement is changed[76].

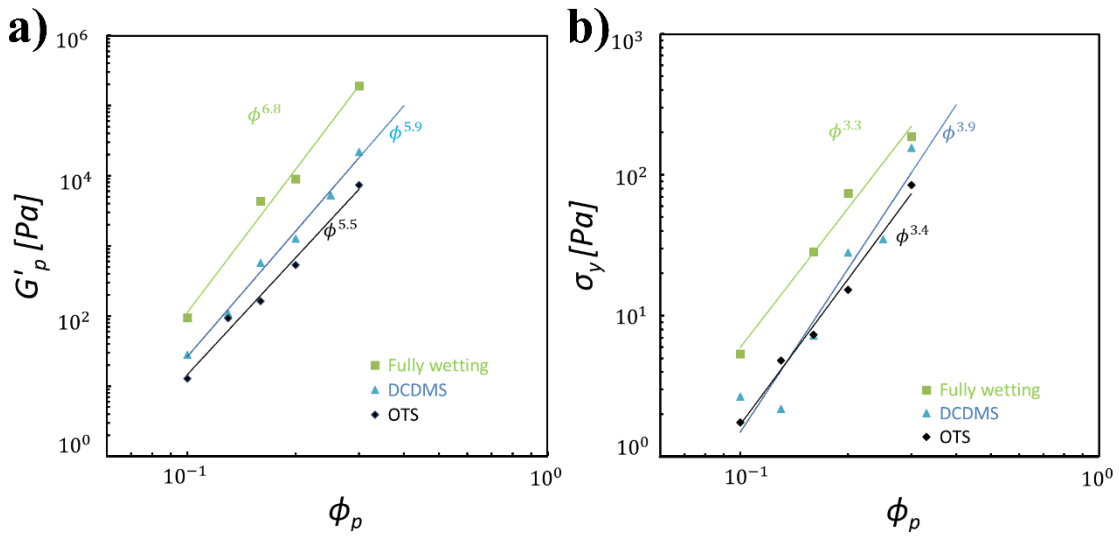

Figure 18. Linear storage modulus dependence on particle loading using different particles at various particle loadings (b) Yield stress dependence on particle loading using different particles at various particle loadings

We now turn to the microstructural picture. The fact that the ternary mixtures of PIB/PEO/silica in Figure 16 all have yield stresses regardless of particle wettability suggests that there are capillary-bound particle networks in all three cases. Previously we have firmly established the existence of a capillary-bound network for the fully-wetting and the DCDMS-modified particles, but not for the OTS-modified particles. In fact the OTS-modified particles are almost completely non-wettable: Figure 15c shows many of them are not bound to the drops at all. This makes it even more critical to verify the microstructure since the particles may be too PEO-

phobic to form a network at all. To verify its microstructure, SEM was conducted on samples extracted from the rheometer at the end of the experiments. The corresponding microstructure of the mixtures with OTS-modified particles is shown in Figure 19. Similar images for blend containing fully wetting particles and the DCDMS-modified particles are shown in Appendix B Figure 42. Figure 19 leaves no doubt that – despite their poor wettability of the OTS-modified particles – PEO does bind them together. Three possible reasons for why PEO binds poorly wetting particles are discussed as followed.

First, as discussed in the introduction, when particles are poorly wetted, a pair-wise meniscus is expected to be repulsive when the particles are nearly in contact (Figure 14c). Yet, at larger separations, the force can be attractive[72]. This is because the total capillary force consists of a Laplace pressure contribution (proportional to the area wetted by the meniscus), and a "perimeter" contribution (proportional to the perimeter length of the meniscus). The Laplace pressure contribution is repulsive for non-wetting particles, but the perimeter contribution is always attractive. Thus it is possible that some particles sustain a pair-wise attraction while maintaining some separation.

Second, the network might not be built from pairwise contacts but from multiparticle clusters[13] (Figure 14c). Energy calculations[51] of capillary-bound clusters of monodisperse particles suggest that multiparticle clusters can be stable even if the meniscus fluid makes a contact angle as high as 160°. Clusters were found to become more stable with increasing number of particles – although of course a larger-volume meniscus was needed to bind all the particles. We believe that polydispersity could make multi-particle clusters even more favorable simply because they can pack more efficiently and allow larger number of particles to join a cluster.

Yet, a close examination Figure 19 suggests that the explanations stated above are not entirely satisfactory. Specifically, there is not a single location in Figure 19 where the PEO phase trapped between two or more particles appears to bulge outwards, as may be expected for a multi-particle cluster with a high contact angle. Nor is there any location where a particle has a small convex drop of PEO sticking to it; while PEO does appear to adhere to the particle surfaces, it appears as irregular patches, not as a convex lens. The latter feature, in particular, was readily evident in the work of Bossler et al[52], albeit with an oil/water system and much bigger particles. These observations suggest a third possibility: variability in contact angle. Such variability is evident in the insets to both Figure 15b and Figure 15c. For instance, in Figure 15c, a few particles are much more deeply embedded in the PEO, some protrude nearly completely out, whereas many more seem to be completely unattached to the PEO. Some of this variability may be intrinsic, i.e. the particles may truly have different contact angles even at equilibrium. A much greater source of variability might be contact angle hysteresis which is very common and can have various causes: surface roughness, chemical heterogeneities on the surface, or irreversible adsorption of either the PEO or PIB on the surface. In fact we have already shown that particles that are pre-dispersed in PIB tend to be more PEO-phobic than those pre-dispersed in PEO[75]. Regardless of cause, if there is sufficient variability in contact angle, one may get network formation due to the more-wetting particles, with the less-wetting particles not attaching to the network at all.

Thus we tentatively propose the following picture: As the wettability of the particles reduces, there is an increasing reliance on multi-particle clusters (rather than pairwise adhesion) to sustain the network. Since the capillary forces corresponding to less-wettable particles are weaker, the corresponding network is expected to be less strong and less stiff as well. This is essentially the physical picture proposed by Koos[51]. But further we propose that in most real-world

cases, the particles have a distribution of wettabilities, either intrinsically or due to contact angle hysteresis. As average wettability of the particles reduces, a certain fraction of particles become too non-wetting to participate in the network, whereas the other particles remain within the network, either bonded pairwise to other particles or as a part of multi-particle clusters. In summary, we propose that the decrease in the solid-like characteristics of the suspension as the particle wettability reduces has two causes: the multi-particle clusters inherently give a weaker network, and moreover, fewer particles contribute to the network.

To seek evidence that some particles do not participate in the network at all, a different experiment was conducted. A small portion of ternary blend consisting OTS-modified particles was deposited on a filter paper. Octane was dripped over this to remove the PIB (which was then absorbed into the filter paper). We presume that any particles that are not aggregated by the PEO would be washed out and redeposited around the boundary. Indeed the result shows that a small cluster of particles bound by PEO, along with numerous particles in the surrounding region suggesting that many particles are not bound to the network.

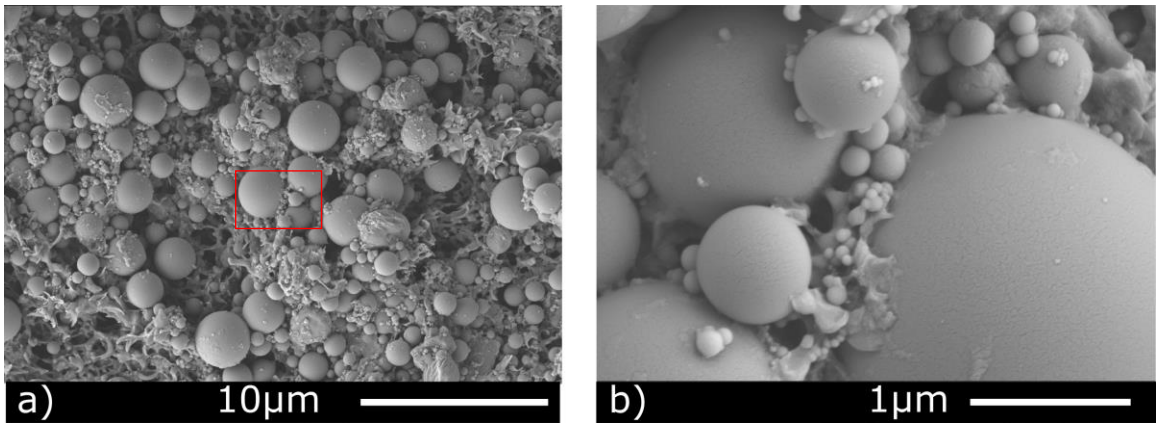

Figure 19. Scanning Electronic microscope images of ternary blend consisting OTS-modified silica particle at composition of PIB/PEO/silica = 76.8/3.2/20. Part b is at higher magnification.

3.6 SUMMARY AND CONCLUSIONS

In summary, we have examined three-phase liquid/liquid/solid suspensions comprising particles suspended in a majority liquid phase, with a small minority of a second liquid phase added. The minority liquid can bind together the particles by capillary forces, giving the suspension strongly non-Newtonian rheology with characteristics such as a non-zero modulus or a yield stress. The central issue underlying this paper is how the rheology depends on the wettability of the particles by the minority fluid. To our knowledge, this is the first study of how suspension rheology changes with particle wettability while holding fixed the particle sizes and distributions, the fluids, and mixture compositions. Therefore all rheological changes can be attributed unambiguously to difference in wettability of the particles.

Three cases were examined: particles that are almost completely-wetted by the minority liquid, nearly equally-wetted by both liquids, and almost completely-wetted by the majority fluid. Broadly, the rheological properties are qualitatively similar in all three cases: the capillary forces induce solid-like mechanical behavior, with the yield stress and the modulus having similar dependence on particle loading. But quantitatively, when ternary mixtures with the same composition are compared, the yield stress and modulus reduce as the minority fluid becomes less wetting towards the particles. On a microstructural scale, the minority phase is found to induce aggregation of particles which is responsible for the change in rheology.

Apart from the quantitative details of the yield stress and modulus, we conclude with two central points. First, these results support the physical picture proposed previously that even a minority fluid that is not preferentially-wetting towards the particles can give the suspension solid-like properties, and that the underlying cause is multi-particle clusters held together by capillary forces[51]. Second, the mean wettability of the particles, as judged by a single contact angle, may be

a poor predictor of suspension behavior. In most systems, there is inevitably polydispersity in contact angle, either inherently or due to contact angle hysteresis. Therefore a minority fluid that appears to be almost completely non-wetting towards most of the particles may still be able to create capillary bonds because some fraction of the particles can still be wetted. The latter result is of obvious relevance to researchers seeking to exploit capillary forces to develop new materials or new methods for materials processing. Specifically, even particles that are expected to be fully wetting towards the minority or the majority fluid may nevertheless stabilize Pickering emulsion type morphologies because some fraction of particles are partially wetting. Conversely, capillary aggregates (which require full wetting of particles by the minority phase) may appear even if the particles are expected to be partially wetting towards both phases.

4.0 ON THE RHEOLOGY OF TERNARY SYSTEM WITH PARTIALLY WETTABLE SILICA PARTICLES

4.1 Chapter Preface

Materials contained in this chapter were published as a research article titled "A microstructure-composition map of a ternary liquid/liquid/particle system with partially-wetting particles" in RSC Advances; figures used in this chapter have been reprinted with permission from: Soft Matter, 13 (2017) 8579-8589. (listed as reference 75 in the bibliography section).

List of Authors: Junyi Yang, David Roell, Martin Echavarria and Sachin S. Velankar

4.2 INTRODUCTION

Ternary mixtures of liquid/fluid/particles show a wide diversity of microstructures, many of which have been reviewed in two recent articles [1, 3]. Much of the structural diversity is attributable to the capillarity-induced interaction between particles: pairwise attraction through capillary bridging [5, 13, 14, 70], many-body cohesion through capillary clustering [5], interfacial assembly of particles [24, 38, 39] or particle bridging of drops[15, 40]. Even a single ternary system can display several different morphologies depending on its composition. A recent article by one of us suggested that given a

pair of fluids and a particulate species, mixtures of various composition can be conveniently classified within a triangular compositional diagram, with different regions of composition space corresponding to distinct morphologies[1]. Previous papers[4-6, 73, 74, 76] from our group examined the morphology of ternary blends composed of two immiscible polymers (polyethylene oxide, PEO and polyisobutylene, PIB), and polydisperse silica particles that have a strong affinity for the PEO. Five types of morphology were identified at various compositions of this single system: (1) pendular/funicular network, (2) capillary aggregates network, (3) particle-filled drops, (4) co-continuous and (5) drops-in-suspension. Schematics of these structures, and their location on a triangular morphological map were presented previously[73, 74] and are reproduced in Figure 45. To our knowledge, this morphological map covers widest composition range for any single liquid/fluid/particle system in the literature.

That research[4-6, 73, 74, 76] was all conducted with particles that are fully-wetted by one of the two phases (PEO). This immediately raises the question of how the morphological map would change if the particles were partially-wetted by both phases. Most studies of partial wettability in three-phase liquid/liquid/particle systems have been conducted in oil/water/particle mixtures. The most heavily-studied example is of Ramsden–Pickering emulsions [2, 36, 80] in which the particles act somewhat like surfactants by adsorbing at the liquid–fluid interface, hence inhibiting drop coalescence and stabilizing the emulsion. There have also been studies of bridged Pickering emulsions, i.e. emulsions in which a monolayer of particles at the interface bridges together two droplets and hence assembles the droplets into volume-spanning networks [15, 40, 81]. The presence of interfacially active particles can also stabilize bicontinuous structures through arrested spinodal decomposition of the fluids[19, 24, 39]. Finally, with partially-wetting particles, particle aggregation into space-spanning networks has also been noted in oil/water/particle mixtures[52].

Going beyond small molecule systems, similar microstructures and phenomena have been noted in ternary systems in which the two fluids are molten polymers[1, 82].

Despite the research cited in the previous paragraph, a comprehensive mapping of the morphology-composition space has never been conducted for situations where the particles are partially-wetted by both liquid phases. Most significantly, the effect of particles at higher loadings remain very poorly understood. Virtually all of the research cited in the previous paragraph has been conducted at relatively low particle loadings, typically lower than 10 % by volume, often lower than 2 %. There are a few articles at particle loadings exceeding 15 vol%[13, 15, 52, 73, 74, 83, 84] but many of these do not cover a wide range of fluid phase fractions. The goal of this paper therefore is to construct a comprehensive morphological map that is completely analogous to Figure S1, but with the key difference that the particles are partially wetted by both liquid phases.

It must be emphasized that the only difference between this work and the research leading to Figure S1 is that the particles in this work are hydrophobically-modified. Other than that, all the remaining materials and methods are identical. Thus, the final morphological maps (Figure 6) in this paper, and Figure 45, constitute two different slices of the composition-wettability prism of a single experimental system. Conceptually, such morphological classification within a prism resembles oil-water- surfactant equilibrium phase diagrams[85, 86], except that the current mixtures are far from equilibrium.

We proceed in the following sequence. Chapter 4.3 describes the materials and methods, including the method used for hydrophobic modification of particles. Chapter 4.4 first verifies that the modified particles are indeed partially-wetted by both fluid phases, and then examines the effect of particles on the morphology at various fluid ratios and particle loadings.

Chapter 4.5 discusses the results, most importantly, the effect of particles on phase inversion and co-continuity, and interfacial jamming.

4.3 EXPERIMENTAL SECTION

4.3.1 Materials and sample preparation

Polyisobutylene (PIB, $\rho \approx 0.908\,\mathrm{g}/mL$, $\mathrm{Mw} \approx 2200\mathrm{g}/mol$) polyethyleneoxide (PEO, $\rho \approx 1.1\,\mathrm{g}/mL$, $\mathrm{Mw} \approx 20{,}000\mathrm{g}/mol$, $T_{melt} \approx 65℃$) and silica particles (#SS1205, Industrial Powders) constitute the ternary experimental system. The particles are spherical with an average diameter of 2μm and a monomodal size distribution. The particles were made hydrophobic by coating them with dichlorodimethylsilane (DCDMS) as follows: a ~100 mL container, quarter-filled with particles was tumbled at a few rpm. Nitrogen was bubbled through a DCDMS vial, any droplets/mist was removed, and the DCDMS-saturated nitrogen was then passed through the tumbling container for 1 hour. SEM (shown later in Figure 20) confirms that DCDMS-modified particles, when added to a PEO/PIB blend, are partially-wetted by both phases. This contrasts with the unmodified particles that when added to a PEO/PIB blend, are fully-wetted by PEO.

Similar to our previous research, a temperature-controlled custom ball mixer was used to mix all three components. A two-step procedure was followed: PEO and PIB were first blended in the desired ratio at 600 RPM at 80℃ for 2 minutes. Then, particles were added to the mixing cup and the three components were blended for an additional 5 minutes. This blending procedure is

similar to that used in our previous research except for some minor modifications (higher speed during blending, and mechanical redesign of how the mixer is held closed during blending). The mixed sample was quenched by cooling to roughly 5℃ to ensure complete crystallization of the PEO.

Sample stubs were prepared for SEM characterization. As previously, we exploit the fact that n-octane can selectively dissolve the PIB while leaving the PEO completely unaffected. For samples with PIB as the continuous phase, a small quantity of sample was first transferred into a vial filled with n-octane, and held overnight to dissolve the PIB matrix. The residual sediment (a composite structure comprising particles and PEO) was then collected, transferred onto a filter (Millipore, 0.1 μm pore size) stuck onto a carbon-taped SEM stub, and rinsed with octane several times. For samples with PEO as the continuous phase, a small portion of sample was first cooled and fractured in liquid nitrogen. The fractured surface was then washed several times with n-octane before placing on the stub. All SEM stubs were then left to dry, and coated with an Au/Pd sputtering target (Cressington) for 90 seconds at 40mA before sent into the SEM chamber.

In addition to scanning electron microscopy, a limited amount of optical microscopy was also conducted on both, molten and quenched blends. All the information from these images are completely consistent with SEM images, but particles are not clearly visible. Hence optical images are not discussed here.

4.4 RESULTS

Before turning to particle effects, we will briefly summarize the morphology of the PEO/PIB blends in the absence of particles. Consistent with our previous research[74], we find that blends of PEO and PIB show simple droplet-matrix morphologies, either PEO drops in a PIB continuous phase (at high PIB content) or PIB drops in a PEO continuous phase (at high PEO content). Phase inversion was reported at about 60% PEO. The drop size was found to increase as phase inversion composition was approached from either size. Unlike in many polymer blends, we did not find any composition region of co-continuity, nor any fibrillar morphologies near phase inversion. This is likely due to the fact that the viscosity of our polymers is two to three orders of magnitude lower than of typical molten plastics, and hence any complex microstructure that may be present during mixing rapidly breaks into a droplet-matrix structure as soon as mixing ceases.

The rest of this Chapter 4.4 deals with the effects of particles on the morphology. A total of 26 blends were examined, and representative SEM images are shown in Appendix A.3 Figure 46. Due to the large number of samples, it is difficult to gauge the wide-ranging effects of particles all at once. Accordingly, the following sections present the results in a more piece-wise fashion proceeding from dilute to concentrated particle loadings. The experimental results for particle effects are organized as follows. In Chapter 4.4.1 we first show that the DCDMS modification is successful in changing the particles from being fully-wettable by PEO to being partially-wetted by both phases. This is followed by four sections that discuss changes in drop size due to particles (Chapter 4.4.2), changes in morphology at low particle loading (Chapter 4.4.3), and changes in phase continuity due to higher particle loadings (Chapter 4.4.4) and particle wettability (Chapter 3.5).

4.4.1 Validation of surface modification

As mentioned in the Introduction, the purpose of this research was to construct a morphological map of ternary blends with partially-wettable particles, and compare with the case (Figure 45) of fully-wettable particles examined previously[5]. Thus it is first critical to verify that the DCDMS treatment actually modifies the surface wettability towards PEO and PIB. This was tested (Figure 20) by comparing the morphology of four particle-containing blends, two with 10% DCDMS-modified silica particles, and two with 10% unmodified silica particles. The blend compositions were selected so that in two cases PEO was in a large majority (70%) and hence PEO became the continuous phase, whereas in the other two cases, PIB was in a large majority (70%) and hence PIB became the continuous phase. Figure 20a&b shows the fracture surface of the two blends with PEO as the continuous phase after extraction of the PIB, leaving behind craters. The inner surface of the craters appears smooth for the sample containing unmodified particles (Figure 20a). In contrast, in Figure 20b, the crater surfaces are covered with DCDMS-modified particles. Figure 20c&d show the two blends with PIB as the continuous phase. In this case, upon extraction of the PIB, the dispersed phase (comprising the PEO and silica) is recovered for imaging. The dispersed phase of the blend with the unmodified particles (Figure 20c) appears smooth indicating that the particles are inside the PEO drops. In contrast, the dispersed phase of the blend with the DCDMS-modified particles is heavily covered with particles suggesting that the particles are partially-wetted by PEO and PIB. Based on these images, the DCDMS surface modification process is deemed to be successful in creating partially-wettable particles, and therefore suitable for constructing a morphology-composition map for a ternary liquid/liquid/particle mixture with partially-wettable particles.

The images also allow some judgement of contact angles of the DCDMS-coated silica. Due to the polydispersity of the particles and also because the PEO/PIB interface is not flat (indeed not even very smooth), it is difficult to judge a contact angle quantitatively. Nevertheless, judging by the visual appearance of the particles (and in particular, how far the particles protrude out of the PEO phase), the particles appear to be at a near 90° contact angle in Figure 20d. In Figure 20b however, the particles protrude less out of the PEO phase suggesting a contact angle of less than 90° as measured through the PEO phase. This comparison of Figure 20b vs d suggests some level of contact angle hysteresis, which may be attributable to the following reason: The blends are prepared by first blending the PEO and PIB in the appropriate proportions, and then adding particles. Thus the particles first encounter (and hence are wetted by) that phase which is continuous prior to particle addition. Accordingly, particles encounter PIB first for Figure 20d, and PEO first for Figure 20b. Evidently this initially-wetting phase affects the final contact angle. Similar contact angle hysteresis can be found in small molecule systems[87]. Furthermore, Figure 20d results in a near-symmetric wetting, and Figure 20b results in a preferential wetting by PEO. We never observe preferential wetting by PIB, suggesting that the particles are somewhat PEO-philic, and not as neutrally-wetting.

Two other features are noteworthy from Figure 20. The first is that in both Figure 20b & d, the dispersed phase is non-spherical in notable contrast to the fully-wetting blends (Figure 20a & c). Such non-spherical dispersed phases are well-known in Pickering emulsions, and indeed were noted even in an early description of Pickering emulsions[2]. The second is that the dispersed phase is much larger when PEO is the dispersed phase than when PIB is the dispersed phase. We will discuss both points later in the paper.

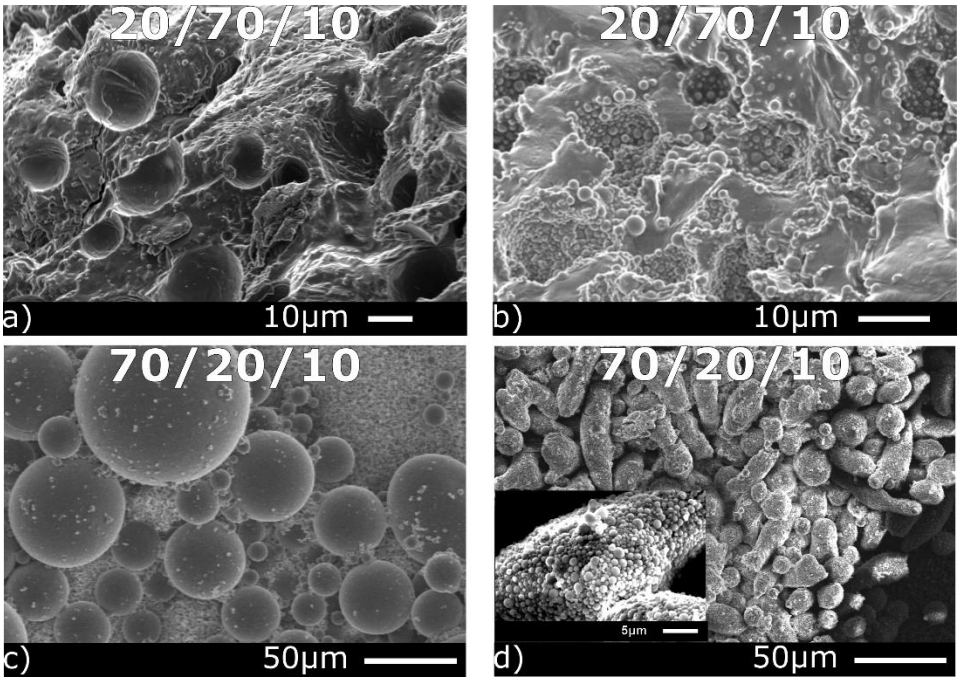

Figure 20. SEM images comparing blends with unmodified silica particles (a&c) vs. blends with DCDMS-modified silica particles (b&d). The inset of d shows a higher magnification for the same blend to show the particles crowded at the interface. The numbers at the top of each image are the blend composition in the format of PIB/PEO/particle volume ratio.

4.4.2 Dilute particle loading: Increase in size of the dispersed phase

To test particle effects at dilute loadings, experiments were conducted on blends with just 1% particles. Even at this low loading, particles sharply increase drop size as illustrated in Figure 21. At a PIB:PEO ratio of 80:20, PIB forms the continuous phase, and the PEO drops are fairly uniform-sized and round with a typical diameter of 2 μm (Figure 21a). Addition of 1 % particles induces a massive increase in the PEO drop size to 20 μm (Figure 21c). Figure 21b shows the

reverse situation: at a PIB:PEO ratio of 20:80, PEO forms the continuous phase, and in the absence of particles, the PIB drop size is several microns. Upon addition of 1% particles, the drop size increases by several fold. Such particle-induced increase in drop size has been noted previously in our research[40, 88] (indeed at even lower particle loading). We attribute this to an increase in coalescence rate due to particles by a mechanism analogous to the "bridging-dewetting" mechanism well-known in in aqueous systems, although as originally proposed, the bridging-dewetting mechanism applies only when the particles are preferentially-wetted by the drop phase[58, 88, 89].

Figure 21 also shows another unexpected feature: even in the absence of particles, there is a large difference in the dispersed phase size: the PEO drops in Figure 21a are far smaller than the PIB drops in Figure 21c. This large size difference appears even though both these blends have the same dispersed phase loading, and even though their viscosity mismatch is only modest. The cause of this asymmetric behavior of the particle-free blends is not clear. Nevertheless, similar asymmetric behavior has been noted previously in other blends of immiscible polymers[90]. We will not discuss this drop size asymmetry in particle-free mixtures further in this article.

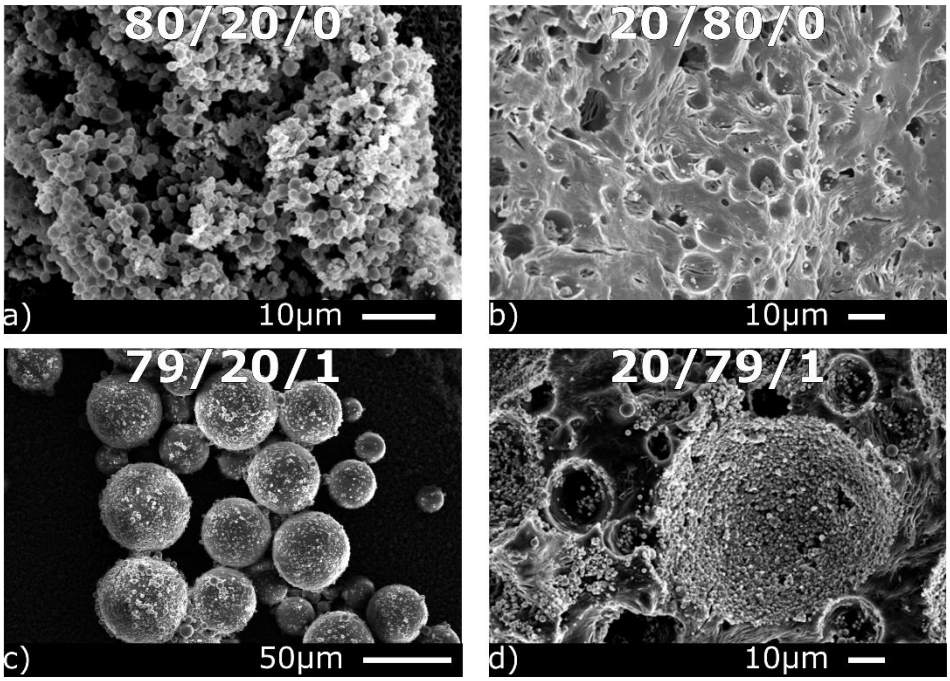

Figure 21. SEM images of the effect of adding DCDMS-coated particles on blends with PIB as the continuous phase (a and c) and PEO as continuous phase (b and d). The PIB/PEO/particle volume ratios are noted in each image.

4.4.3 Morphological changes with composition at 10% particles

We now turn a higher particle loading of 10%, which is already higher than used in much of the past literature on oil/water Pickering emulsions or particle-filled polymer blends. Nine blends with various PIB:PEO volumetric ratios ranging from 87:3 to 3:87 were examined, all at 10 % particles (Figure 46). Six of these have been selected in Figure 22 to illustrate the morphological changes with composition. The magnifications are selected to match the appropriate length-scale of each sample, and we will discuss each in turn.

In Figure 22a, at 3% PEO, the particles appear to be aggregated together by PEO, which resembles the "pendular/funicular" morphology obtained previously for fully-wetting particles. At

even lower PEO loading (the composition of 89/1/10 in volume in Figure 46), many of the particles appear to be bonded to each other pairwise (i.e. pendular menisci), whereas in Figure 22a, multiple particles are bonded by a single “funicular” meniscus. It is noteworthy that of all the morphologies in Figure 22, this is the only one that also exists in the fully-wetting case studied previously. All the other morphologies in Figure 22 are altogether different from those seen in Figure 45.

Upon increasing the PEO content to 20% (Figure 22b) the morphology changes drastically: the dispersed phase PEO now adopts irregular elongated shapes of several tens of microns in size. With a further increase in the PEO loading, the size scale of the dispersed phase increases, e.g. compare Figure 22b, Figure 46h and Figure 22c, respectively at 20, 30 and 36 % PEO. Along with the increase in drop size, the interface becomes much more smooth, Higher magnification images at these compositions all show that the surface of such dispersed phases is tightly covered with particles. An example is shown in the inset to Figure 22c.

With a further increase in PEO fraction, phase inversion occurs. At 45 % PEO (Figure 22d), the morphology qualitatively resembles an inverted version of Figure 22c: an irregularly-shaped dispersed phase that is coated with particles. Similarly, Figure 22e comprises particle-covered PIB drops, which is an inverted version of Figure 22b, albeit with a much smaller size scale. Finally, at the lowest PIB loading, Figure 22f, the sample still consists of PIB drops, but now the drop size is comparable to that of the particles.

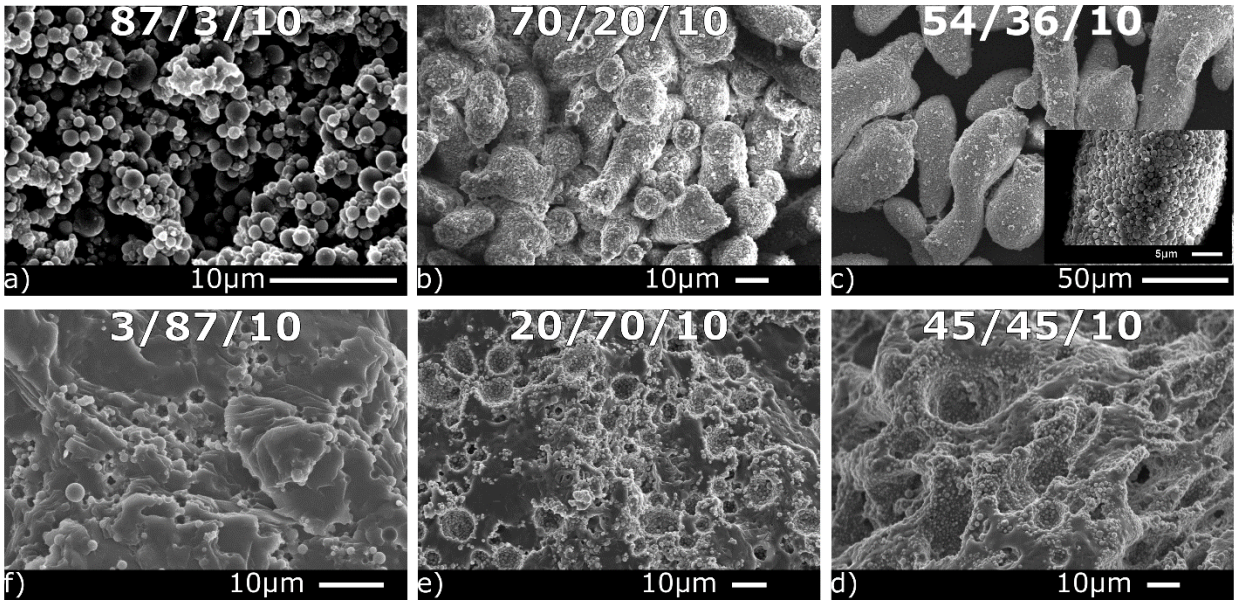

Figure 22. Ternary blend morphology at various PIB/PEO/particle ratios listed in each image. The particle loading is 10% in all cases.

4.4.4 High particle loadings and co-continuous morphologies

We now turn to a much higher particle loading of 20% and 30%, values far higher than used in most of the existing literature on Pickering emulsions or on filled polymer blends. A total of nine blends were prepared at these two loadings (Figure 46). The morphological trends were found remain broadly similar to those at 10% but with some differences. One difference is the sharp decrease in the lengthscale of the dispersed phases as particle loading increases. The second is the appearance of highly branched morphologies that appear, at least visually, to be co-continuous. Various methods including image analysis, solvent extraction, electrical conductivity measurements and rheological measurement have been considered for judging the phase continuity of polymer blends[91].

Here however, well-established quantitative methods of judging phase continuity, which typically involve blends of solid samples, are difficult to apply since PIB is a liquid. Instead, we rely on qualitative visual judgment. To illustrate these two trends, the morphologies at selected compositions are shown in Figure 23. The compositions of Figure 23 were selected such that the middle column (Figure 23b and e) correspond to morphologies that appear (at least visually) to be co-continuous. The left and right columns correspond respectively to the blends with somewhat lower and somewhat higher PEO content respectively.

At 10 % particles, co-continuous morphologies are not evident, and hence only dispersed phase morphologies are shown (Figure 23g&h). As the particle loading reaches 20 %, the branched PEO structures are found to join together into the morphology of Figure 23e which appears co-continuous (indeed it remains intact when the PIB is dissolved). With further increase in particle loading, the lengthscale of the morphology reduces further (Figure 23b). The inset to Figure 23b shows a higher resolution SEM of the fractured surface which reveals that the PEO-phase itself contains a smaller-scale microstructure that incorporates both the particles and the PEO. This latter point will be discussed further below.

On the PIB-rich side of phase inversion (left column of Figure 23), at 10 % particles, the 54/36/10 blend (Figure 23g) shows a branched dispersed phase, which may be regarded as a precursor to a truly co-continuous morphology. With increase in particle loading to 20 % (Figure 23d), the branching increases, and the 53/27/20 sample is nearly co-continuous (upon extracting the PIB, the sample fragmented to some degree). At 30 % particle loading however (Figure 23a), the morphology looks distinctly different: it is no longer highly branched, and the surface appears highly irregular. Indeed this visually resembles a capillary aggregate morphology seen in mixtures with fully-wetting particles[6] although in the present case, the particles are not fully-wetting and

capillary aggregates are unlikely to form. The likely reason for this morphology is that the particle loading now exceeds the dispersed phase loading. Since the particles have a strong preference to stay at the interface, a highly irregular interface, by offering a larger interfacial area, may be able to accommodate more particles at the interface.

On the PEO-continuous side (the right column in Figure 23), the dispersed phase (now PIB) appears interfacially-jammed. This is somewhat analogous to the left column in Figure 23, but with two differences. First, highly elongated and branched dispersed phases do not appear when PIB is the dispersed phase (compare for instance Figure 23d vs Figure 23f). Second, consistent with the previous section, the size-scale of the morphology is much smaller when the dispersed phase is PIB vs when the dispersed phase is PEO.

Finally, it is noteworthy that the phase inversion composition shifts significantly due to particles. In the discussion below, we will present a morphological map of this ternary system, and the corresponding Figure 25 shows that particles increase the PIB:PEO ratio at phase inversion, i.e. particles help maintain PEO phase continuity even when the PEO loading reduces.

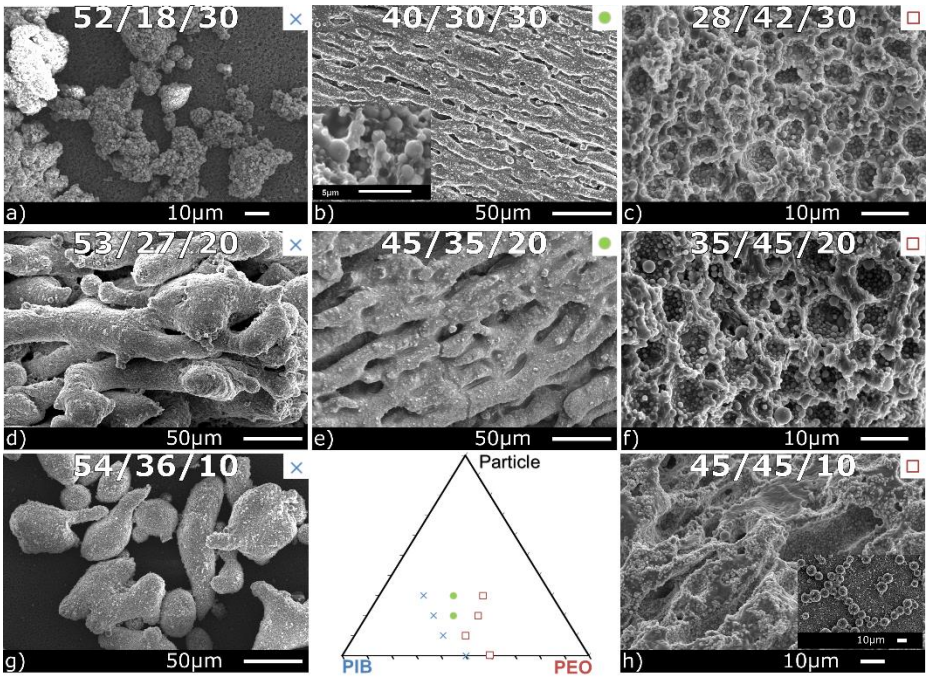

Figure 23. Morphologies near phase inversion at various particle loadings. The PIB/PEO/silica ratios are listed in each image. Left column are PIB-continuous, right column are PEO-continuous, and mid column are co-continuous. The inset in (b) shows a magnified image of structure inside the percolating branches. The inset in (h) shows the PEO dispersed phase using OTS-modified silica particles at same composition. The top right of each image shows the symbol used in the triangle for each type of phase continuity.

4.4.5 Effect of particle wettability on phase inversion

The previous Chapter 4.4.4 concluded that the DCDMS-modified silica particles, which are partially-wetting towards both phases, shift the phase inversion point towards higher PIB:PEO ratio. In fact our previous research on the unmodified silica particles (which are fully-wetted by PEO) showed a similar shift[73, 74]. The fact these two particle types with very different wettability have a similar effect (increase the PIB:PEO ratio at phase inversion) raises the following question:

Does the shift in phase inversion composition depend on particle wettability at all? Or is there some inherent asymmetry in the PEO and PIB fluids themselves that tends to favor PEO-phase continuity regardless of the nature of particles added?

To address this question, a limited number of blends were prepared using the same silica particles, but modified with a different silane, octadecyltricholorosilane (OTS). Since OTS has a long alkyl chain, it makes the particles much more hydrophobic, and hence much more PIB-philic, than DCDMS-modified particles[40]. Two blend compositions, PIB/PEO/silica = 45/45/10, and 36/54/10 were prepared, and the corresponding morphologies are shown in Figure 24. In the 45/45/10 blend (PIB:PEO=1:1) PEO forms the dispersed phase, and particles protrude far out of the PEO drops (Figure 24a) confirming that they are more PIB-philic than the DCDMS-modified particles. Indeed the particles protrude sufficiently far that they can bridge together PEO drops as shown in the inset to Figure 24a. Such bridging was already seen previously, albeit with monodisperse OTS-silica particles at much lower loading[40, 58]. In the 36/54/10 blend (PIB:PEO=2:3) an elongated or co-continuous morphology appears (Figure 24b). We may then summarize the phase continuity results in Table 2. It is immediately obvious that at certain PIB:PEO ratios, the phase continuity does depend on the particle type. Most importantly, at the 1:1 PIB:PEO ratio, the phase continuity of the blends with OTS-modified particles is "flipped" as compared to the unmodified or the DCDMS-modified particles. We therefore conclude that the changes in phase continuity does depend on the wettability of the particles. Specifically, addition of particles favors continuity of the phase that is preferentially-wetted by the particles, as has also been observed in oil/water Pickering emulsions[42, 87, 92-94].

Table 2.Volume ratio of phases near phase inversion

Particles	Approx. PIB: PEO ratio of samples bracketing phase inversion		
	3:2	**1:1**	**2:3**
None		PIB-cont. (Figure 46b)	PEO-cont. (Figure 46c)
unmodified[74]	PIB-cont. (Figure 45)	PEO-cont. Figure 45)	
DCDMS-modified (10%)	PIB-cont. (Figure 22c)	PEO-cont. (Figure 22d)	
OTS-modified (10%)		PIB-cont. (Figure 24a)	Co-cont. (Figure 24b)

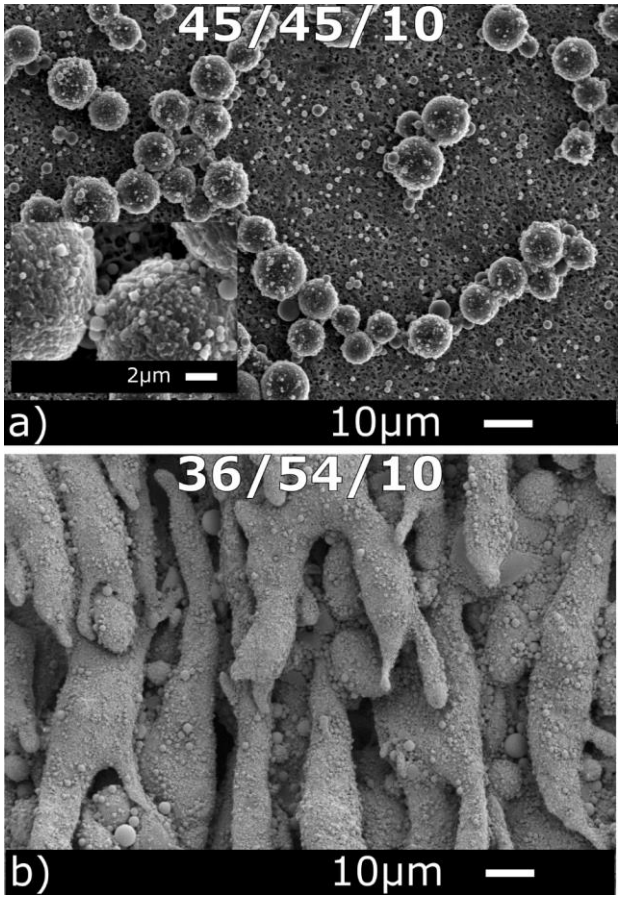

Figure 24. Testing phase continuity of polymer blends containing OTS-modified silica particle at the two compositions (in the format PIB/PEO/silica) indicated in each image

4.5 DISCUSSION

4.5.1 State map and phase inversion

A major goal of this paper was to construct a state map of the microstructure as a function of composition and contrast it with the previously-constructed map for fully-wettable particles. The morphological observations of Chapter 4.4 suggest the morphological state map of Figure 25, where the various morphologies are shown in schematic form. Pendular/funicular structures appear when PIB is the continuous phase and the volume fraction of PEO (ϕ_{PEO}) is less than that of particles (ϕ_p) PEO-in-PIB Pickering emulsion microstructures appear when $\phi_p < \phi_{PEO}$. On the PEO-continuous side, PIB-in-PEO Pickering emulsions occur at all particle loadings, including when volume fraction of PIB (ϕ_{PIB}) is less than that of particles(ϕ_p). In this latter situation, since the particle loading exceeds the PIB drop loading, there must be numerous particles that are not covering the visible PIB drops. We infer that there may be a population of very small PIB-bound particle aggregates dispersed in the PEO phase which are not readily identifiable by our SEM imaging method. The two Pickering emulsion states are separated by a co-continuous morphology, and Figure 24b shows that such a co-continuous state appears even with particles of a very different wettability. To our knowledge, such co-continuous morphologies have never been reported in small-molecule oil/water systems prepared by mixing (co-continuous bijels can be prepared as an arrested state after spinodal decomposition, but not by blending particles into a two-phase oil/water mixture[24, 95]).

We believe that the much lower viscosity of oil/water systems is responsible for this: any complex morphology that may exist under flow conditions rapidly reverts to a conventional spherical-drop morphology immediately after mixing stops. There are sharp differences compared with the state map for fully-wetting particles[74]. The pendular/funicular microstructure of particles bound by PEO is the only one that appears with both unmodified silica (Figure 45) and with the DCDMS-coated silicas (Figure 25). Another feature in common with Figure 45 is that particles stabilize co-continuous morphologies, whereas in the particle-free blends, co-continuous morphologies do not appear. However the microstructural details of the co-continuity are altogether different: the co-continuity in Figure 45 is due to internal jamming of the PEO phase, whereas those in Figure 23e and Figure 24b are likely attributable to interfacial jamming of particles as well as the particle-covered drops within the PEO phase (see below). In the very apt description of Spicer et al[96, 97], the former is endoskeletal jamming, whereas the latter is exoskeletal. Finally, partially-wetted particles greatly affect the morphology across all compositions including low and high particle loadings, and across the entire range of PIB:PEO ratios. In contrast, fully-wetted particles affected the morphology significantly only when ϕ_p exceeded or was comparable to the wetting phase loading, ϕ_{PEO} [73, 74].

The morphological map of Figure 25 is notably asymmetric. The asymmetries include the following:

Pendular/funicular microstructures appear unambiguously only when PEO is the dispersed phase. However we acknowledge that it is difficult to make a firm judgement about morphologies such as Figure 22f. On one hand, the appearance of PIB craters suggests a Pickering emulsion of PIB drops surrounded by PEO. However the drops may also be bonded to each other, similar to particle network dubbed “capillary state suspension” by Koos et al[13].

For the Pickering emulsion microstructures, the dispersed phase has a larger size when PEO is the dispersed phase as compared to when PIB is the dispersed phase.

Near phase inversion, the PEO phase is itself a Pickering emulsion, i.e. the PEO phase contains particle-covered PIB drops.

Addition of particles shifts the phase inversion composition "leftwards" on the composition diagram, i.e. in the presence of particles, the PEO can retain continuity at a higher PIB:PEO ratio than in the absence of particles. Analogously, at $\phi_p \geq 0.2$ where co-continuous morphologies appear, the PIB:PEO ratio for the co-continuous morphologies exceeds 1:1.

The latter three trends all seem to be attributable to preferential wettability of the PEO towards the particles. More specifically, the Pickering emulsion literature suggests that an emulsion is highly stable against coalescence if the continuous phase is preferentially-wetted by the particles, but much less stable if the dispersed phase is preferentially-wetted by the particles[98]. Such differential stability would immediately explain item 2 above, i.e. the PIB drops are small because PEO wets the particles preferentially making the PIB-in-PEO emulsion very stable. Moreover, if the PIB-in-PEO Pickering emulsion is highly stable, but ϕ_{PEO} is too small to ensure PEO phase continuity, it is easy to envision the stable emulsion itself becoming dispersed into PIB (item 3 above). Finally, item 4 above may be attributable to two related causes: faster coalescence of PEO drops implies that continuity of the PEO phase is favored[99], and furthermore, the PEO phase tends to incorporate significant amounts particle-coated PIB drops near phase inversion. Thus, the volume fraction of the PEO phase is effectively "expanded", making it easier for that phase to become continuous.

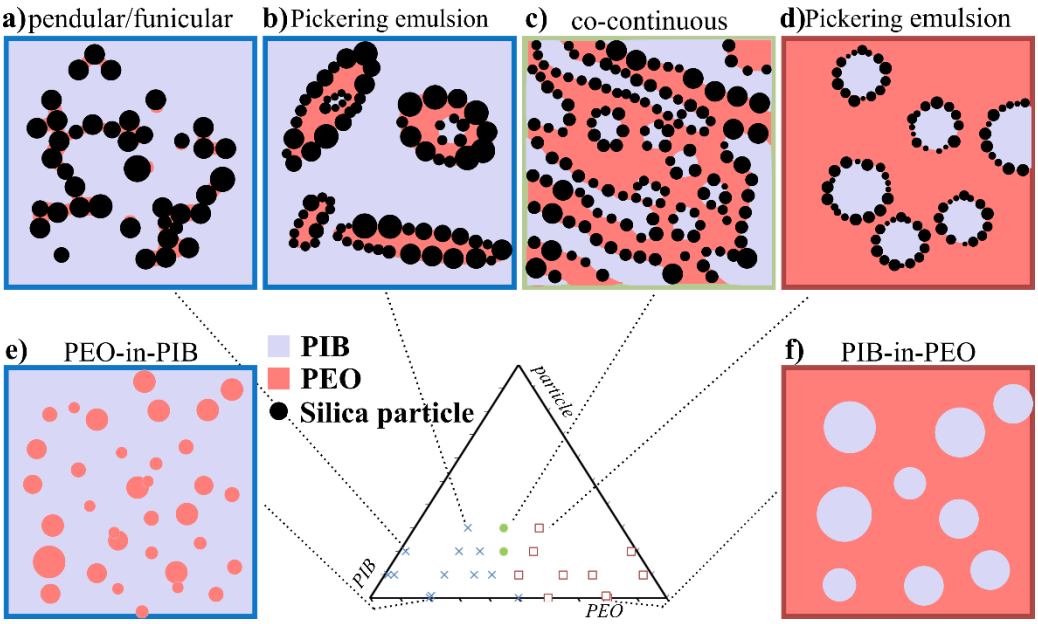

Figure 25.A summary of all the composition studied and different morphology sketches at various compositions. From left to right: (a) pendular/funicular state when PEO is the minority phase; (b) PEO-in-PIB Pickering emulsion; (c) co-continuous state; (d) PIB-in-PEO Pickering emulsion; (e) PIB-in-PEO suspension; (f) PIB-in-PEO suspension.

4.5.2 Interfacial jamming

In the oil/water Pickering emulsion literature, it has been long-recognized that particles can crowd at the interface and give rise to non-spherical drop shapes, a phenomenon generally called interfacial jamming[38, 100]. Similar phenomena have been noted in air/water systems, and the corresponding jammed dispersed phases are often called particle-covered bubbles or liquid marbles[27, 28]. Furthermore, the same idea of interfacial jamming can be exploited to stabilize co-continuous morphologies[24, 101]. Interfacially-jammed morphologies readily appear in our systems at a variety of compositions (Figure 25), and we will discuss them here.

Interfacial jamming appears because particles adsorb at liquid-liquid interfaces very strongly, with the adsorption energy typically being several orders of magnitude higher than kT[98, 102]. As a result, the desorption of individual particles from the interface is unlikely. Moreover, since the particles have homogeneous surfaces (i.e. are not patchy), unlike surfactants, they cannot form micelles. Thus crowding particles lead to interfacial jamming.

Accordingly, the simplest "morphological model" is that interfacial jamming occurs when the liquid-liquid interfacial area is exactly what is needed to accommodate all the particles at the interface. The corresponding area per unit volume (i.e. the cross sectional area of the particles per unit volume) can be estimated as $\phi_p/2D_p$ where D_p is the diameter of the particles. Consider now an emulsion-type morphology (with either PEO or PIB as the dispersed phase) with L being lengthscale of the morphology. For example, L may be regarded approximately as a mean drop size (if the dispersed phase is in the form of round drops), or a mean cylinder size (if the dispersed phase is roughly cylindrical). The interfacial area per unit volume of the morphology is therefore roughly ϕ_{disp}/L where ϕ_{disp} is the volume fraction of the dispersed phase. The pre-factor of 4 is the exact value for monodisperse cylindrical geometry (the corresponding pre-factor would be 6 for monodisperse spheres, and 2 for lamellae). If the morphology is on the verge of jamming, we can equate the above two areas per unit volume to obtain $L^* = D_p \frac{\phi_{disp}}{\phi_p}$. This L^* is the largest possible lengthscale for the dispersed phase if all the particles reside at the interface; specifically, if $L < L^*$ (e.g. under intense mixing conditions), then interfacial jamming cannot happen and hence the dispersed phase will remain spherical. On the other hand if the flow is relatively weak, the

dispersed phase will coarsen, but become no bigger than L^*. We acknowledge that this model does not predict a value for average droplets size of the dispersed phase, which is determined by the volume fraction of the dispersed phase, the rate of coalescence of the dispersed phase, and flow strength. This model only predicts the largest size the dispersed phase can have, which is also the sizescale below which the dispersed phase must be unjammed and hence spherical. This model is based on assumption that the particles are monodisperse, whereas in reality, the smallest particles are most effective in covering interfaces. Nevertheless, L^* provides a first order estimate of the largest sizescale of the microstructure that can avoid jamming.

Of all the samples examined, Figure 21c is the only morphology that is not jammed, i.e. has unambiguously spherical drops whose interface is not crowded with particles. Indeed, for this sample $L^* = 20D_p = 40\,\mu m$ is predicted, whereas most drops are comparable or smaller in diameter. This is consistent with the idea that if $L < L^*$, interfacial jamming will not happen. For most samples with PIB as the dispersed phase, the L^* is found to be close to the morphological lengthscale estimated from SEM images. For instance, for Figure 4f, $L^* = 1.75\,D_p = 3.5\,\mu m$ is calculated, and a majority of PIB drops appear to have a diameter near $10\,\mu m$. In contrast, for the samples with PEO as the dispersed phase, the calculated values of L^* underestimate the morphological sizescale. For instance, for Figure 23d $L^* = 1.35\,D_p = 2.7\,\mu m$ is calculated whereas the interfacially-jammed dispersed phase has a typical width of a few tens of microns.

For these PEO-dispersed phase samples, the fact that $L \gg L^*$ suggests that at least one of the assumptions underlying the calculation of L^* must be incorrect. For instance, if some of the particles stay dispersed into one of the bulk phases (i.e. behave similar to fully-wetted particles), the basic assumption that the all the particles are interfacially-adsorbed is violated. In fact, the Section 4.1 and the inset to Figure 23b support a different view, that the morphology is more "topologically" complex than a simple emulsion. Specifically, the PEO phase is itself a Pickering emulsion which incorporates particles.

The central conclusion therefore is that in such ternary particle/liquid/liquid systems, co-continuous morphologies cannot be readily tuned by changing particle loading. For instance, in the bijel literature, the lengthscale of the co-continuous structures was found to be proportional to the reciprocal of the particle loading[24, 95]. This was based on the same picture of interfacial jamming as above (indeed above we also calculated $L^* \propto \frac{1}{\phi_p}$). However in the co-continuous morphologies developed by blending, such simple tuning of lengthscales may not be possible; the system "decides" whether particles should be located at the interface of the co-continuous structure or on drops within one of the phases. Indeed other microstructures may be possible under some conditions, e.g. a co-continuous morphology in which one of the phases is a pendular network.

4.6 CONCLUSION

To summarize, we have conducted a comprehensive morphology-composition mapping of a ternary mixture composed of two molten immiscible polymers (polyisobutylene and polyethylene oxide) and spherical silica particles which are partially-wetted by both polymer phases. To our knowledge, this study, similar to our previous study of the fully-wetting case, encompasses the widest composition range examined for a single ternary liquid/liquid/particle system. The partially-wettable particles significantly affect the morphology across the entire range of compositions. The various morphologies observed include pendular/funicular aggregates of particles, Pickering emulsions, co-continuous morphologies, and (when the particle strongly prefer one fluid) particle-bridged Pickering emulsions. The particles induce coalescence of the dispersed phase at dilute particle loading, create interfacially-jammed Pickering emulsions, and stabilize interfacially-jammed co-continuous morphologies. At least one of the morphologies appears to be topologically-complex: a co-continuous morphology where one phase is a Pickering emulsion. This suggests that such ternary blends may adopt microstructures that are difficult to predict based on simple considerations of wettability and composition.

Many of the particle effects are asymmetric, i.e. the morphology is sharply different depending on which fluid is the continuous phase. The asymmetries are likely attributable to the modest preference of the particles towards one of the phases, polyethylene oxide. Most importantly, the particles shift the phase inversion composition such that polyethylene oxide, the phase that preferentially-wets the particles, tends to become the continuous phase.

In combination with the previous research on the fully-wetting case, this research represents the most detailed morphological mapping of a ternary liquid/fluid/particle mixture in the parameter space defined by the composition and the wettability of the particles. It would be

interesting to see if other systems with different chemistry and particle sizes show similar morphologies at similar composition and particle wettings. If so, they would confirm the idea that diverse ternary systems share a somewhat universal microstructural map.

5.0 RECOVERY OF PARTICLE-FILLED DROPLETS IN IMMISCIBLE POLYMER BLEND

5.1 CHAPTER PREFACE

Materials contained in this chapter will be submitted as a research article.

List of Authors: Junyi Yang, and Sachin S. Velankar

5.2 INTRODUCTION

It has been long-recognized that a blend of two immiscible Newtonian liquids is viscoelastic. The source of this viscoelasticity is interfacial tension. Specifically, under flow conditions, the interfacial area within the blend is larger than under quiescent conditions and moreover it has some net orientation, i.e. the area tensor is not isotropic. The interfacial energy associated with this excess surface area provides a mechanism whereby mechanical energy of deformation can be stored rather than dissipated. The interfacial orientation provides a mechanism for developing net stress so that blend becomes viscoelastic.

Such viscoelasticity is manifested in a variety of rheological phenomena including gradual growth of stress during startup of flow, time-dependent stress relaxation or time-dependent elastic recoil after cessation of flow, and additional relaxation processes appearing in oscillatory frequency sweep experiments.

On the other hand, interfacial tension can also be a cause for yielding phenomena in particulate systems. The most familiar example of this is when a small amount of water is mixed with dry sand to yield wet sand which has a yield stress (and a non-zero modulus prior to yield)[9, 13]. The same occurs when a small amount of particle-wetting fluid is added to a suspension of particles in another fluid. In such cases, the particle-wetting fluid is present in the form of small menisci that bind together the particles into a large scale network[5, 7, 12, 103]. Since flow of such a suspension requires breaking some of the capillary "bonds" between the particles, the suspension develops a yield stress. As will be discussed later, such a suspension is not especially viscoelastic; for example wet sand does not show significant recoil after being deformed[8, 9].

Therefore, considering a ternary mixture comprising particles suspended in fluid with another particle-wetting fluid added, one may imagine two extremes of composition. In the first, the particle-wetting fluid is dilute whereas the particles are concentrated, and hence the mixture has the morphology of a meniscus-bound network (Figure 26a). Rheologically such a network may be regarded as elastoplastic: it has a modulus at small deformation, and a yield stress. In the other extreme, it the particle-wetting fluid is concentrated whereas the particles are dilute, thus the mixture has a droplet-matrix morphology (Figure 26c). Such a mixture is expected to be a viscoelastic fluid with no yield stress. This transition from elastoplastic behavior to a viscoelastic fluid behavior due to composition changes is the topic of this paper.

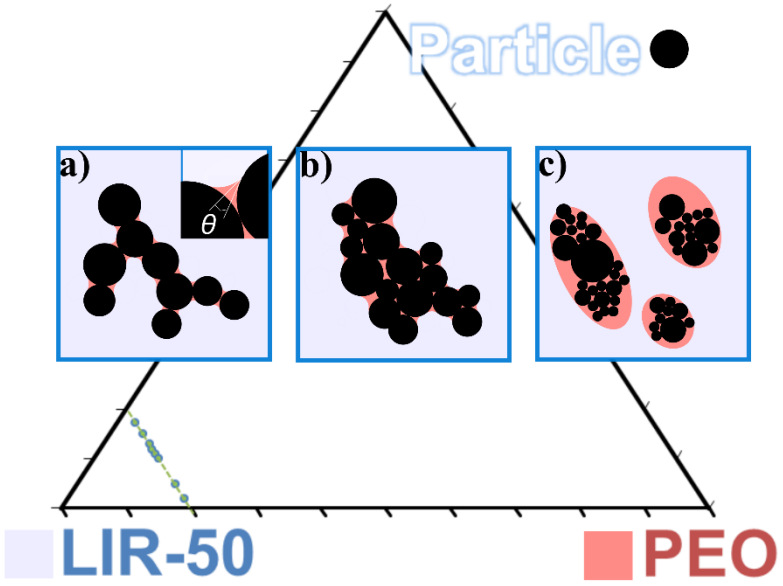

Figure 26. Compositions examined following a 20 vol% combined phase dashed line. From left to right, three morphologies are sketched: a) pendular state; b) capillary aggregates; c) particle-filled droplets.

In Figure 26, where compositions are indicated on a triangular composition diagram. The three vertices correspond to the materials used in this paper (details below): silica particles, liquid polyisoprene (which is the continuous phase liquid in all the samples in this paper) and liquid polyethylene glycol which is a minority liquid phase which preferentially-wets the particles. The dashed line shows a composition trajectory that spans the two extremes of composition mentioned in the previous paragraph. In this paper, we conduct rheological and in situ morphological investigations of several samples along this composition trajectory. The focus is on one specific aspect of viscoelasticity, viz. creep recoil upon cessation of shear, and we investigate how the magnitude and the kinetics of recoil vary along the composition trajectory.

The outline of this paper is as follows. In Section 5.3 we describe the materials and methods. Section 5.4.1 describes the in situ morphological observations during creep recoil, and Section 5.4.2 describes the corresponding rheological measurements. Section 0 briefly discusses the dependence of retardation on composition.

5.3 EXPERIMENTAL SECTION

5.3.1 Materials and sample preparation

Polyethylene oxide (PEO, $\rho \approx 1.1$ g/ml, Mw$\approx$600 g/mol, viscosity < 0.1 Pa·s) and polyisoprene (LIR30, viscosity 130 Pa·s) was purchased from Fluka and Kuraray respectively. The particles used are hydrophilic glass particles with average diameter of ~10μm obtained from Karlsruhe Institute of Technology.

5.3.2 Rheological Measurement and Testing protocol

Rheology tests were conducted on the Anton Paar rheometer with a 40 mm parallel glass plate geometry and built *in in-situ* microscope at 20 °C. The sample was loaded within a gap of 200 μm

. Video capture function was activated to simultaneously record the rheological parameters and corresponding optical image of localized microstructure.

Oscillatory shear, steady state flow and creep-recovery tests were. An example of testing protocol is shown in Figure 27: the sample was first sheared at 480 Pa for 2 minutes in order to attain enough strain units to reach steady state flow condition. A 0.7-second step shear was applied

at same stress level (480Pa) then removed for 5 minutes for strain recovery. The video recording starts from the end steady state flow toward the end of third recovery to 1) capture the instantaneous elongated particle filled droplet morphology; 2) measure the time required for such structure to recover; 3) investigate the relaxation and aspect ratio dependence on stress and composition. After the first sequence, same testing protocol was conducted twice more at lower stress level (240Pa/120Pa). The initial steady state shearing time varied for different stresses to ensure same strain units were applied before the following creep-recovery process (ie. 480Pa for 2 minutes and 240Pa for 4 minutes, etc). Oscillatory shear experiment was conducted right after the creeping, both storage and loss moduli were retrieved from a frequency sweep range of 0.05% to 300% at fixed strain amplitude of 1%. The modulus results along with the in-situ visualization can be used to determine whether the system is in pendular network state or capillary aggregate state. Limited steady state flow experiment were also conducted to measure the yield stress (σ_y) and infinite shear viscosity ($\dot{\gamma}_\infty$) by increasing shear rate from 0.1/s to 100/s for selected compositions.

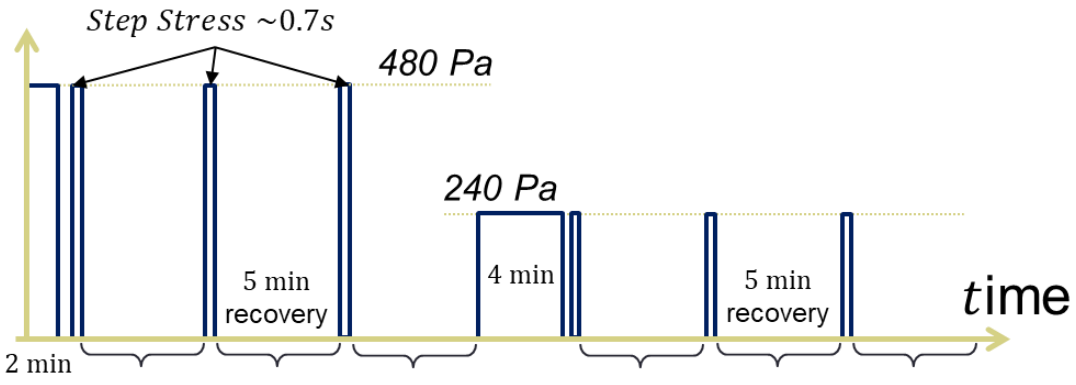

Figure 27. Schematic diagram of test protocol of creep-recovery sequence (only 480Pa and 240Pa are showing here).

5.4 RESULTS

5.4.1 In-situ visualization on droplet recovery

As is mentioned in the introduction, the sole source of viscoelasticity in the current mixtures is interfacial tension, and more specifically, shape relaxation of the interface. The advantage of in-situ visualization is to be able to correlate the morphology evolution deformation to instantaneous mechanical response. Accordingly, we will first discuss the structural changes during recover in this section, and the corresponding mechanical recovery in the following section. Similar results can be obtained, albeit with much more effort, by imaging the morphology quenched from various stages of morphological evolution, and comparing the sequence of images with the rheological changes[43, 104].

Only the 480 Pa stress is discussed for illustration, since a stress level 480 Pa is beyond the yield stresses for all compositions. Similar results are obtained at the two lower stresses, and are shown in the ESI. Of the eight blend compositions ranging from 2.75 vol% to 18 vol% of PEO, four were chosen in Figure 28 showing their morphologies at different time set during relaxation. Our previous studies showed under quiescent condition, the structure of ternary blends varies from *pendular/funicular network*, *capillary aggregates*, to *particle-in-PEO droplets* depending on the relative volume ratio of wetting phase (PEO) to particles[1, 74]. And images captured during relaxation suggest that morphologies respond differently upon stress removal after steady state shear flow.

The top row of Figure 28 corresponds to dilute PEO loading where the ϱ value is 0.33(Figure 28a to d). At this ϱ value, there is not adequate PEO to completely engulf the particles,

and the images indicate pendular/funicular clusters of glass particles bonded by PEO menisci. During shearing process, those clusters predominantly showed tumbling movement rather than deformation along the shearing direction, i.e. the particulate clusters were more-or-less rigid. Once the shearing ceased, there was almost no visible change in clusters suggesting negligible deformation during shear. Upon increasing the amount of PEO (second row), a capillary particle aggregate state emerges (Figure 28e to i) corresponding to complete encapsulation of particles by PEO. However the resulting combined phase is highly filled with an internal particle volume fraction of 65%. The images show that the capillary aggregates are highly elongated along the shearing direction, and upon cessation of shear, they do not undergo significant shape relaxation over the entire 5 minute observation period. This arrest of non-spherical drop shapes is entirely attributable to the internal jamming within the drops. Further increase in PEO loading (third row) lowers the internal particle fraction sufficiently that the combined phase is capable of "normal" deformation and relaxation, although a few non-spherical shapes are still evident. We presume that some drops have slightly higher particle loading than others, this leading to slower shape recovery (Figure 28h to k). Incidentally, the largest drops in this blend have diameters of ~ 50 microns which is comparable to the gap size, and hence at this composition at least, the morphology may be affected by finite gap width effects.

The last row corresponds to a ϱ value of 3, and hence the combined phase has a particle loading of only 25%. Under these dilute conditions, the behavior resembles that expected from a typical droplet-matrix blend where the drop viscosity is far lower than the matrix viscosity: under steady shear conditions, the dispersed phase is highly elongated and in the form of fibrils, with rapid reversion to spherical shapes after cessation of shear (Figure 28i to o).

Incidentally we note that much of the reversion to spherical shapes occurs by capillary instabilities of the elongated fibrils, rather than shape recovery of the fibrils.

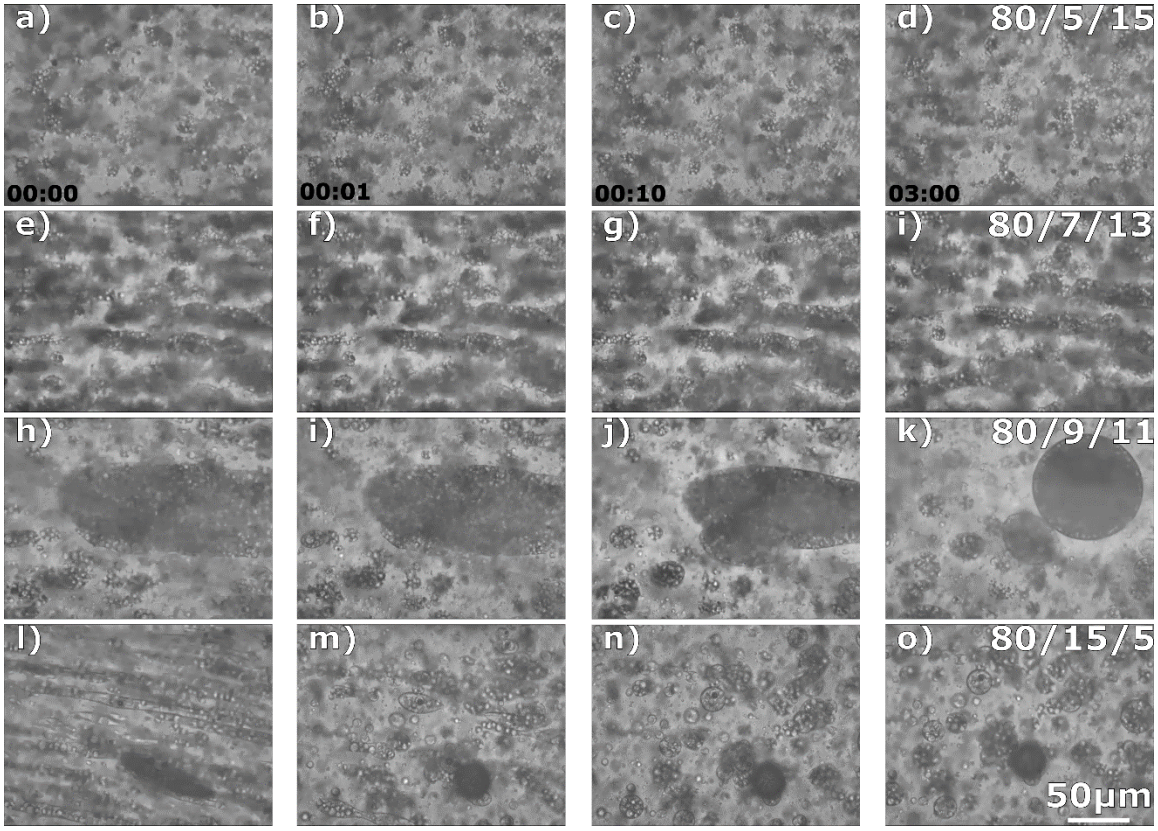

Figure 28. Screenshots of the structure recovery process 1 second, 10 seconds, and 3 minutes after the shearing ceases from in-situ microscope. The compositions are labeled on the up right corner of each row in the format of LIR/PEO/particle volume ratio. The shearing direction went horizonal to the right.

5.4.2 Composition dependence on strain recovery

We now turn to the creep recovery after cessation of shear by comparing the strain recovery measurements for compositions selected in Figure 28. In general, Figure 29 complies with conclusion made in previous section with serval noteworthy difference: First, while there appeared no significant changes in shape from 10 seconds to 3 minutes mark for some compositions, the recovery continued accordingly; Second, even at dilute PEO condition (2.75%) whose deformation of the structure was not obvious by eyes, a 5% strain recoil is still detectable at the end of observation window; Third and most importantly, the speed of recovery is not monotonic. Here we use the time it took to reach 60% of its ultimate recoverable strain as the total retardation time by first approximation. For both highest and lowest PEO content sample, 60% of the ultimate recoverable strain reaches within the first 10 seconds, whereas it takes more than 20 and 40 seconds for 80/7/13 and 80/9/11 blend respectively.

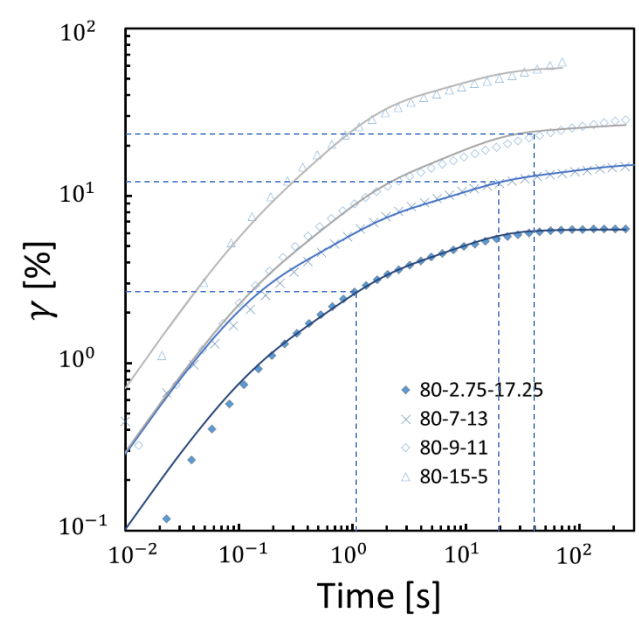

Figure 29. Strain recovery at various compositions. (the legends display in a format of LIR-PEO-particle in volume fraction). The smooth lines are corresponding fitting curves. The dashed lines indicate the time required to reach 60% of the ultimate recovery strain.

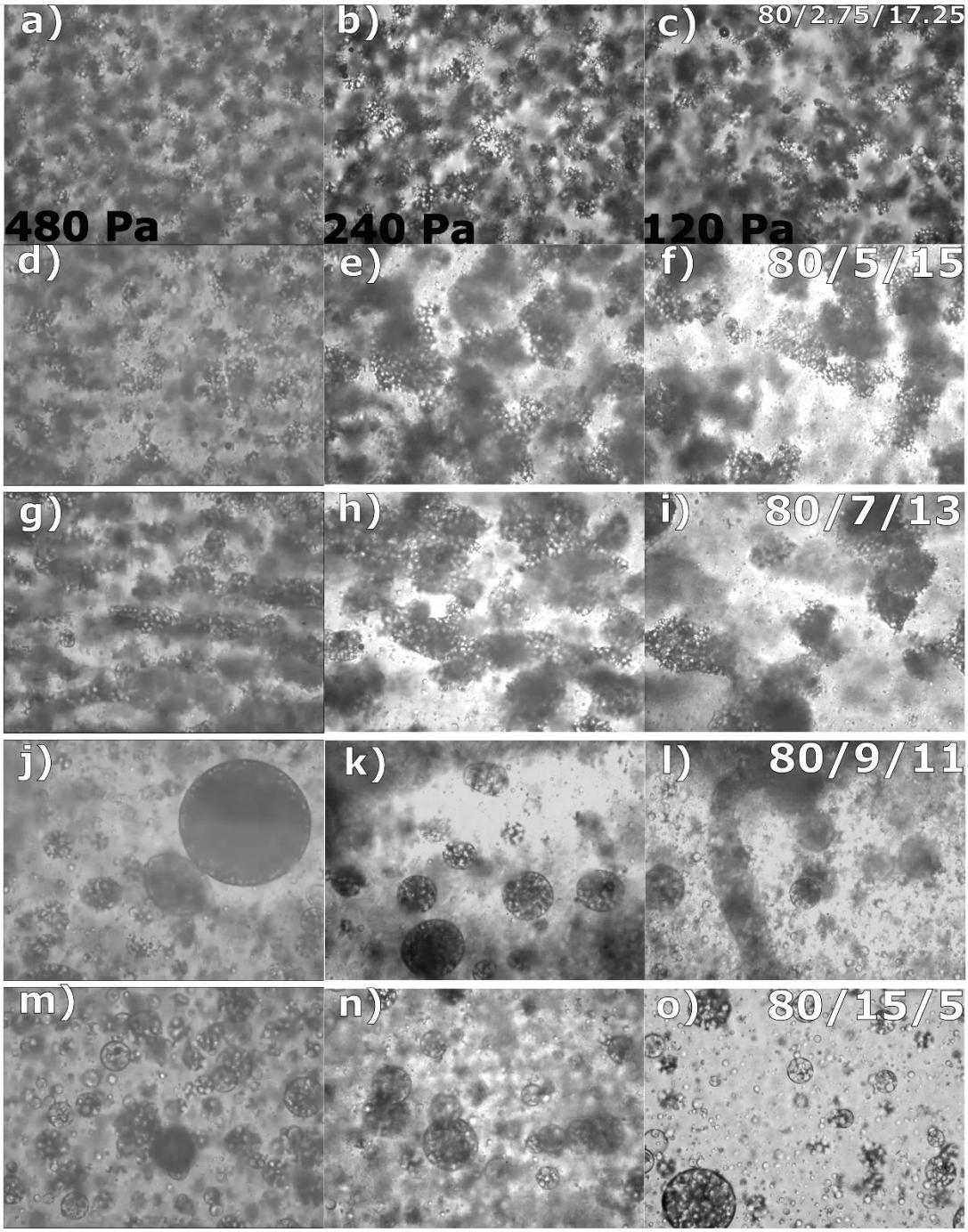

Figure 30. Screenshots of ternary blend after fully recovery from different stress level. The compositions are labeled on the upper right corner of each row in the format of LIR/PEO/particle volume ratio. The shearing direction went horizonal to the right.

5.5 DISCUSSION

5.5.1 Retardation spectrum at various compositions

As is stated in the section above, the total retardation time of the blends does not increase accordingly with the increasing amount of PEO. In order to get a more qualitive judgement on retardation time, Vinckier et al[43] proposed the recovery behavior following exponential kinetics:

$$\gamma_r = \gamma_\infty \left(1 - exp\left(-\frac{t}{\tau}\right)\right) \quad \textbf{(7)}$$

Where γ_∞ is the ultimate recovery, τ is the retardation time. However, this model with single exponential kinetics provides very poor fits to the experimental data. Strictly, one needs to describe the results using a continuous retardation spectrum $L(\tau)$. Yet evaluation of a continuous spectrum requires sophisticated numerical techniques with attendant questions of whether other spectra may capture the measured data equally well. Accordingly, we will adopt a discrete version of the same where:

$$\gamma_r = \sum_{i=1}^{n} \gamma_i \left(1 - exp\left(-\frac{t}{\tau_i}\right)\right) \quad where \quad \gamma_\infty = \sum_{i=1}^{n} \gamma_i \quad \textbf{(8)}$$

We attempted fits with various values of n, i.e. *n* equally-spaced retardation times were specified, and the corresponding γ_i values were treated as fitting parameters. By trial and error we

found that $n = 4$, with retardation times of 0.01s, 1s, 10s and 100s, were adequate to both capture all the data accurately, but at the same time as avoid problems with uniqueness. The corresponding fitting curves are shown as solid lines in Figure 29. The values of the fitted $\gamma_i's$ are shown for all compositions shown in Figure 31 below, and may be regarded as the approximate retardation spectrum at each composition.

Two trends are immediately obvious in the spectra. The first is the increase in the maximum γ_i value with increasing PEO content. This is simply a reflection of the increasing γ_∞, i.e. increasing elasticity, as PEO loading increases. The second is the non-monotonic position of the peak: the composition 80/9/11 has its peak shifted farthest to the right, i.e. to the longest retardation times, whereas the peak is shifted to shorter times a both lower or higher PEO contents.

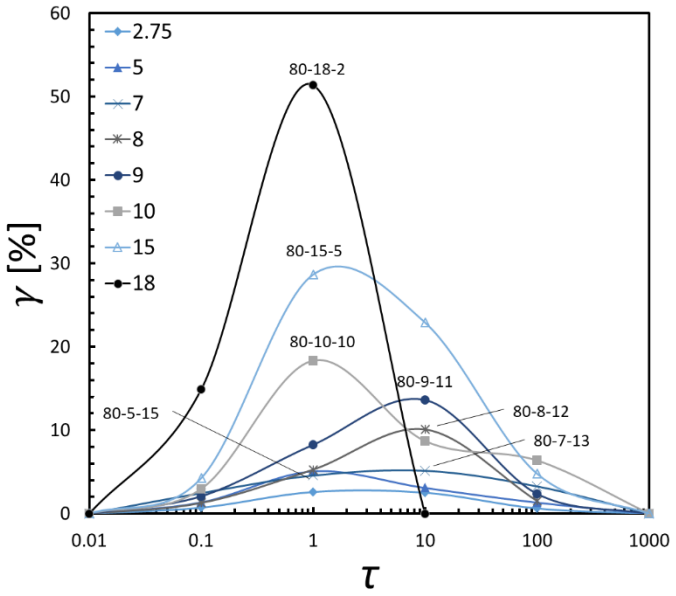

Figure 31. Relaxation spectrum of LIR-PEO-particle system at various compositoins. τ_1, τ_2, τ_3 *and* τ_4 are chosen as 0.1, 1, 10 and 100 seconds listed in the x-axis. When PEO volume fraction is more than 50% in the combined phase, the highest relaxation time scale falls at 1 second. Otherwise, the highest relaxation period falls at 10 second indicating a slower relaxation. The legends show the PEO fraction and the data labels show the peak position for each of the composition.

For simplicity of comparison, it would be convenient to quantify the recovery using just two parameters, one that captures the magnitude of the recovery, and the other its mean timescale. Obviously $\gamma_\infty = \sum_{i=1}^{n} \gamma_i$ is the best measure of the strength of the recovery. A mean timescale can be defined as:

$$log\, \tau_{ave} = \frac{\sum_i \gamma_i log\, \tau_i}{\sum_i \gamma_i} \quad \textbf{(9)}$$

We acknowledge that this is not the only possible definition, and other definitions have been used previously with different weightings for each more[105]. The values of $\gamma_\infty$and τ_{ave} are

shown in Figure 32. The ultimate recovery increases monotonically with increase PEO loading, whereas the mean retardation time is not monotonic. The reasons for this non-monotonic behavior can be immediately related to the microstructure: with decreasing ϱ (PEO-to-particle volume ratio), the combined phase becomes increasingly filled, thus developing high viscosity and possibly solid-like rheology. The combined phase retains sufficient mobility to coalesce, and hence the drop size, and interfacial deformation under steady shear conditions, both grow. While interfacial tension driven relaxation still occurs (as proved by the recovery), this process requires significant rearrangement of the particles within the drops and hence is greatly slowed. Once the rho value reduces below 0.66, or the particle fraction in the combined phase reaches over 60%, the droplets loses sufficient mobility that it cannot coalesce readily and the size of the dispersed phase reduces sharply. Recovery no longer requires large shape changes, and hence proceeds more rapidly.

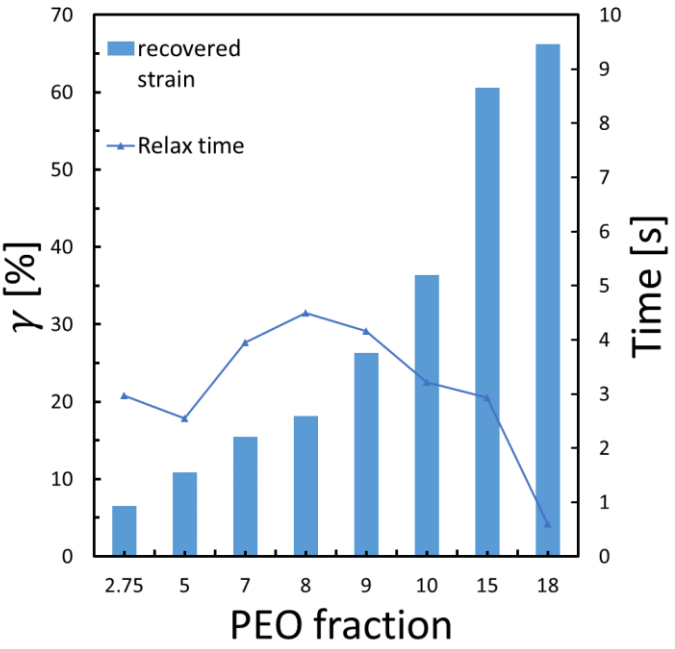

Figure 32. Summary of both ultimate recovered strain and average relaxation time for each composition whose PEO fraction is listed in the x-axis.

5.5.2 Dependence of droplets recovery on shear stress

To further understand the effect of creep stress on droplets recovery, the creep-recovery process was repeated twice more at lower stress levels (240Pa & 120Pa). The summarized ultimate strain recoil and retardation time for each stress level are shown in Figure 33 respectively. It is apparent from the images that the stress dependence on either strain recoil or retardation time is determined by its morphology. When the blend is within particle-fill droplets state (shown in open symbols), the ultimate recovery is proportional to the stress applied while the retardation time is almost independent with stress. On the other hand, when there is not enough PEO to engulf all the surface of the glass particles (i.e. capillary aggregates), the dependence alters (shown in filled symbols):

the retardation time is now inverse-proportional to stress and ultimate recoil is indifferent from stress variation. Similar behavior can be found in the emulsion literature which suggests that both the level and time scale of the immiscible blend recovery after steady state shear are very sensitive to the morphology and shearing condition. More specifically, according to the model predicted by Vinckier[43, 46], the ultimate recoil can be given by:

$$\gamma_{r,\infty} = \frac{\sigma_{12}^{0} R \eta_m}{\eta_0 \alpha} f(p, \phi) \qquad \textbf{(10)}$$

where σ_{12}^{0} is the shear stress, R is the radius of the droplets, η_m matrix viscosity, η_0 emulsion viscosity, α interfacial tension, p the viscosity ratio, ϕ volume fraction of the droplets. $f(p, \phi)$ is a function which increases with the viscosity ratio. Noted that in our experimental scenario, the observation area is too narrow to gather enough droplets and make quantitative analysis on size distribution in a single frame of image. Thus, we only use this model to predict the stress proportionality with strain recoil. Since the volume fraction of PEO-and-particle combined phase was fixed at 20 vol%, and interfacial tension and matrix/emulsion viscosity can be considered constant, the strain recoil is merely depending on radius of the droplets and viscosity ratio according to Equation 10. Judging from Figure 30 d through Figure 30 f as the blend is at capillary aggregate state, the size scale of the aggregates expands with decreased shear stress since lower shear rates prompt coalescence of particle clusters[76]. In fact, under steady state condition, the radius of the droplets is inverse-proportional to the shear stress: $R \propto \frac{1}{\sigma_{12}^{0}}$. This explains that the recoil strains are linear in the capillary aggregates state. However, with increasing ϱ value, the

maximum average radius of the droplets reaches to a plateau at around 50 μm regardless of the shear stress Figure 30 g through Figure 30 o. Because there is a 200 μm gap constrain in our experimental scenario. Therefore, according to Equation 10, $\gamma_{r,\infty} \propto \sigma_{12}^{0}$ once particle-filled droplets are formed. Similarly, the retardation time for emulsion characteristics is given by Graebling et al[104]:

$$\tau = \frac{R\eta_m}{4\alpha} f(p, \phi) \tag{11}$$

According to Equation 11, the retardation time is proportional to radius of the droplets. The results in Figure 33 also suggest that the retardation time is inverse-proportional to stress at capillary aggregates state (filled symbols) and almost independent to stress at particle-filled droplets state (open symbols).

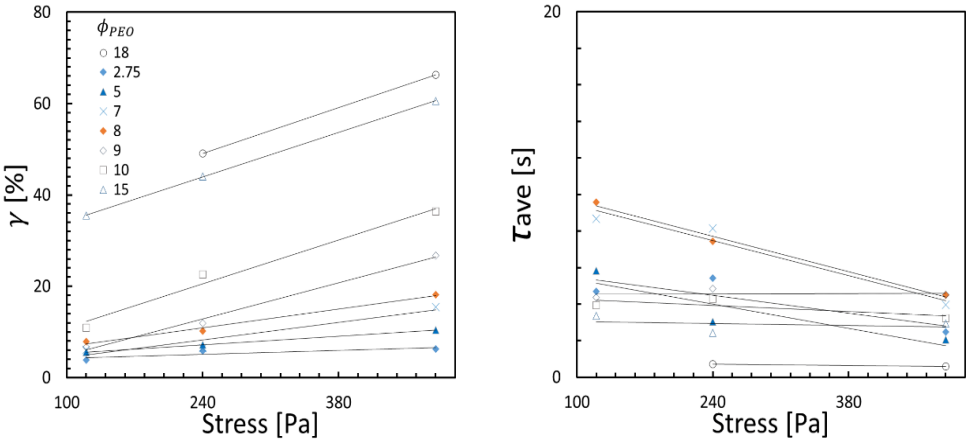

Figure 33. The dependence of ultimate strain recoil and retardation time on steady state shear stress.

5.6 CONCLUSION

To summarize, we have conducted a comprehensive morphology and rheology study on strain recoil after steady state shear with particle-filled polymer suspension. The volume of dispersed combined phase droplets (glass particle and PEO) were fixed but the morphology of the droplets varies with various particle content inside the droplets. To our knowledge, such study on strain-recovery has never been done on particle-filled droplets. In general, the strain-recovery behavior follows a multi-stage exponential kinetics. The ultimate recovery strain increase with increasing particle loading while the average retardation time is longest with around 50% of the particle loading.

Simultaneous video capture function was activated during the creep-recovery measurement to help explain the relationship between droplets morphology and blend recovery profile. Depending on particle content in the droplets, various morphologies were observed including pendular/funicular network, aggregates of particles and particle-filled droplets. Both pendular/funicular and particle aggregates display rapid recovery and small recoil (in the order of 1%). Once particle-filled droplets are formed, the creep-recovery profile is determined by two factors: on the one hand, the extend of the recovery is dominated by the interfacial tension; on the other hand, the fact whether the droplets are internally jammed significantly extends the total retardation time required.

The effects of creep stress are also discussed in the paper. Under steady state condition, the droplets size up with decreasing shear stress, and corresponding strain recoil is proportional to the shear stress. However, such effect is limited when the droplets size reach to the gap constrain.

APPENDIX A

SUPPLEMENTARY MATERIAL TO "PREPARATION AND YIELDING BEHAVIOR OF PENDULAR NETWORK SUSPENSIONS"

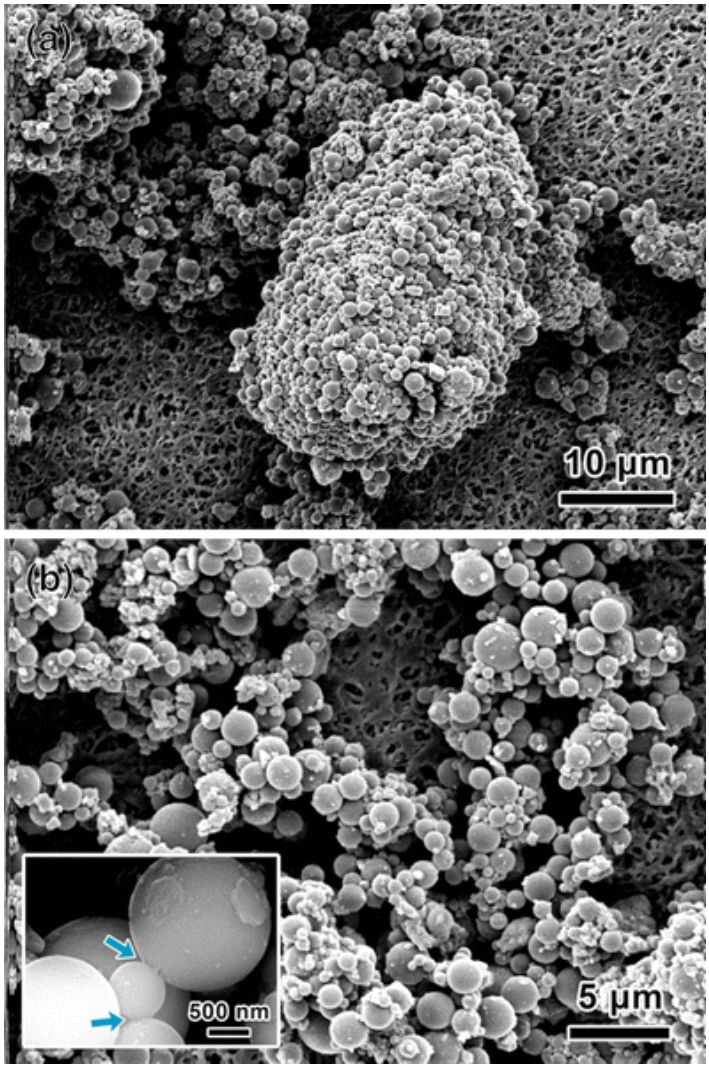

Figure 34. SEM pictures of the PIB/PEO/SP–A blend after dissolution of the PIB matrix. (a) A capillary aggregate. (b) Pendular network. The inset shows a closer view of capillary bridges (pointed out by the blue arrows) between particles of different sizes in a branch of the pendular network. Figure reproduced from Domenech and Velankar, Rheol. Acta, 53, 593, 2014, with permission from Springer.

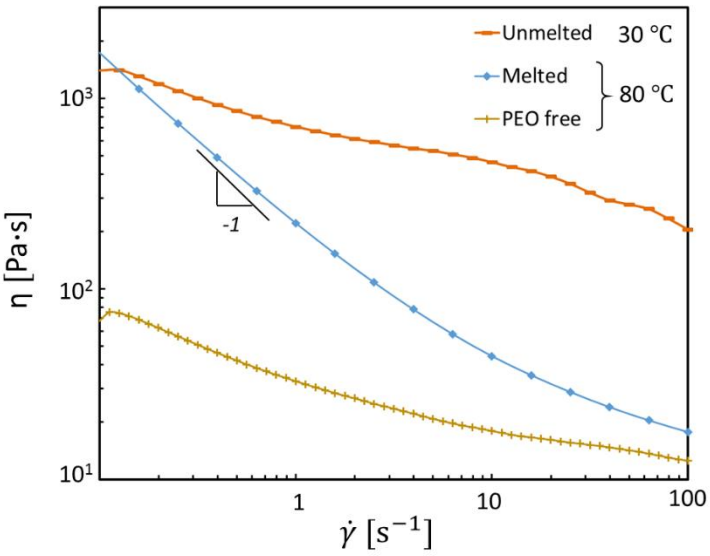

Figure 35. Viscosity versus shear rate curves for polymer blend (PIB/PEO/SP =76.8/3.2/20): 1. At 30℃ below melting temperature; 2. at 80℃ above melting temperature; and 3. Binary PEO free blend at 80℃ (replacing PEO with corresponding amount of particle in volume).

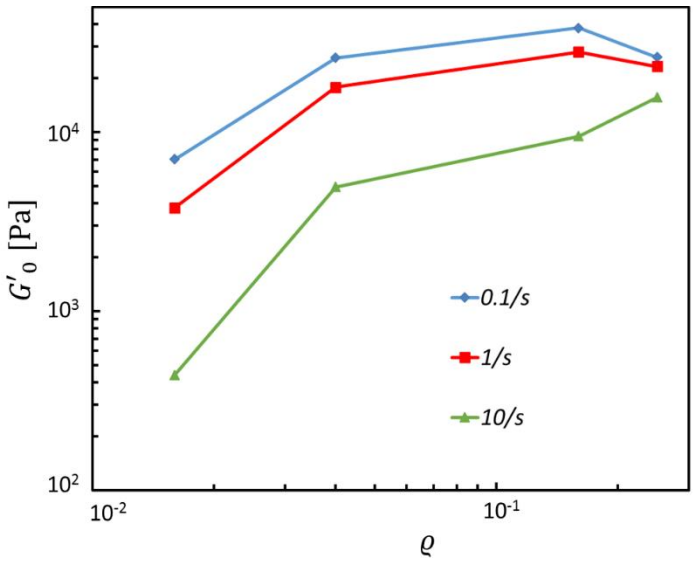

Figure 36. Zero shear storage modulus (values in amplitude sweep tests at 0.01% strain) for polymer blend with same particle loading (20^{vol}%) but various ϱ values and different pre-shear history: after 10 minutes shear at 0.1/s (blue diamond), 1/s (red square) and 10/s (green triangle).

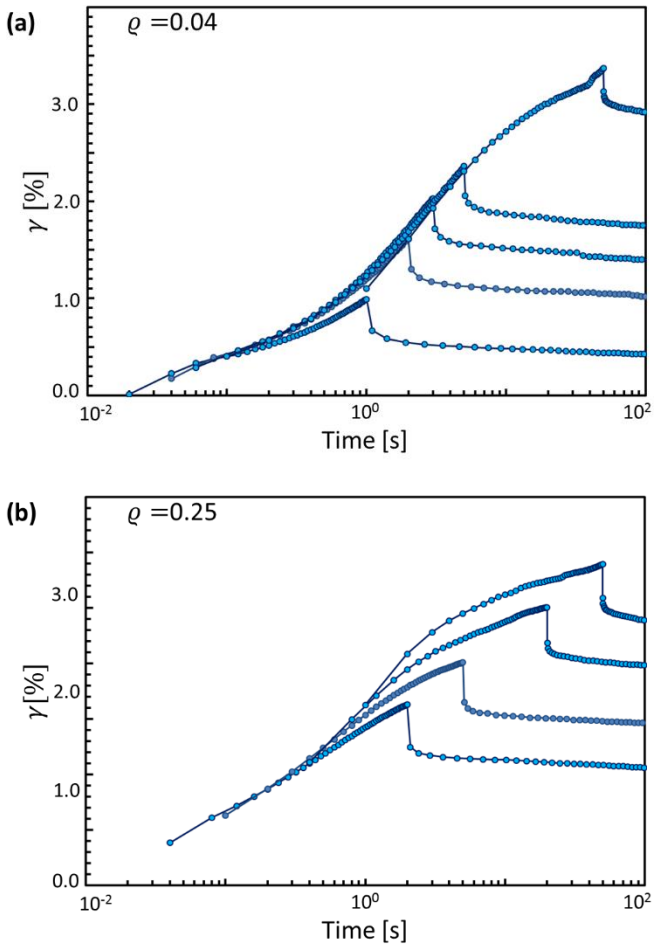

Figure 37. Creep-recovery test results for ternary mixtures blends with 20^{vol}% particles at two different PEO loadings: (a) PIB/PEO/SP= 79.2/0.8/20 at 20 Pa; (b) PIB/PEO/SP= 75/5/20 at 120 Pa. Both stresses were set below the yield stress for the corresponding sample. The creep step was interrupted at various times before recovery

The following two figures use materials and methods different from those in the main paper. The ternary mixtures are composed of polyisoprene (LIR30 from Kuraray, viscosity 130 Pa.s) as the continuous phase, glass particles (~10 micron diameter), and glycerol as the wetting fluid. The sample composition by volume is LIR30/glycerol/glass = 94/1.1/4.4 giving a ϱ value of 0.25. The glycerol was pre-dispersed into the LIR30, followed by adding the particles. All mixing was performed by hand with a spatula.

For flow visualization experiments, the sample was loaded in a shear cell at room temperature. The shear cell is a parallel plate device capable of linear translation. The maximum usable strain was roughly 15 strain units, and hence instead of steady shear, oscillatory strain was applied on the sample. Figure 38 illustrates the formation of aggregates at low frequency (which corresponds to a low maximum shear rate), followed by breakdown upon increasing the frequency, followed by reformation of the aggregates at low frequency. Figure 38 also includes LAOS modulus data obtained with the same sample and indeed the storage and loss moduli decrease when the pendular network is ruptured, but recover (at least partially) when sheared. Note that the particle volume fraction in these samples (4.4%) is far less than in the main paper (20%) and hence these samples are only weakly-solidlike. Hence the rheological changes corresponding to network rupture are only modest.

Figure 39 illustrates morphological changes during LAOS, and the same sequence of images are available as a movie file entitled LAOSSequence.mpg.

We are grateful to Dr. Erin Koos for permitting use of her shear cell and microscope, and assistance with setting up the experiment.

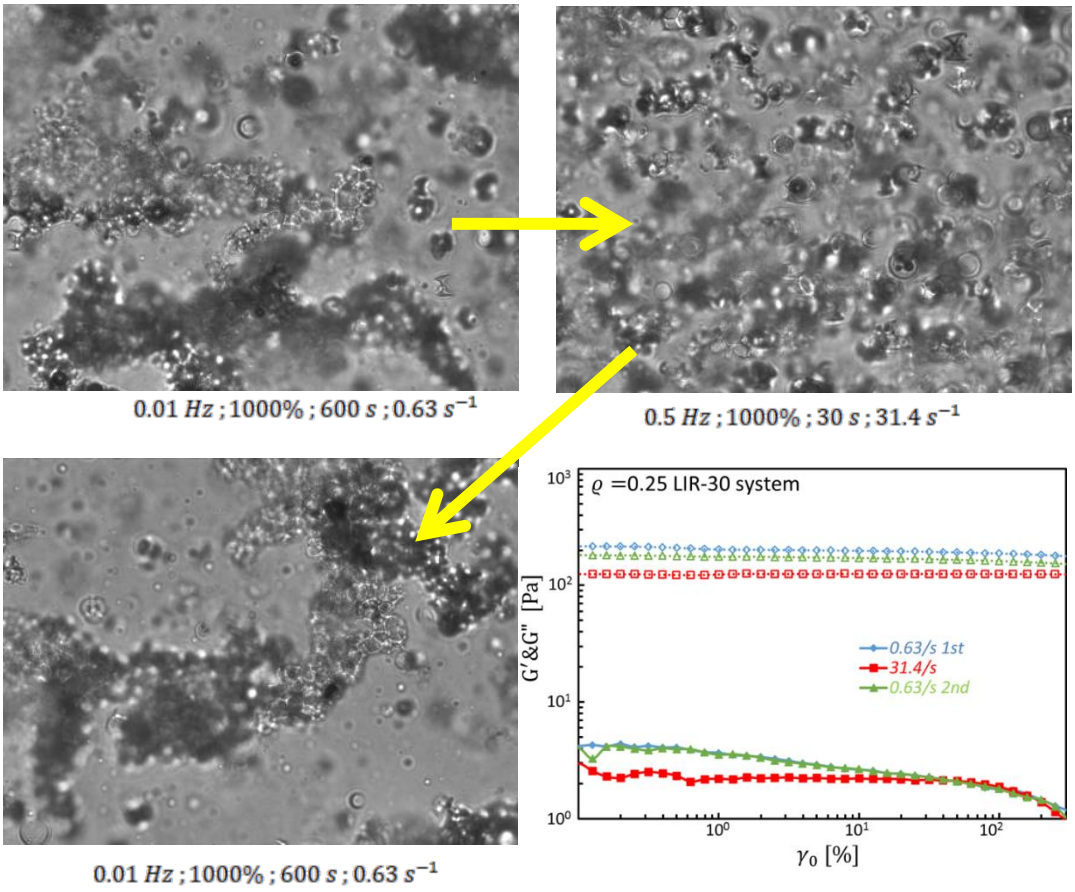

Figure 38. Optical micrographs after oscillation under the conditions (frequency, strain, duration, and maximum shear rate during the oscillation) shown below each image. Thick yellow arrows indicate the sequence of shearing. Bottom right shows changes in oscillatory moduli using the same shear protocol.

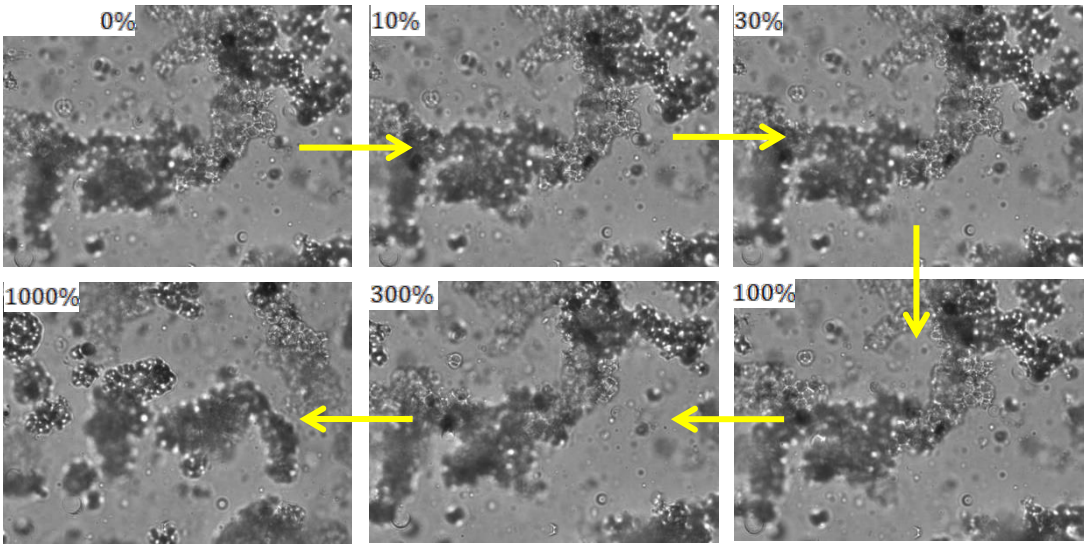

Figure 39. Images taken after applying increasing amounts of oscillatory strain (listed in the image) at a frequency of 0.1 Hz. Yellow arrows indicate sequence of strain increase. Up to 300% strain, the changes in microstructure involve small rotations of the network (more clear in the movie LAOS Sequence.mp4 of the same images). At 1000% strain, the rupture of the network is evident.

APPENDIX B

SUPPLEMENTARY MATERIAL TO "THE EFFECT OF PARTICLE WETTABILITY ON YIELDING OF TERNARY LIQUID/LIQUID/PARTICLE POLYMER BLENDS"

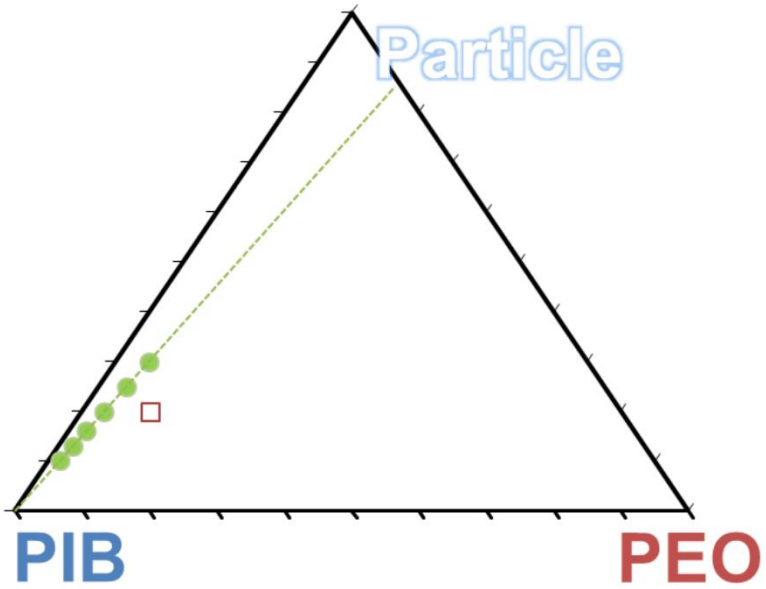

Figure 40. Composition diagram of all samples examined. The green dashed line follows a fixed PEO:particle ratio of 0.16. The red square represents the sample solely in Figure 2.

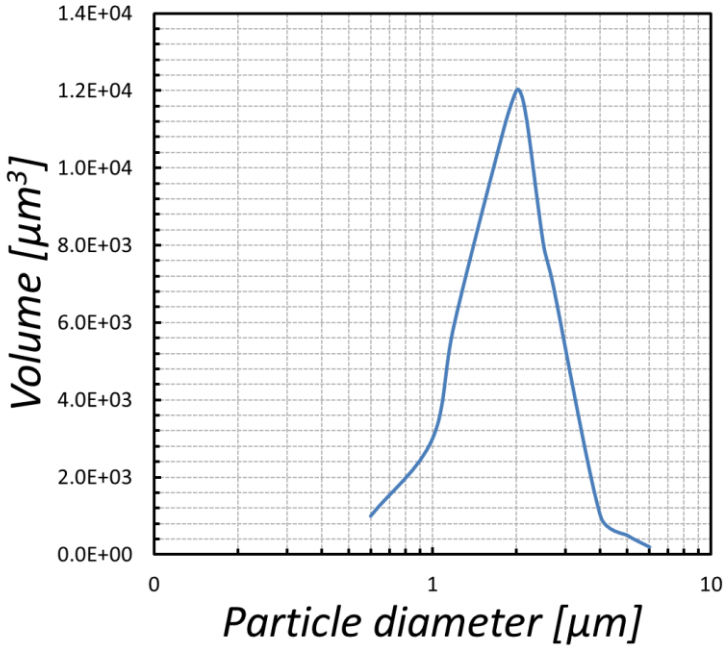

Figure 41. Particle size distribution of unmodified silica particles showing the average diameter is around 2µm.

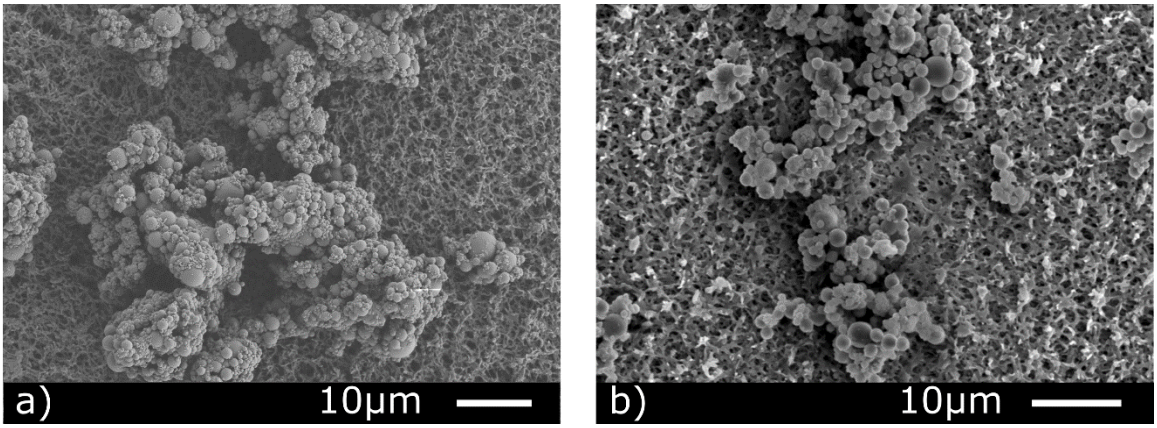

Figure 42. Scanning Electronic microscope images of ternary blend consisting: a) fully wetting silica particle at composition of PIB/PEO/silica = 76.8/3.2/20. b) DCDMS-modified silica particle at PIB/PEO/silica = 89/1/10 reproduced with permission from RSC. (J. Y. Yang, D. Roell, M. Echavarria and S. S. Velankar, Soft Matter, 2017, 13, 8579-8589).

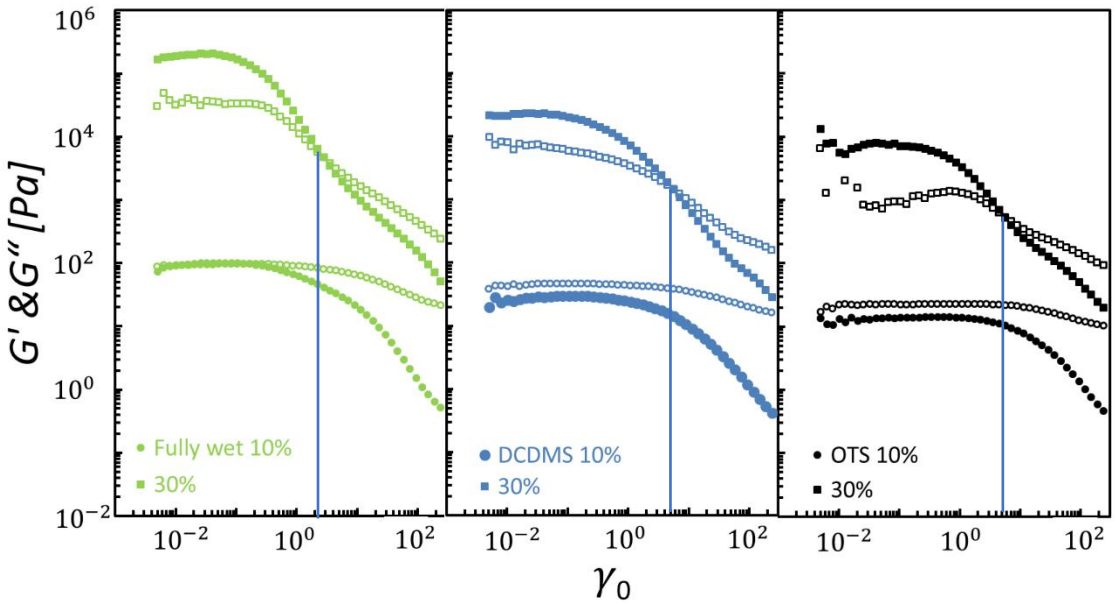

Figure 43. Large amplitude strain sweep results for ternary blends with different silica particles (from left to right: unmodified silica, DCDMS-modified silica and OTS-modified silica). Two compositions are shown in each case: PIB/PEO/silica=66.2/4.8/30 (square) and 88.4/1.6/10 (round). Filled symbols show storage modulus, Open symbols show loss modulus.

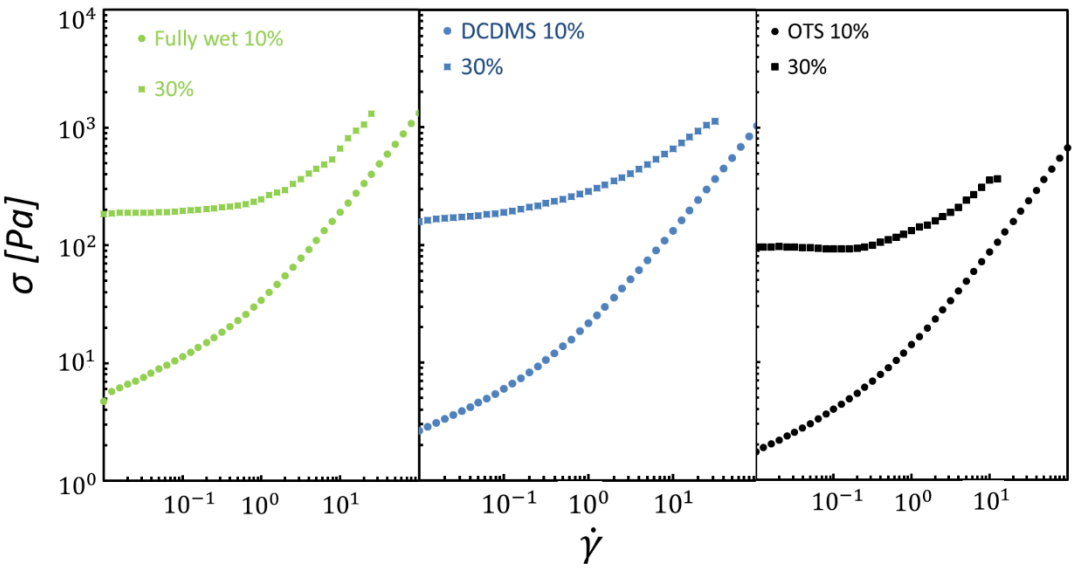

Figure 44. Steady flow behavior for three ternary blends containing, from left to right, unmodified silica, DCDMS-modified silica and OTS-modified silica at two compositions: PIB/PEO/silica=66.2/4.8/30 (square) and 88.4/1.6/10 (round). At 30% particles, some data at high shear rates have been omitted due to indications of slip, e.g. non-monotonic changes in stress as rate increases.

B.1 EXPERIMENTAL DETAILS

B.1.1 Materials

The two fluids used here are identical to those used in our previous research[1, 4-6, 73, 74, 76]: polyisobutylene (PIB, ρ=0.908 g/mL, MW = 2200 g/mol), and polyethylene oxide (PEO ρ=1.1 g/mL, MW = 20000 g/mol). Both fluids are Newtonian under the conditions of the rheological experiments. The size distribution of silica particles is shown in Figure 41.

B.1.2 Surface modification of silica

Dichlorodimethylsilane (DCDMS) and octadecyltricholorosilane (OTS) were used to increase hydrophobicity of particle surface. For DCDMS modification, the process was identical to that in Yang et al[75]. A gas stream laden with DCDMS vapor was fed into a tumbling barrel half-filled with particles for 60 minutes. For OTS modification, the procedure was similar to that used previously[40]. The silica particles were first heated at 380℃ in a vacuum oven to remove any residual organic compounds on the surface. Particles were then suspended in toluene, the OTS was added, and allowed to stir at 99℃ to accomplish hydrophobization. The mixture was stirred overnight, then washed five times with toluene, centrifuged, and dried to remove the solvent.

B.1.3 Blend preparation

Samples for validating changes in wettability due to silane modification were prepared as previously[73], by mixing the three components at 80 ℃ where both polymers are molten. 70 vol% of PIB, 20 vol% of PEO and 10 vol% of particles were held inside the mixer at 80 ℃ for 15 minutes to ensure complete melting, and then mixed at 500 RPM for 5 minutes. The blend was then cooled in a refrigerator, the PIB removed by dissolving into octane, and the dispersed phase (PEO and particles) examined by SEM. This procedure and composition refers to Figure 15 only.

The samples to be tested rheologically were all prepared by the "cold mixing" method described in Yang et al[76]. In this method, a PEO-in-PIB dispersion was first prepared under molten conditions and cooled to freeze the PEO drops. Particles were then mixed while this mixture was still at room temperature at which the PEO drops are still solidified. The details are as follows: A master batch of 80 wt% PIB and 20 wt% PEO was made using a custom mixer described

previously[5, 74-76]. The appropriate weight percentages of PEO and PIB were transferred into the mixer container and covered with a metal cap until it reached 80°C to ensure complete melting of the PEO. Once the temperature was reached, the PEO was blended into the PIB at 500 RPM for 5 minutes. The blend was immediately transferred into a petri dish, sealed with parafilm, and placed in a refrigerator at about -5℃ for 20 minutes to complete the crystallization of the PEO drops.

Separately, particles were dispersed into PIB. For the unmodified or the DCDMS-modified particles, simply adding the dry powder into the PIB and mixing by hand was adequate to realize a good dispersion. The OTS modification however was done in a toluene solvent, and those particles were dried at the end, resulting in some aggregation. Simply mixing the dried powder of OTS-modified particles into PIB gave a poor dispersion (large aggregates were evident). Accordingly, the OTS-modified particles were first dispersed in a small amount of heptane and sonicated for 1 hour. Excellent dispersion of particles was verified by optical microscopy. The appropriate amount of PIB was then added to this solution and the sample mixed with a spatula until most of the heptane evaporated, followed by complete drying of the heptane while stirring in the hood. Since the particles were never dry during this process, they transferred from a well-dispersed state in heptane to a well-dispersed state in PIB.

In either case, suitable quantities of the particles-in-PIB blend were then mixed with the PEO-in-PIB masterbatch to realize the desired composition for the ternary mixture. This mixing was done by hand with a spatula in a petridish at room temperature to keep the PEO drops solid (hence the term “cold mixing”). The samples were placed in vacuum overnight to eliminate air bubbles. The samples were then sealed with parafilm and stored in the refrigerator (to minimize sedimentation) until the rheology tests.

Before any rheological experiments, each dish was given about 20 minutes to reach room temperature before the parafilm was removed to avoid humidity condensing onto the sample. All the samples used for rheological experiments (i.e. except for Figure 15) used a PEO:particle ratio of 0.16 (Figure 40). A limited number of samples without PEO were also examined. For microstructure validation, SEM characterization was conducted using ZEISS Sigma500 VP on ternary blends after selectively removal of continuous PIB.

APPENDIX C

SUPPLEMENTARY MATERIAL TO "A MICROSTRUCTURE-COMPOSITION MAP OF A TERNARY LIQUID/LIQUID/PARTICLE SYSTEM WITH PARTIALLY-WETTING PARTICLES"

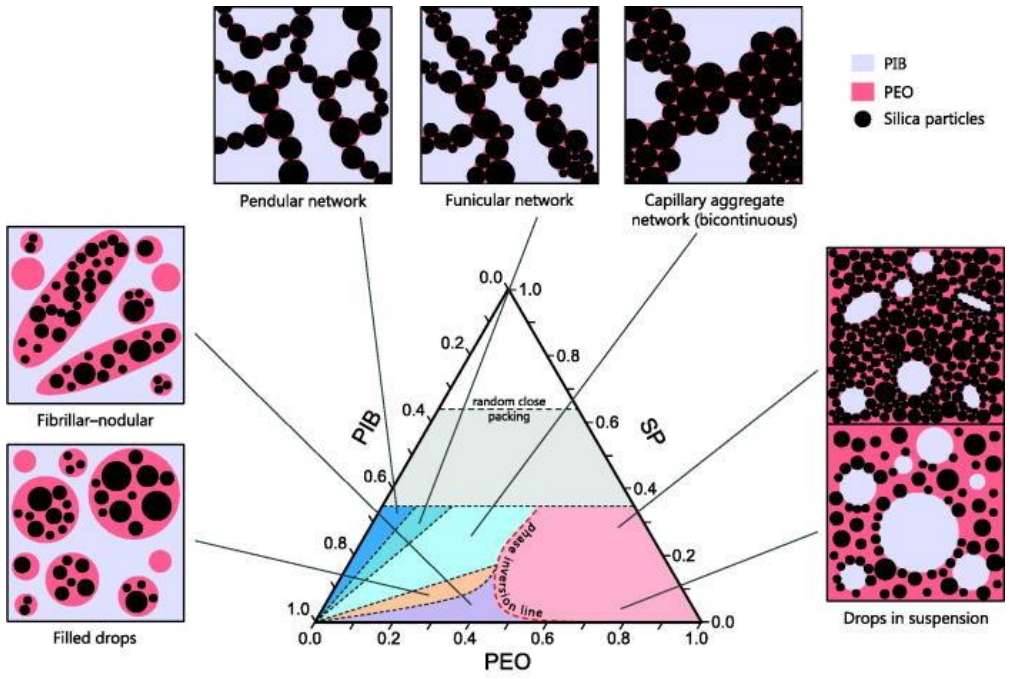

Figure 45. Morphological map and schematic structures of the investigated PIB/PEO/fully wettable silica ternary system. The ternary composition diagram is based on volume fractions. The red dashed path in the ternary diagram represents the phase inversion boundary, with the liquid continuous phase being PIB (non-wetting phase) on the left-handside and PEO (wetting phase) on the right-handside. The grey region of the ternary diagram corresponds to high particle concentrations, which was not explored. Figure reproduced from T. Domenech and S. S. Velankar, J. Rheol., 2017, 61, 363-377. with permission

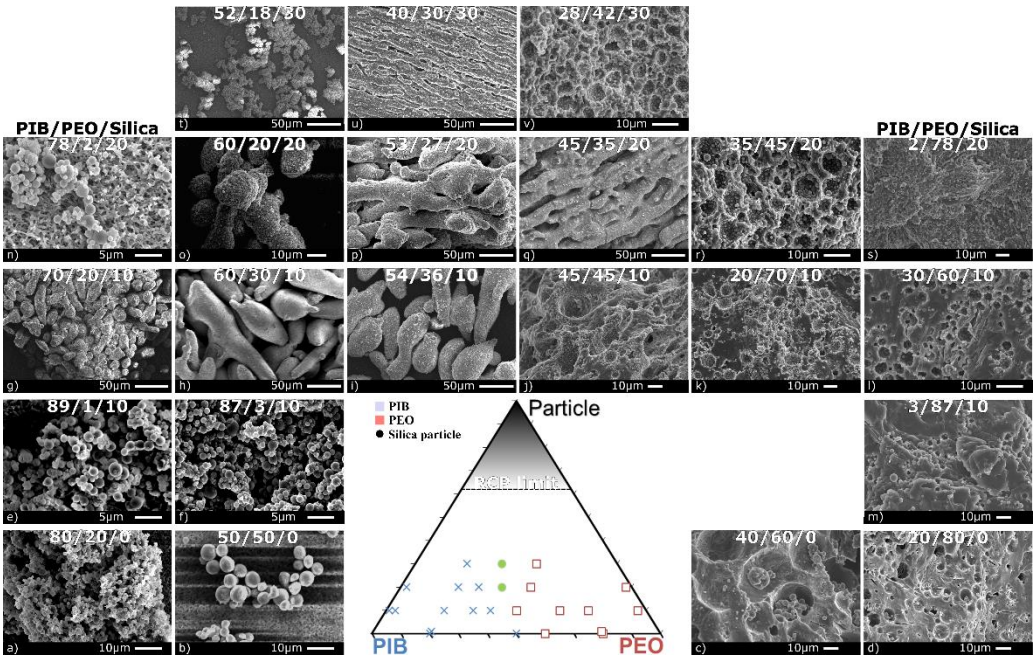

Figure 46. Summary of scanning microscope images at all compositions which are labelled in the pictures separately. The compositions, all listed in the form of PIB/PEO/silica, are as follows: (a) 80/20/00; (b) 50/50/0; (c) 40/60/0; (d) 20/80/0; (e) 89/1/10; (f) 87/3/10; (g) 70/20/10; (h) 60/30/10. (i) 54/36/10; (j) 45/45/10; (k) 20/70/10; (l) 30/60/10 (m) 3/87/10. (n) 78/2/20; (o) 60/20/20. (p) 53/27/20; (q) 45/35/20; (r) 35/45/20; (s) 2/78/20; (t) 52/18/30. (u) 40/30/30; (v) 28/42/30; *sign refers to Figure 2c&d where the difference of addition partial wet particles is shown.

BIBLIOGRAPHY

1. S. S. Velankar, *Soft Matter*, 2015, **11**, 8393-8403.
2. S. U. Pickering, *Journal of the Chemical Society, Transactions*, 1907, **91**, 2001-2021.
3. E. Koos, *Current Opinion in Colloid & Interface Science*, 2014, **19**, 575-584.
4. T. Domenech and S. Velankar, *Rheol. Acta*, 2014, **53**, 593-605.
5. T. Domenech and S. S. Velankar, *Soft Matter*, 2015, **11**, 1500-1516.
6. T. Domenech, J. Y. Yang, S. Heidlebaugh and S. S. Velankar, *PCCP*, 2016, **18**, 4310-4315.
7. S. J. Heidlebaugh, T. Domenech, S. V. Iasella and S. S. Velankar, *Langmuir*, 2014, **30**, 63-74.
8. T. C. Halsey and A. J. Levine, *Phys. Rev. Lett.*, 1998, **80**, 3141-3144.
9. S. Herminghaus, *Adv. Phys.*, 2005, **54**, 221-261.
10. T. Schanz, *Unsaturated Soils: Experimental Studies: Proceedings of the International Conference "From Experimental Evidence towards Numerical Modeling of Unsaturated Soils", Weimar, Germany, September 18-19, 2003*, Springer Berlin Heidelberg, 2006.
11. B. Andreotti, Y. Forterre and O. Pouliquen, *Granular Media: Between Fluid and Solid*, Cambridge University Press, 2013.
12. S. Vankao, L. E. Nielsen and C. T. Hill, *J. Colloid Interface Sci.*, 1975, **53**, 367-373.
13. E. Koos and N. Willenbacher, *Science*, 2011, **331**, 897-900.
14. J. McCulfor, P. Himes and M. R. Anklam, *AlChE J.*, 2011, **57**, 2334-2340.
15. M. N. Lee, H. K. Chan and A. Mohraz, *Langmuir*, 2012, **28**, 3085-3091.

16. J. Dittmann, E. Koos and N. Willenbacher, *J. Am. Ceram. Soc.*, 2013, **96**, 391-397.

17. J. Zhang, H. Zhao, W. F. Li, M. H. Xu and H. F. Liu, *Scientific Reports*, 2015, **5**, 8.

18. K. Haibach, A. Menner, R. Powell and A. Bismarck, *Polymer*, 2006, **47**, 4513-4519.

19. M. N. Lee and A. Mohraz, *Adv. Mater.*, 2010, **22**, 4836 - 4841.

20. A. Barbetta, G. Rizzitelli, R. Bedini, R. Pecci and M. Dentini, *Soft Matter*, 2010, **6**, 1785-1792.

21. P. Thareja, B. P. Ising, S. J. Kingston and S. S. Velankar, *Macromol. Rapid Commun.*, 2008, **29**, 1329-1334.

22. E. Dickinson, *Current Opinion in Colloid & Interface Science*, 2010, **15**, 40-49.

23. H. J. Jin, W. Z. Zhou, J. Cao, S. D. Stoyanov, T. B. J. Blijdenstein, P. W. N. de Groot, L. N. Arnaudov and E. G. Pelan, *Soft Matter*, 2012, **8**, 2194-2205.

24. E. M. Herzig, K. A. White, A. B. Schofield, W. C. K. Poon and P. S. Clegg, *Nat. Mater.*, 2007, **6**, 966-971.

25. C. L. Flemmer, *Powder Technol.*, 1991, **66**, 191-194.

26. S. Strauch and S. Herminghaus, *Soft Matter*, 2012, **8**, 8271-8280.

27. P. Aussillous and D. Quere, *Nature*, 2001, **411**, 924-927.

28. B. P. Binks and R. Murakami, *Nat. Mater.*, 2006, **5**, 865-869.

29. J. M. Rallison, *Annual Review of Fluid Mechanics*, 1984, **16**, 45-66.

30. M. Minale, J. Mewis and P. Moldenaers, *AlChE J.*, 1998, **44**, 943-950.

31. B. E. Burkhart, P. V. Gopalkrishnan, S. D. Hudson, A. M. Jamieson, M. A. Rother and R. H. Davis, *Phys. Rev. Lett.*, 2001, **87**, art. no.-098304.

32. S. Duzyol and A. Ozkan, *Sep. Sci. Technol.*, 2011, **46**, 876-881.

33. C. D. Willett, M. J. Adams, S. A. Johnson and J. P. K. Seville, *Langmuir*, 2000, **16**, 9396-9405.

34. M. E. D. Urso, C. J. Lawrence and M. J. Adams, *J. Colloid Interface Sci.*, 1999, **220**, 42-56.

35. J. Colombo and E. Del Gado, *J. Rheol.*, 2014, **58**, 1089-1116.

36. T. Ngai, S. A. F. Bon, H. J. Butt, I. Hamley, H. A. Stone, C. Wu, B. J. Park, P. Clegg, S. Biggs and H. Zhao, *Particle-stabilized Emulsions and Colloids: Formation and Applications*, Royal Society of Chemistry, London, 2014.

37. S. J. Huang, L. Bai, M. Trifkovic, X. Cheng and C. W. Macosko, *Macromolecules*, 2016, **49**, 3911-3918.

38. R. Aveyard, B. P. Binks and J. H. Clint, *Adv. Colloid Interface Sci.*, 2003, **100**, 503-546.

39. M. E. Cates and P. S. Clegg, *Soft Matter*, 2008, **4**, 2132-2138.

40. S. P. Nagarkar and S. S. Velankar, *Soft Matter*, 2012, **8**, 8464-8477.

41. B. P. Binks, M. Kirkland and J. A. Rodrigues, *Soft Matter*, 2008, **4**, 2373-2382.

42. B. P. Binks and S. O. Lumsdon, *Langmuir*, 2000, **16**, 8622-8631.

43. I. Vinckier, P. Moldenaers and J. Mewis, *Rheol. Acta*, 1999, **38**, 65-72.

44. J. G. Oldroyd, *Proceedings of the Royal Society of London Series a-Mathematical and Physical Sciences*, 1953, **218**, 122-132.

45. P. H. M. Elemans, J. M. H. Janssen and H. E. H. Meijer, *J. Rheol.*, 1990, **34**, 1311-1325.

46. J. F. Palierne, *Rheol. Acta*, 1990, **29**, 204-214.

47. K. Okamoto, M. Takahashi, H. Yamane, H. Kashihara, H. Watanabe and T. Masuda, *J. Rheol.*, 1999, **43**, 951-965.

48. H. J. Butt and M. Kappl, *Adv. Colloid Interface Sci.*, 2009, **146**, 48-60.

49. W. Herschel and R. Bulkley, *Am. Soc. Test Proc*, 1926, **26**, 621-633.

50. P. Coussot, *Phys. Rev. Lett.*, 1995, **74**, 3971-3974.

51. E. Koos and N. Willenbacher, *Soft Matter*, 2012, **8**, 3988-3994.

52. F. Bossler and E. Koos, *Langmuir*, 2016, **32**, 1489-1501.

53. R. Buscall, I. J. McGowan, P. D. A. Mills, R. F. Stewart, D. Sutton, L. R. White and G. E. Yates, *J. Non-Newtonian Fluid Mech.*, 1987, **24**, 183-202.

54. E. Koos, W. Kannowade and N. Willenbacher, *Rheol. Acta*, 2014, **53**, 947-957.

55. G. P. Lian, C. Thornton and M. J. Adams, *J. Colloid Interface Sci.*, 1993, **161**, 138-147.

56. K. N. Pham, G. Petekidis, D. Vlassopoulos, S. U. Egelhaaf, W. C. K. Poon and P. N. Pusey, *J. Rheol.*, 2008, **52**, 649-676.

57. N. Koumakis and G. Petekidis, *Soft Matter*, 2011, **7**, 2456-2470.

58. P. Thareja and S. Velankar, *Rheol. Acta*, 2008, **47**, 189-200.

59. H. Sedgwick, S. U. Egelhaaf and W. C. K. Poon, *J. Phys.-Condes. Matter*, 2004, **16**, S4913-S4922.

60. J. P. Pantina and E. M. Furst, *Langmuir*, 2004, **20**, 3940-3946.

61. C. J. Dibble, M. Kogan and M. J. Solomon, *Physical Review E*, 2006, **74**, 11.

62. F. Cardinaux, A. Stradner, P. Schurtenberger, F. Sciortino and E. Zaccarelli, *Epl*, 2007, **77**, 5.

63. S. Buzzaccaro, R. Rusconi and R. Piazza, *Phys. Rev. Lett.*, 2007, **99**, 4.

64. S. J. Antony, W. Hoyle and Y. Ding, *Granular Materials: Fundamentals and Applications*, Royal Society of Chemistry, 2004.

65. A. Mohraz, *Current Opinion in Colloid & Interface Science*, 2016, **25**, 89-97.

66. L. Bai, J. W. Fruehwirth, X. Cheng and C. W. Macosko, *Soft Matter*, 2015, **11**, 5282-5293.

67. A. F. Sirianni, C. E. Capes and Puddingt.Ie, *Can. J. Chem. Eng.*, 1969, **47**, 166.

68. S. H. Lee, M. Bailly and M. Kontopoulou, *Macromol. Mater. Eng.*, 2012, **297**, 95-103.

69. A. N. Alexandrou, A. V. Bazilevskii, V. M. Entov, A. N. Rozhkov and A. Sharaf, *Fluid Dyn.*, 2010, **45**, 952-964.

70. J. Zhang, H. Zhao, W. Li, M. Xu and H. Liu, *Scientific Reports*, 2015, **5**, 16058.

71. J. P. Wang, E. Gallo, B. Francois, F. Gabrieli and P. Lambert, *Powder Technol.*, 2017, **305**, 89-98.

72. D. Megias-Alguacil and L. J. Gauckler, *Powder Technol.*, 2010, **198**, 211-218.

73. D. Amoabeng, D. Roell, K. M. Clouse, B. A. Young and S. S. Velankar, *Polymer*, 2017, **119**, 212-223.

74. T. Domenech and S. S. Velankar, *J. Rheol.*, 2017, **61**, 363-377.

75. J. Y. Yang, D. Roell, M. Echavarria and S. S. Velankar, *Soft Matter*, 2017, **13**, 8579-8589.

76. J. Y. Yang and S. S. Velankar, *J. Rheol.*, 2017, **61**, 217-228.

77. F. Bossler, J. Maurath, K. Dyhr, N. Willenbacher and E. Koos, *J. Rheol.*, 2018, **62**, 183-196.

78. E. Koos, J. Johannsmeier, L. Schwebler and N. Willenbacher, *Soft Matter*, 2012, **8**, 6620-6628.

79. P. C. Hiemenz and R. Rajagopalan, *Principles of Colloid and Surface Chemistry, Third Edition, Revised and Expanded*, CRC Press, 2016.

80. B. P. Binks, *Current Opinion in Colloid & Interface Science*, 2002, **7**, 21-41.

81. T. S. Horozov and B. P. Binks, *Angew. Chem.-Int. Edit.*, 2006, **45**, 773-776.

82. P. Cassagnau, *Polymer*, 2008, **49**, 2183-2196.

83. K. Premphet and P. Horanont, *Polymer*, 2000, **41**, 9283-9290.

84. B. P. Binks, A. J. Johnson and J. A. Rodrigues, *Soft Matter*, 2010, **6**, 126-135.

85. M. Kahlweit and R. Strey, *Angew. Chem.-Int. Edit. Engl.*, 1985, **24**, 654-668.

86. H. T. Davis, *Colloid Surf. A-Physicochem. Eng. Asp.*, 1994, **91**, 9-24.

87. B. P. Binks and S. O. Lumsdon, *PCCP*, 2000, **2**, 2959-2967.

88. P. Thareja, K. Moritz and S. S. Velankar, *Rheol. Acta*, 2010, **49**, 285-298.

89. P. R. Garrett, in *The Science of Defoaming: Theory, Experiment and Applications*, CRC Press, Boca Raton, 2013, pp. 115-308.

90. C. DeLeo, C. A. Pinotti, M. D. Goncalves and S. Velankar, *J. Polym. Environ.*, 2011, **19**, 689-697.

91. J. A. Galloway and C. W. Macosko, *Polym. Eng. Sci.*, 2004, **44**, 714-727.

92. B. P. Binks and S. O. Lumsdon, *Langmuir*, 2000, **16**, 2539-2547.

93. B. P. Binks and S. O. Lumsdon, *Langmuir*, 2000, **16**, 3748-3756.

94. E. S. Read, S. Fujii, J. I. Amalvy, D. P. Randall and S. P. Armes, *Langmuir*, 2004, **20**, 7422-7429.

95. J. A. Witt, D. R. Mumm and A. Mohraz, *Soft Matter*, 2013, **9**, 6773-6780.

96. M. Caggioni, P. T. Spicer, D. L. Blair, S. E. Lindberg and D. A. Weitz, *J. Rheol.*, 2007, **51**, 851-865.

97. A. B. Pawar, M. Caggioni, R. W. Hartel and P. T. Spicer, *Faraday Discuss.*, 2012, **158**, 341-350.

98. B. P. Binks and J. H. Clint, *Langmuir*, 2002, **18**, 1270-1273.

99. J. T. Davies, *Proceedings of the International Congress of Surface Activity*, 1957, **1**, 426-438.

100. V. Pauchard and T. Roy, *Colloid Surf. A-Physicochem. Eng. Asp.*, 2014, **443**, 410-417.

101. K. Stratford, R. Adhikari, I. Pagonabarraga, J. C. Desplat and M. E. Cates, *Science*, 2005, **309**, 2198-2201.

102. G. Gillies, K. Buscher, M. Preuss, M. Kappl, H. J. Butt and K. Graf, *J. Phys.-Condes. Matter*, 2005, **17**, S445-S464.

103. H. K. Chan, *Colloid Surf. A-Physicochem. Eng. Asp.*, 2006, **284**, 50-55.

104. D. Graebling, R. Muller and J. F. Palierne, *Macromolecules*, 1993, **26**, 320-329.

105. V. Shaayegan, P. Wood-Adams and N. R. Demarquette, *J. Rheol.*, 2012, **56**, 1039-1056.